



JNCC Report

No: 570

Geological investigation of pockmarks in the Scanner Pockmark SCI area

Gafeira, J. & Long, D.

August 2015

© JNCC, Peterborough 2015

0963 8091

For further information please contact:

Joint Nature Conservation Committee
Monkstone House
City Road
Peterborough PE1 1JY
www.jncc.defra.gov.uk

This report should be cited as:

Gafeira, J. & Long, D. 2015. Geological investigation of pockmarks in the Scanner Pockmark SCI area. *JNCC Report No 570*. JNCC Peterborough.

Foreword

This report is the product of a desk study by the British Geological Survey (BGS) for the Joint Nature Conservation Committee (JNCC). The scope of the desk study included a comparison of the JNCC 2012 multibeam/sidescan dataset from the Scanner and Braemar pockmarks areas in the northern North Sea with similar historic datasets noting morphological change. Also within scope were a record of gas seepage and Methane-Derived Authigenic Carbonate (MDAC) observations and an examination of sedimentation rates and evidence of anthropogenic causes of sedimentation.

The Scanner Pockmark area is located in UKCS Block 15/25, near the centre of the Witch Ground Basin. As a site of active gas seepage it has been a focus of surveys since 1983. The Scanner Pockmark site proposal was submitted to the European Commission on 31st August 2008 for the following interest feature under the EC Habitats Directive: *1180 Submarine structures made by leaking gases*. Following submission, it was accepted as a Site of Community Importance (SCI). The Scanner Pockmark SCI includes four unusually large pockmarks, which constitute two pockmark complexes named *Scanner* and *Scotia* Pockmark Complexes.

This report contains the analysis of the Scanner Pockmark SCI area. The results from the Braemar Pockmarks SCI are given in a separate report.

Prior to publication this report was subject to JNCC's Evidence Quality Assurance (EQA) process and peer reviewed by Dr Alan Judd and Peter Croker. The JNCC EQA policy can be found on the JNCC website. <http://jncc.defra.gov.uk/default.aspx?page=6675>

Acknowledgements

We thank Dr Alan Judd, Peter Croker and JNCC for their comments on an earlier version of this rep



**British
Geological Survey**

NATURAL ENVIRONMENT RESEARCH COUNCIL

Contents

Foreword	i
Acknowledgements	ii
Contents	iii
Summary	viii
1 Introduction	1
2 Data sources	4
2.1. Data supplied by JNCC	4
2.2. BGS-acquired data	5
2.3. Third party data held by the BGS	6
2.4. Multibeam surveys	6
3 Scanner and Scotia Pockmark Complex	7
4 Pockmark morphology	10
4.1. Semi-automated mapping	10
4.2. Scanner Pockmark Complex	14
4.3. Scotia Pockmark Complex	17
4.4. Pockmark Morphology	20
4.5. Survey Comparison	22
5 Evidence of Gas Seepage	31
5.1. Direct evidence of gas seepage	31
5.2. Methane-Derived Authigenic Carbonate (MDAC)	38
5.3. Bacterial Mats	40
5.4. Seep-associated fauna	40
5.5. Shallow gas accumulations	41
6 Sedimentation	42
7 Anthropogenic Activities	44
7.1. Oil and Gas Exploration and Production	44
7.2. Fishing Activity	47
8 Comments	50
9 Conclusions	56
Appendix 1. List of Cruises	58
Appendix 2. Pockmark attributes	59
Appendix 3. Current data provided by BODC	62
Appendix 4. UK Benthos data for the Blenheim Platform	63

Appendix 5. Previous depictions of the Scanner Pockmark Complex	66
Appendix 6. Pockmarks Summary	75
Glossary.....	77
References	78

FIGURES

Figure 1. Location of block 15/25 and the oil and gas fields within the UK Northern North Sea..	1
Figure 2. Variation in pockmark density across the Witch Ground Basin.....	2
Figure 3. Detail from the JNCC multibeam dataset showing the limits of the Scanner Pockmark SCI and the areas considered as part of both the Scanner and Scotia pockmark complexes. ...	3
Figure 4. BGS regional data around Scanner Pockmark SCI and seismic lines acquired by BGS for the Marine Biological Association (MBA).....	5
Figure 5. Map showing both multibeam datasets used during this study.	6
Figure 6. Deep-towed sparker line collected in 1983, across the Western Scanner Pockmark, during the Geoteam cruise.....	7
Figure 7. Map showing the distribution of shallow gas in UK block 15/25d as seen in boomer records and in 3D seismic volumes (From Holmes and Stoker, 2005).	8
Figure 8. Detail view showing two pockmarks of different sizes (blue outline) that had previously been manually mapped as of similar size (red outline). This image exemplifies the consistency resulting from using an automated method to map seabed features.	11
Figure 9. Outline of the 67 pockmarks mapped with the pockmark semi-automated mapping method.	12
Figure 10. Outline of the 67 pockmarks mapped within and surrounding the Scanner Pockmark SCI showing their identification number and both their deepest point (red dot) and the polygons centre (blue dot).	13
Figure 11. Bathymetry of the Scanner Pockmark Complex area (contour lines at 0.5m intervals).	14
Figure 12. Slope angle and depth map of the Scanner Pockmark Complex area.	15
Figure 13. Slope angle map of the Scanner Pockmark Complex area overlying the shaded-relief map.	16
Figure 14. Curvature map of the Scanner Pockmark Complex area overlying the shaded-relief map.	16
Figure 15. Bathymetry of the Scotia Pockmark Complex area (contour lines at 0.5 m intervals).	17
Figure 16. Slope angle and depth map of the Scotia Pockmark Complex area.	18
Figure 17. Slope angle map of the Scotia Pockmark Complex area overlying the shaded-relief map.	19
Figure 18. Curvature map of the Scotia Pockmark Complex area overlying the shaded-relief map	20
Figure 19. Relationship between the Pockmark Depth and Pockmark Area for the 63 unit pockmarks mapped within the Scanner SCI area.	21
Figure 20. Relationship between Pockmark Area and Pockmark Depth for the unit pockmarks mapped within the Scanner SCI area (yellow dots) compared to the relationship found in 15 other sites within the Witch Ground Basin (Gafeira <i>et al.</i> , 2012).....	21
Figure 21. Detailed view of the raster generated by subtracting the depth values of the SEA 2, Box 4 dataset from the JNCC multibeam dataset values.....	22
Figure 22. Profiles from A to B (on Figure 21) extracted from 1) the SEA2 dataset (in dark red), 2) the JNCC dataset (blue) and 3) the depth corrected SEA2 dataset (orange).....	23
Figure 23. The difference of pockmark depth derived for the JNCC survey and the SEA2 survey, box 4.	24

Figure 24. Detailed image showing the difference between pockmark depths extracted from the two surveys compared in this study.....	25
Figure 25. Difference values between the pockmark's Maximum Water depths extracted from the two datasets used in this study.....	25
Figure 26. Horizontal distance between the positions of the deepest points of each pockmark, extracted from the SEA and JNCC datasets.	26
Figure 27. Bathymetric profiles extracted from both surveys across Pockmark 46, showing apparent erosion of the northern sidewall.....	26
Figure 28. Bathymetry profiles extracted across Southern Scotia from both surveys.	28
Figure 29. Bathymetry profiles extracted from both surveys across the Northern Scotia pockmark.	28
Figure 30. Shade-relief map (JNCC dataset) of the Eastern Scanner Pockmark, with contour lines every 50 cm.	30
Figure 31. Towed Sidescan sonar image across the Western Scanner Pockmark.	32
Figure 32. Single beam echosounder record acquired over the Scanner Pockmark Complex by the vessel Lador as the ROV Solo surveyed the pockmark at a constant depth (~130 m)....	33
Figure 33. Data collected during the RRS Challenger Cruise 70 (Dando, 1990), overlying the pockmarks outlines (JNCC, 2012).....	33
Figure 34. 1000 kHz side-scan sonar record (BGS 91/03 Line 22) across Southern Scotia Pockmark.	34
Figure 35. Shade-relief map of the Southern Scotia pockmark showing the location of the side-scan sonar (BGS 91/03, Line 22) shown in Fig 34 (purple line).....	35
Figure 36. Scan image showing seep plumes from the major pockmarks in the Witch Ground Basin collected by the Heincke 180 cruise in 2002.....	35
Figure 37. Methane profiles of the gravity cores collected during the He208 cruise from Eastern Scanner (St 713) and Southern Scotia (St 717).	37
Figure 38. Image of bubbles escaping from Scanner pockmark collected by Statoil 1985.	37
Figure 39. A large slab of MDAC found by Statoil near the centre of the Western Scanner pockmark in UK Block 15/25. Taken from Judd (2001).....	38
Figure 40. Image extracted from STN92 video SCDC06 at 13:55:46 UTC, located near the rim of the Eastern Scanner Pockmark. This image shows accumulation of deposits interpreted as possible MDAC.	39
Figure 41. Left: Location of Stn 92 026, on the southern edge of the Eastern Scanner Pockmark. Right: The still image extracted at Stn 92 026, described as possible MDAC ledge.	40
Figure 42. Seabed photograph showing anoxic sediments (black) and bacterial mat (white) adjacent to MDAC at area of gas seepage in UK Block 15/25.	41
Figure 43. Profile of core K1-958 in 146m water depth, Witch Ground Basin (Erlenkeuser, 1979).	43
Figure 44. Profile of core K1-959 in 125m water depth, Witch Ground Basin (Erlenkeuser, 1979).	43
Figure 45. Oilfields and subsea infrastructure features on the vicinity of the Scanner Pockmark SCI.....	45
Figure 46. Spatial relationship between the Scanner Pockmark SCI Boundaries and the sample stations collected in the vicinity of the Blenheim platform.	46

Figure 47. The concentrations of hydrocarbon in the sediments versus distance from the sample station to the Blenheim oil platform.	47
Figure 48. Multibeam backscatter from CEFAS cruise showing several pairs of trawlmarks (~50m apart) crisscrossing the Scanner SCI area (red outline).	48
Figure 49. Comparison between the positions of Pockmark 37 within the two acoustic datasets acquired during the cruise CEND19x/12, multibeam on left and sidescan sonar image on the right.....	49
Figure 50. Bathymetric imaged collected during the ALKOR 259 cruise, showing the location of Scanner and Scotia pockmark complexes, Challenger Pockmark and Alkor Pockmark (that was first found during that cruise).	51
Figure 51. Earthquake epicentres between 2000 and 2014 located near the Scanner SCI.	53
Figure 52. Rose diagrams showing the current direction of modern bottom waters (generally less than 15m above seafloor).	62
Figure 53. Figure presented by Hovland and Sommerville (1985) showing the location of gas seepage within the Scanner Pockmark Complex.....	66
Figure 54. Figure from the Dando et al. (1991) paper, showing the location of the samples collected during the FRV Scotia and MV Resolution cruises in 1989.....	67
Figure 55. Location of stations samples during RRS Challenger Cruise 70 to the Scanner and Challenger pockmarks in 1990.	68
Figure 56. Location of stations sampled during the 1991 RRS Challenger Cruise 82.	69
Figure 57. Figure extracted from the 1991 Challenger 82 cruise report (Dando, 1991).....	70
Figure 58. Figure extracted from Judd et al. (1994).....	71
Figure 59. Map showing the pockmarks Challenger, Scotia, and Scanner, compiled from MBES data acquired by the UK government (Department of Trade and Industry) in 2000 as part of the Strategic Environmental Assessment process.	72
Figure 60. 3D view of the Scanner Pockmark Complex. Figure extracted from Judd (2001).....	73
Figure 61. 3D view of the Scotia Pockmark Complex. Figure extracted from Judd (2001).....	73
Figure 62. Bathymetric data collected, in 2005, during the IFM-GEOMAR cruise (ALKOR 259), on board of the RV Alkor.	74

TABLES

Table 1. List of data collected during the CEND19x/12 cruise that was provided to BGS, from the Scanner Pockmark SCI study area.....	4
Table 2. Details of earthquakes located near Scanner SCI recorded between 2001 and 2014	53
Table 3. Scanner SCI survey area Pockmark morphological attributes.	59
Table 4. BODC data sets with bottom water data examined by Gafeira <i>et al.</i> 2012.	62
Table 5. Data extracted from the UK Benthos dataset for the sample stations collected in the vicinity of the Blenheim platform (58° 16.33'N, 01° 00.27'E).....	63
Table 6. Pockmark characteristics inferred from the interpretation of the JNCC multibeam dataset.	75

Summary

This report describes the findings of the desk study carried out by the British Geological Survey (BGS) for the Joint Nature Conservation Committee (JNCC) covering the Scanner Pockmark Site of Community Importance (SCI) area. The Scanner Pockmark SCI is located in UKCS block 15/25, near the centre of the North Sea Witch Ground Basin. This site was submitted to the European Commission on 31st August 2008, under the EC Habitats Directive: *1180 Submarine structure made by leaking gases*, and was approved as an SCI by the European Commission. This SCI comprises four unusually large pockmarks, which constitute two pockmark complexes named *Scanner* and *Scotia* Pockmark Complexes and several smaller pockmarks.

This study's focus is on the pockmarks found in Scanner Pockmark SCI area, and looks at evidence of gas seepage and specific factors that influence the formation and exposure of methane-derived authigenic carbonate (MDAC) structures within the pockmarks.

The new data collected by Centre for Environment, Fisheries & Aquaculture Science (CEFAS) at the end of 2012, cruise CEND19x/12 commissioned by JNCC, provided the main dataset for this study. The multibeam dataset collected was used to semi-automatically map and characterise the morphology of the pockmarks. The information extracted from the mapped pockmarks was then compared to the information extracted from previous surveys. Backscatter data and side scan sonar data was used to characterise the nature of the seafloor, in particular the presence of methane-derived authigenic carbonate (MDAC). The study confirmed changes in the volume of sediment infill of the pockmark but no clear sediment source was identified.

1 Introduction

The Scanner Pockmark Complex is situated in the south of UK licence block 15/25 (Figure 1), approximately 185 km off the north-east coast of Scotland (58°16'54.0"N, 0°58'14.6"E). It is located near the centre of the Witch Ground Basin, close to many oil and gas condensate fields.

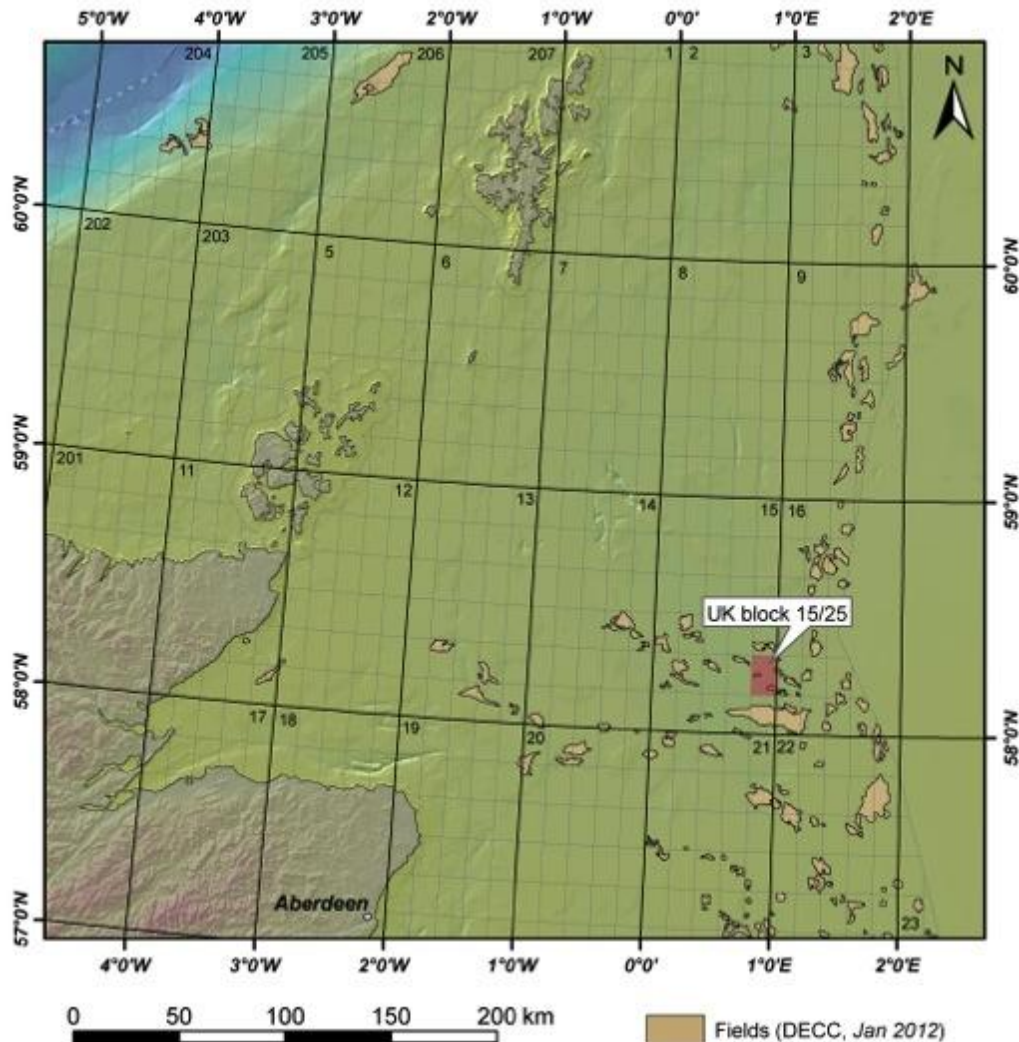


Figure 1. Location of block 15/25 and the oil and gas fields within the UK Northern North Sea.

The North Sea Witch Ground Basin was an important depocentre for fine grained sedimentation during deglaciation at the end of the Weichselian glaciation about 15,000 to 13,000 years ago when sediments were deposited very rapidly creating a thick sequence of very soft muds. Pockmarks can be found in vast numbers across the Witch Ground Basin, in densities generally up to 30 pockmarks per square kilometre (BGS, 1986). The frequency of pockmarks tends to increase with water depth but not directly correlative (Figure 2). They are evident in fine grained sediments but tend to become smaller and less frequent when the mud content is reduced. Acoustic turbidity is often evident in the shallow section, below the Witch Ground Formation, suggesting shallow gas is trapped at selected horizons within the Quaternary sequence (Andrews *et al.*, 1990); such accumulations support the hypothesis that the pockmarks found in this basin were formed by gas escape at irregular intervals since deglaciation (Long, 1992).

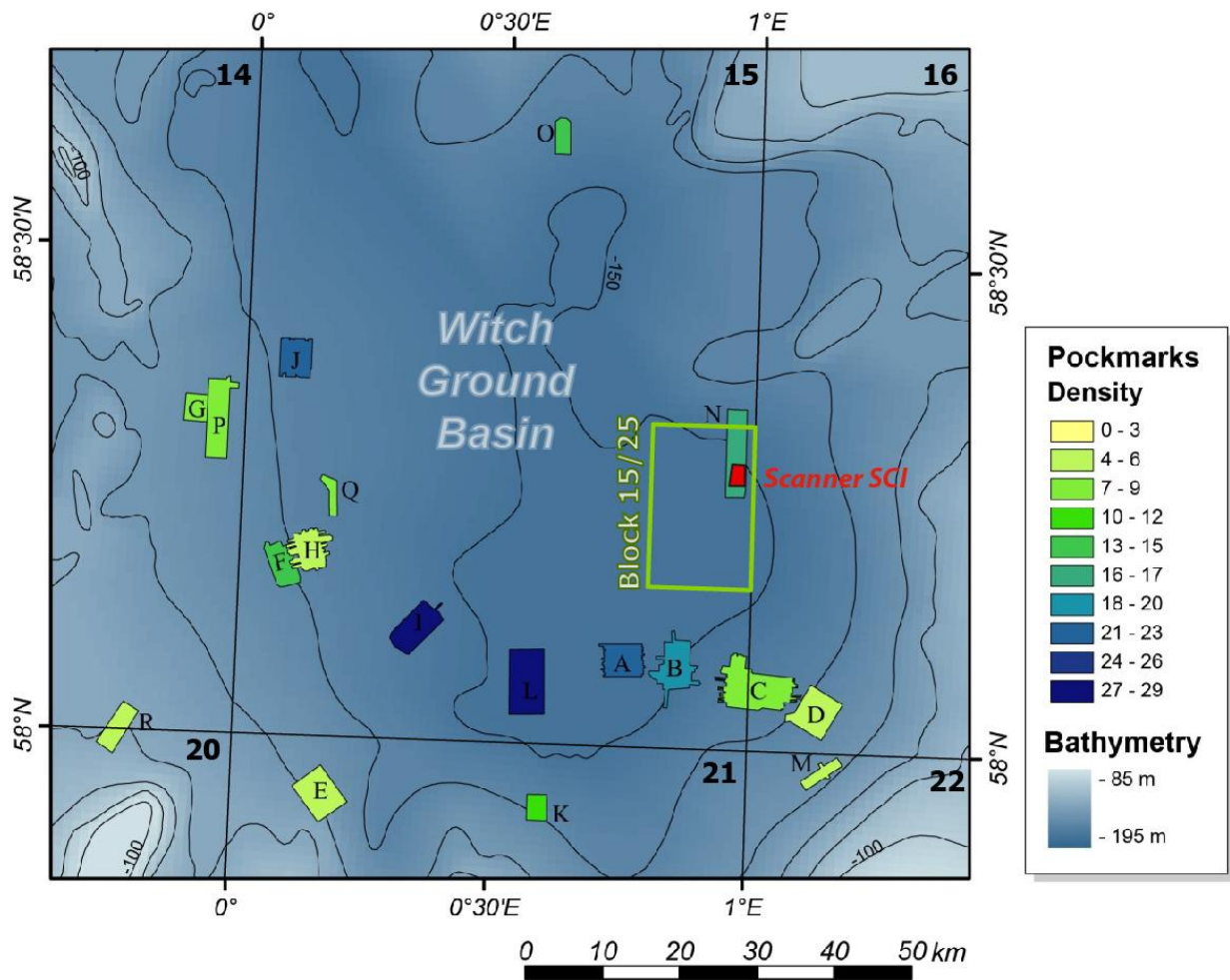


Figure 2. Variation in pockmark density across the Witch Ground Basin.

Note that the density of pockmarks decreases from nearly 30/km² in the centre of the basin, where water depths exceed 150 m, to less than 5/km² on the edge of the basin where water depths are around 120 m.

The seabed in the Witch Ground Basin has remained essentially unchanged by erosion or sedimentation since sea level stabilised after the last glaciation. Subsequently, the pockmarks present on the seabed represent the cumulative effects of gas escape activity over a period of at least 8,000 years.

Most pockmarks in the Witch Ground Basin are less than 3 metres deep, with the exception of a few unusually large pockmarks. The large pockmarks present in the Block 15/25 area have long been known as sites of active seepage (Hovland and Sommerville, 1985; Dando *et al.*, 1991; Judd *et al.* 1994) and have been submitted as a candidate Special Area of Conservation (cSAC) under the European Habitats Directive: 1180 - *Submarine structures made by leaking gases* and have subsequently been approved by the European Commission as Sites of Community Importance (SCI). This SCI extends over 3.35 km² and includes four unusually large pockmarks, which constitute two pockmark complexes named the *Scanner* and *Scotia* Pockmark Complexes (Figure 3).

They are important sites, as methane-derived authigenic carbonate formed by the anaerobic oxidation of escaping methane, cementing the grains of sediment just below the seabed can become exposed by subsequent pockmark activity, thereby providing a hard substrate at seabed that can attract a diverse fauna. Fish (e.g. hagfish, haddock, wolf-fish and small redfish) appear to be using the pockmark depressions and the carbonate structures for shelter. These habitats also host a highly specialized fauna that can exploit the gas released. Two species found on the Scanner Pockmark Complex had not previously been reported from the Fladen Ground in the

northern North Sea (Dando *et al.*, 1991): *Thyasira sarsi* (which is known to contain endosymbiotic sulphide-oxidising bacteria) and the mouthless and gutless nematode, *Astomonema sp.*, present in very high numbers which also contains endosymbiotic bacteria.

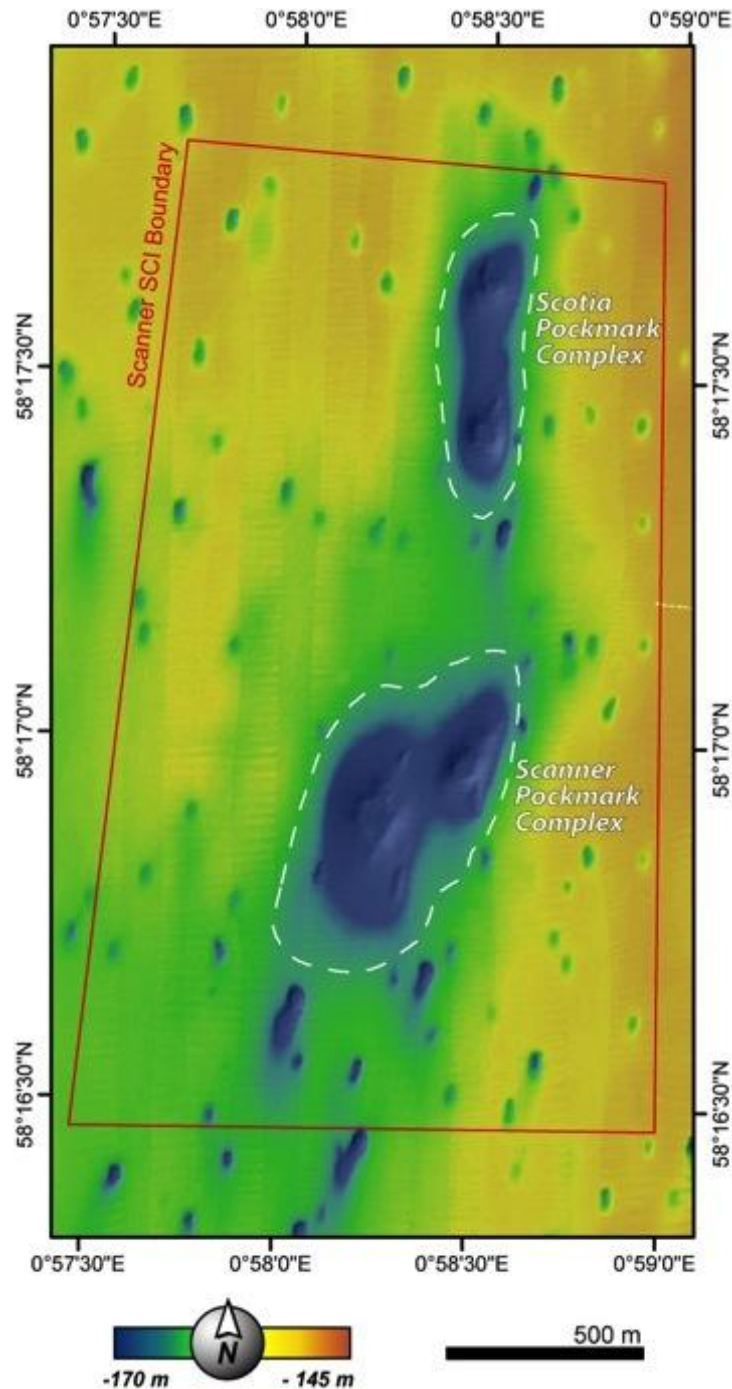


Figure 3. Detail from the JNCC multibeam dataset showing the limits of the Scanner Pockmark SCI and the areas considered as part of both the Scanner and Scotia pockmark complexes.

2 Data sources

2.1 Data supplied by JNCC

JNCC supplied BGS with digital copies of the seabed data collected by CEFAS during a cruise commissioned by JNCC. The survey took place between the 17th November and the 1st December 2012 onboard the *CEFAS Endeavour*. These data were transferred via an external hard disk received by post on 17th June 2013. The dataset received is summarized in Table 1. JNCC also supplied, via Dropbox, the CEFAS's survey report for the cruise CEND19x/12.

Table 1. List of data collected during the CEND19x/12 cruise that was provided to BGS, from the Scanner Pockmark SCI study area.

Data provided
Multibeam Echosounder (<i>Simrad EM2040</i>)
Full MBES data coverage across the Scanner SCI area. <ul style="list-style-type: none"> • 32 files of raw data were made available, • processed data for both the backscatter and the bathymetric datasets, and • CARIS project with the multibeam data.
Backscatter
Several geotiffs and raster files were provided, including: <ul style="list-style-type: none"> • IMAGINE image file <i>SCNR_FPBS_Null.img</i> with full coverage, mosaic at a 0.3 m resolution, and • geotiff <i>SCNRHD_BS_0m3.tiff</i> with 3 lines at higher frequency over the main pockmark feature, giving a mosaic at 0.1 m resolution.
Bathymetry
Several geotiffs and raster files were provided, including: <ul style="list-style-type: none"> • IMAGINE image file <i>SCNR_15032013_2d0_MBFU_UTM31N.img</i>. This raster has a cell size of approximately 2 m.
Side-Scan Sonar (<i>Edgetech 4200 MP</i>)
<ul style="list-style-type: none"> • Full data coverage across the Scanner SCI at 300 kHz frequency and partial coverage at 600 kHz frequency. <i>Low Frequency</i>: Full coverage. Both the mosaic and four individual lines. • <i>High Frequency</i>: Limited coverage. Eight lines split into 12 sections files. Both the raw data and the processed data were made available.
Groundtruthing
Drop Camera
A total of 16 video clips and 402 stills plus: <ul style="list-style-type: none"> • 6 Excel files, • CEFAS' <i>PMPA Video Analysis Report</i> summarising the analysis of the data, and • Shapefile "<i>Video tow lines.shp</i>" showing the route of the video tows.
Grab
0.1 m ² grab samples was subsampled for Particle Size Analysis (PSA), the remaining material was washed on board ship over 5 mm and 1 mm sieves to retain benthic fauna. <ul style="list-style-type: none"> • Particle Size Analyses - also provided as ArcGIS' point shapefile (<i>Scanner_PSA.shp</i>), • photos of the grabs on 5mm sieves, and • 3 Microsoft Excel files summarising sample details, the PSA results and benthic fauna data matrix.

Additional to the raw and processed datasets, some interpretations of the data by CEFAS for JNCC were also made available as ArcGIS shapefiles. These are *SCNR_Biotope.shp*, *SCNR_Sediment.shp*, *SCNR_Pockmark.shp* and *SCNR_Trwl_scar.shp*.

2.2 BGS-acquired data

As well as the BGS published maps (Fladen, Sheet 58° N-00°, 1:250,000 Series, Seabed Sediments (published 1986) and Quaternary Geology (published 1988)) and the regional report (Johnson *et al.*, 1993), the original sampling records (seabed grab, vibrocore) and geophysical data (primarily deep tow boomer and sparker) provide information on the shallow geological conditions. This data was mainly collected as part of the regional mapping programme in the 1970s and 1980s, on behalf of the Department of Energy, later Department of Trade and Industry, now Department of Energy and Climate Change (DECC). It has been supplemented by additional data from commercial and governmental sources. Details from the Sea Bed Sediments maps are available digitally within the DigBath250 and DigSBS250 products and have been used in this study to provide information at a regional level. A suite of 25 shallow seismic lines across the Scanner Pockmark SCI area (Figure 4) were also acquired with the BGS deep tow boomer in July 1991, during the Marine Biological Association (MBA) cruise on board the RRS *Challenger* (Dando, 1991) (Appendix 1).

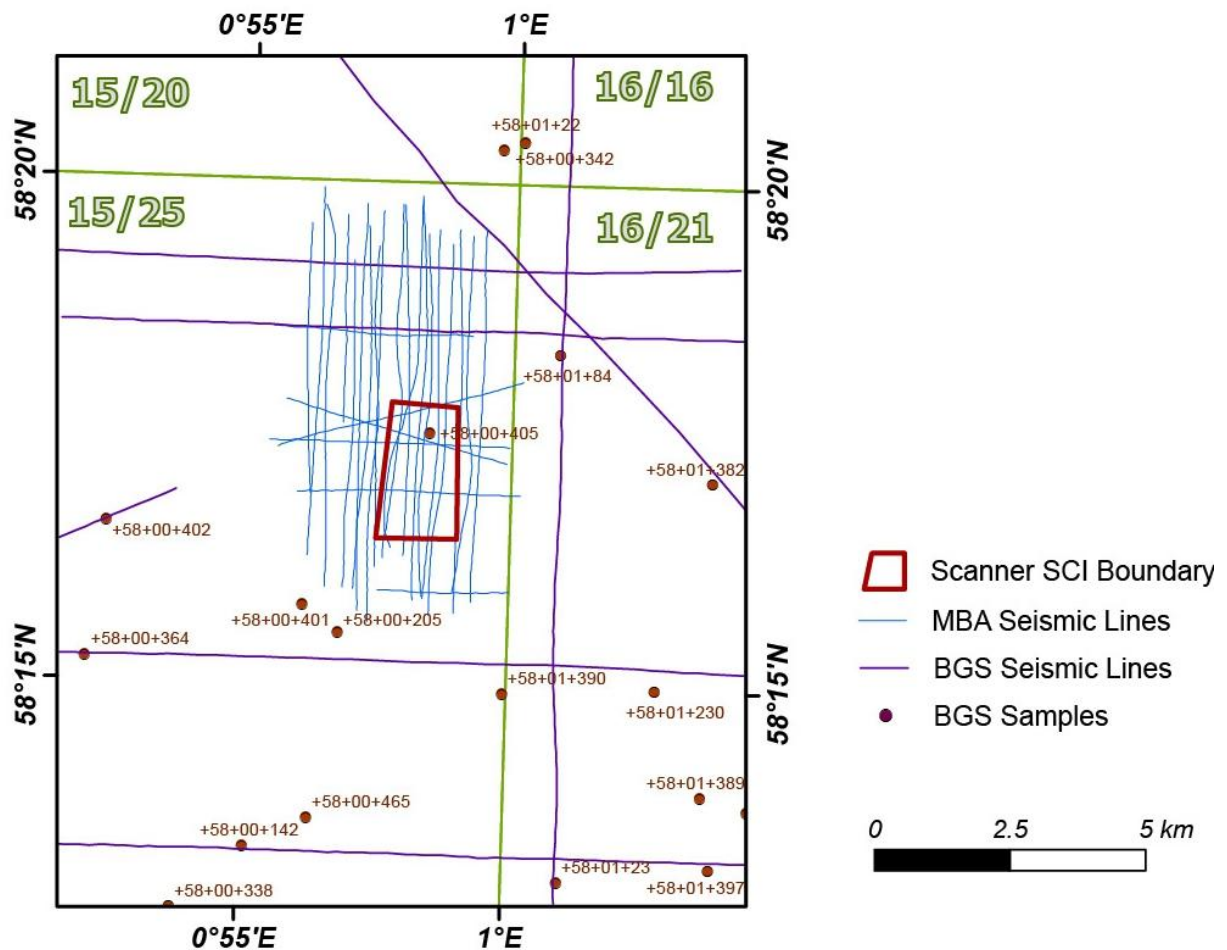


Figure 4. BGS regional data around Scanner Pockmark SCI and seismic lines acquired by BGS for the Marine Biological Association (MBA).

Lines in green indicate the UK blocks limits.

2.3 Third party data held by the BGS

BGS regularly requests operators to deposit copies of site investigations and other shallow data within its national archives. This data is held as commercial in confidence but is used to update regional maps and interpretation. None of the commercial site investigation reports are in digital format. They were retrieved in hard copy from the BGS archives. Most rig site surveys contain interpretations of seabed and sub-seabed conditions to about 1000 m below seabed in a 3 x 3 km area and include surveys using echosounder, side-scan sonar, single-channel high resolution seismic reflection profile and multi-channel 2D high resolution seismic profile data. The first survey of the Scanner SCI area was site survey for Conoco (Appendix 1).

2.4 Multibeam surveys

A significant part of this study was based on the interpretation and analyse of the multibeam datasets acquired by CEFAS, for JNCC in 2012 and by OSAE for the SEA2 Project in 2001. The SEA2 survey included nine box areas of pockmarks in the Witch Ground Basin, box 4 of that survey overlaps with most of the area recently surveyed for JNCC (Figure 5). During the SEA2 survey, OSAE used the Simrad EM1002 multibeam echosounder and the acquired dataset was imported into ArcMap as a 6 m grid, whereas the JNCC multibeam dataset was acquired with the Simrad EM2040 multibeam echosounder (CEFAS and JNCC, 2013) and imported into ArcMap as a 2 m cell size grid.

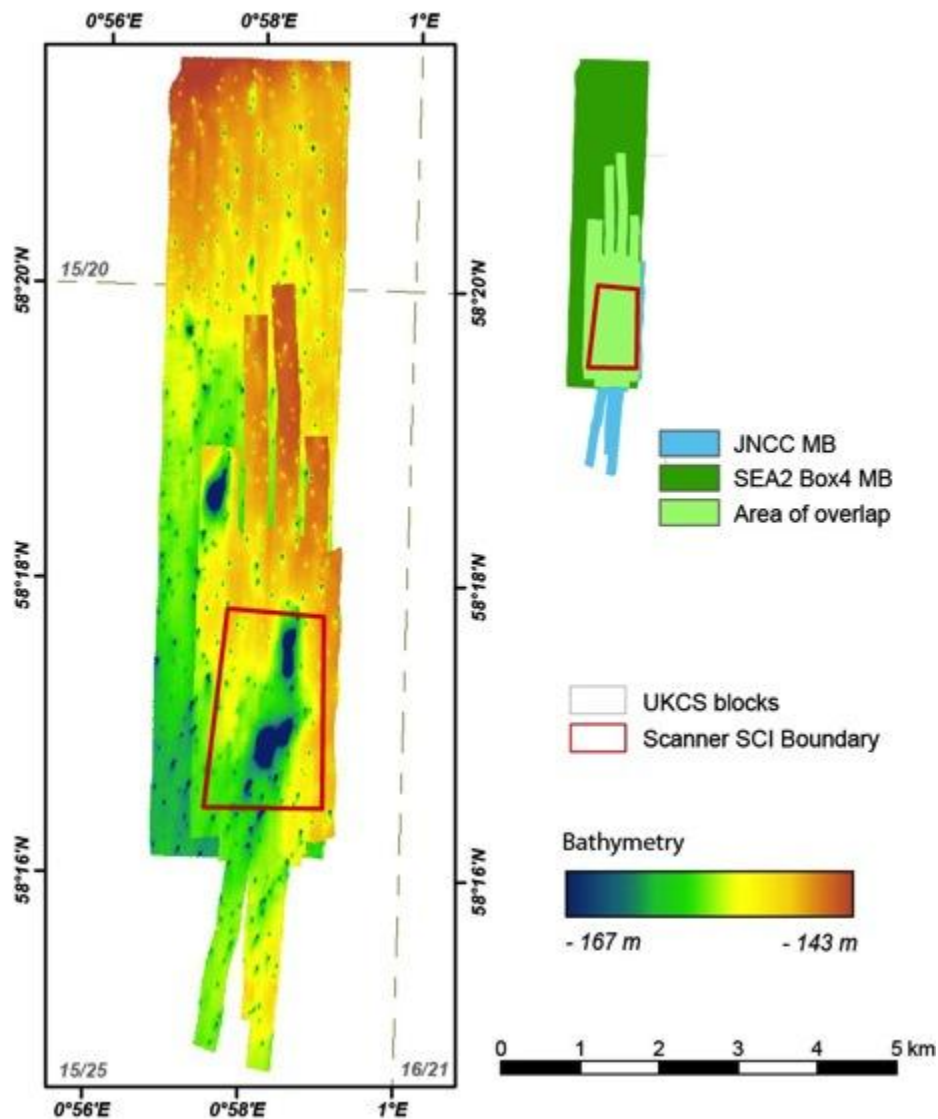


Figure 5. Map showing both multibeam datasets used during this study.

3 Scanner and Scotia Pockmark Complex

The Scanner Pockmark Complex was discovered during a site survey in 1983 for proposed well (GEOTEAM, 1983; Hovland and Sommerville, 1985), and named after the survey ship involved. It has been studied in great detail since then: shallow seismic and side-scan sonar surveys (1983, 1991, 1992, 2001, and 2002), seabed sediment sampling (1988, 1989, 1990, 1991, 2002, 2004 and 2005), ROV inspection (1985 and 2004) and manned submersible survey (1990). Collectively, these surveys have provided a wealth of detailed information which has been presented in various publications, most notably: Hovland and Sommerville (1985), Dando *et al.* (1991), Judd *et al.* (1994), and Dando (2001), and cruise reports (e.g GEOTEAM, 1983; Dando, 1990, 1991; Boetius, 2004; and Pfannkuche, 2005, 2006). The list of cruises known to be relevant to this study is presented in Appendix 1.

The earliest descriptions of the Scanner Pockmark Complex indicated the existence of only one unusually large pockmark. Subsequent mapping of the area revealed that instead of one large single pockmark, the Scanner Pockmark Complex comprises two large depressions more than 250 meters apart and several smaller pockmarks. Additionally, the Scotia Pockmark Complex, which similarly comprises two large pockmarks, was also identified one kilometre further north.

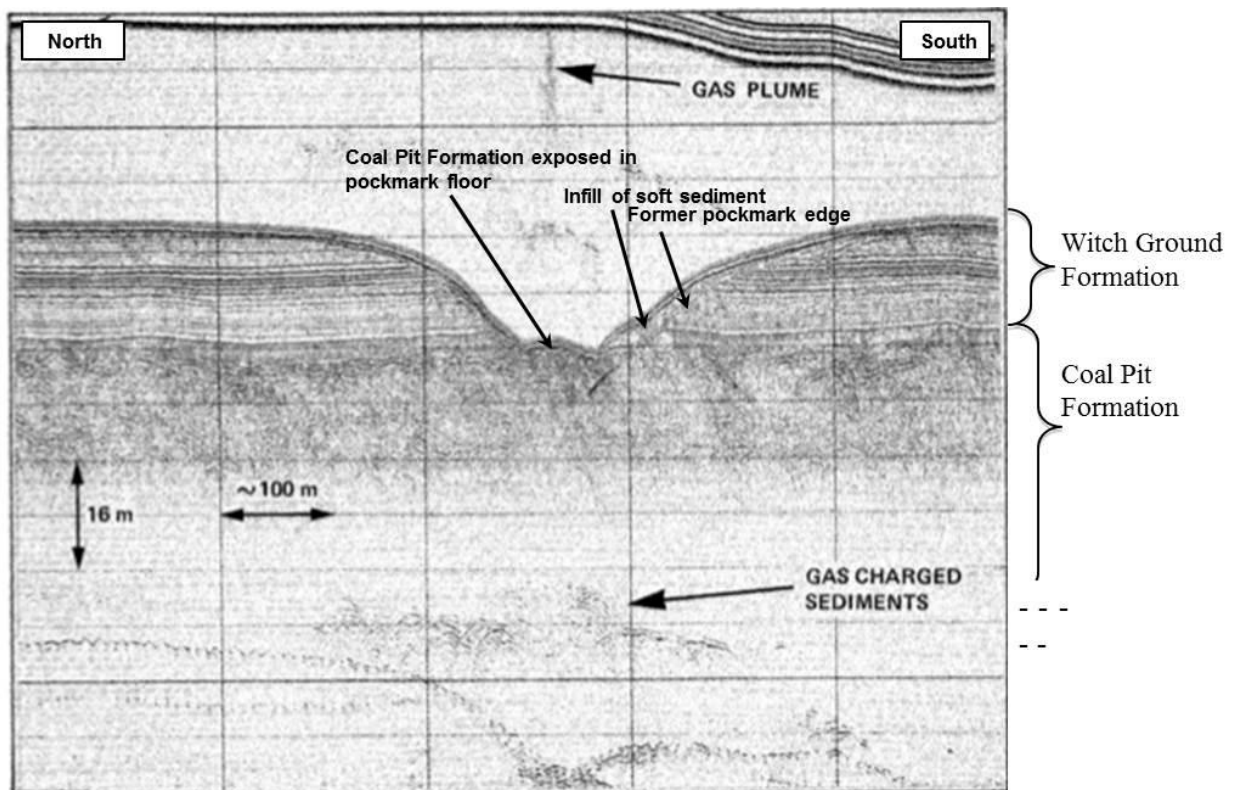


Figure 6. Deep-towed sparker line collected in 1983, across the Western Scanner Pockmark, during the Geoteam cruise.

It shows gas in both the water column and in the sediments. Image after Hovland and Sommerville (1985) with additional annotations.

Based on the interpretation of seismic records, it became evident that the complete sequence of layered, glaciomarine soft silty clays (the *Witch Ground Formation*) has been eroded away from the centre of these unusually large pockmarks by seepage processes (Hovland and Sommerville, 1985). This left exposed at seabed the stiff, dark grey, clay of the *Coal Pit Formation*, that had been subjected to ice-loading during the late Weichselian (Figure 6). The *Witch Ground Formation* is typically very soft to soft clays and silts with some thin sandier horizons with undrained shear strengths of 5-30 kPa and medium to high plasticity. Whereas the *Coal Pit*

Formation is typically firm to stiff muds and sandy muds, of medium plasticity and undrained shear strengths 50-100 kPa (British Geological Survey, 1988). The acoustically well-layered soft muds of the Witch Ground Formation show evidence of buried pockmarks indicating that pockmark formation has been an ongoing process (Long, 1992).

According to Holmes and Stoker (2005) the seabed gas seepages in the northern part of block 15/25d are fed from an almost continuous blanket of gas-charged sediments situated between the sub-glacial channel margins at approximately 280-300 ms two-way time (around 120 m below seabed). The gas has accumulated at shallower levels, with the shallowest being located ~32 m beneath the largest pockmarks (Figure 6). This shallow gas covers a wide area mapped by Judd *et al* (1994) using BGS boomer data and combined with 3D exploration seismic volumes by Holmes and Stoker (2005) to show how the shallow gas distribution is constrained by the sub-glacial channels (Figure 7).

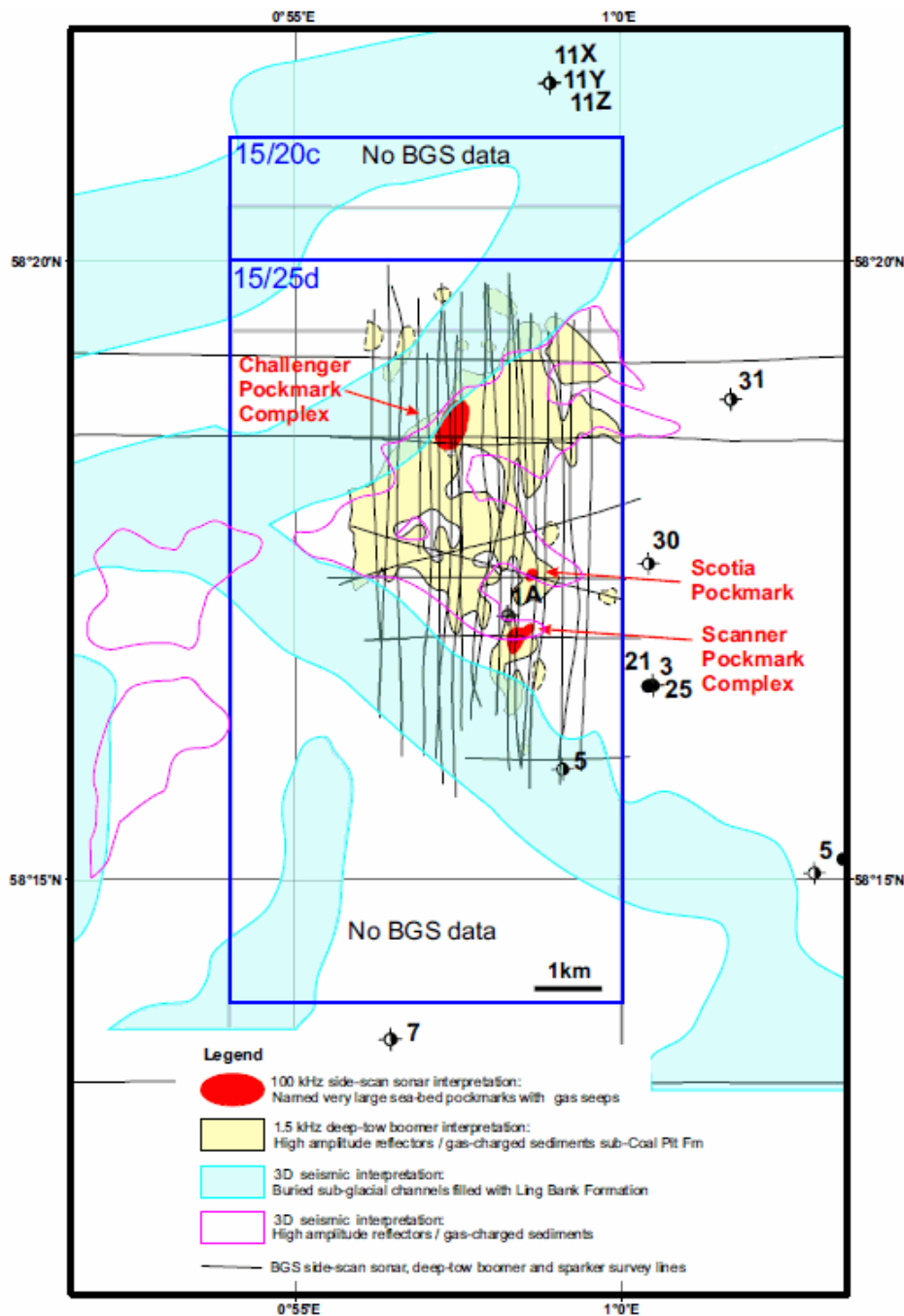


Figure 7. Map showing the distribution of shallow gas in UK block 15/25d as seen in boomer records and in 3D seismic volumes (From Holmes and Stoker, 2005).

Note how the distribution of buried channels constrains the shallow gas.

Isotopic ratios derived from the gas and from the methane-derived authigenic carbonate have been used to infer whether the gas had a biogenic or thermogenic origin, thereon leading to estimates for the depth of origin of the gas seeps at seabed. Carbon isotope ratios ($\delta^{13}\text{C}$) of methane gas varied between -40‰ (in sediment gases) and -79‰ (in bubbles from the water column) (Clayton and Dando, 1996). The -40‰ values suggest a thermogenic origin (especially as the methane was associated with higher hydrocarbon gases), but the -70‰ is more typical of a microbial origin. The Kimmeridge Clay and Tertiary peats are possible sources (Clayton and Dando, 1996; Judd and Hovland, 2007). Carbon isotope ratios of carbonate cement from the MDAC samples ($\delta^{13}\text{C}$ -52‰ and -36‰; Hovland and Irwin, 1989 and Dando et al., 1991 respectively) shows that the carbon was derived from the methane and has similar values to those of the gas within the sediments

4 Pockmark morphology

A semi-automated method of mapping and morphometric characterization, described in 4.1, was used to map the pockmarks within both multibeam surveys used in this study. The pockmark morphological description presented in 4.2, 4.3 and 4.4 was based mainly on the JNCC multibeam bathymetry dataset and the morphological characteristics extracted using the semi-automated mapping method. The two bathymetric datasets used in this study are compared in section 4.5.

4.1 Semi-automated mapping

The semi-automated method used allows the systematic application of a sequence of well-defined tools available within the ESRI ArcGIS toolbox (Gafeira *et al.*, 2012). The input data set required is merely a digital depth model (DDM) that is used to generate three output shapefiles:

- 1) a polygon shapefile that delineates the pockmarks at seabed,
- 2) a point shapefile that shows the centroid of the referred polygons, and
- 3) a point shapefile that marks the deepest point within each pockmark mapped.

This last shapefile is likely to correspond to the main source point, or vent, of the fluid escape that originated the formation of the pockmark. These output shapefiles include, within their table of attributes, a series of morphometric attributes measured for each mapped pockmark: Area (m^2), Perimeter (m), Area/Perimeter Ratio, Depth (m), Maximum water depth, Minimum water depth, Maximum Slope, Mean Slope, Azimuth and Major Axis Length.

This semi-automated method requires the definition, by the user, of three threshold values for the pockmarks: *Minimum Depth*, *Minimum Area*, and *Minimum Area/Perimeter Ratio*. The thresholds used for this study were 40 cm, 400 m^2 , and 4.5 respectively. The user must also define a *Buffer Distance* that will reflect approximately the distance in plan-view, from the internal contour line delineated by the automated method, to the actual rim of the pockmark. The *Buffer Distance* used for this study was 10 m.

This method creates the possibility to extract morphologic information on a vast number of pockmarks from multiple surveys in a fast, systematic and consistent way. This is a significant improvement to the study of pockmarks, considering that it would be highly unlikely for one or multiple interpreters to maintain the same criteria throughout the laborious process of manually mapping such a large number of pockmarks, therefore compromising the possibility of doing any valid statistical comparison between pockmark populations.

Figure 8 shows an example of the advantage of using this method, by comparing the outline of two pockmarks obtained using this method and using the manual picking previously done by JNCC. Previously they had been mapped as having similar size (red outline) whereas the new outline (in blue) better describes their shape.

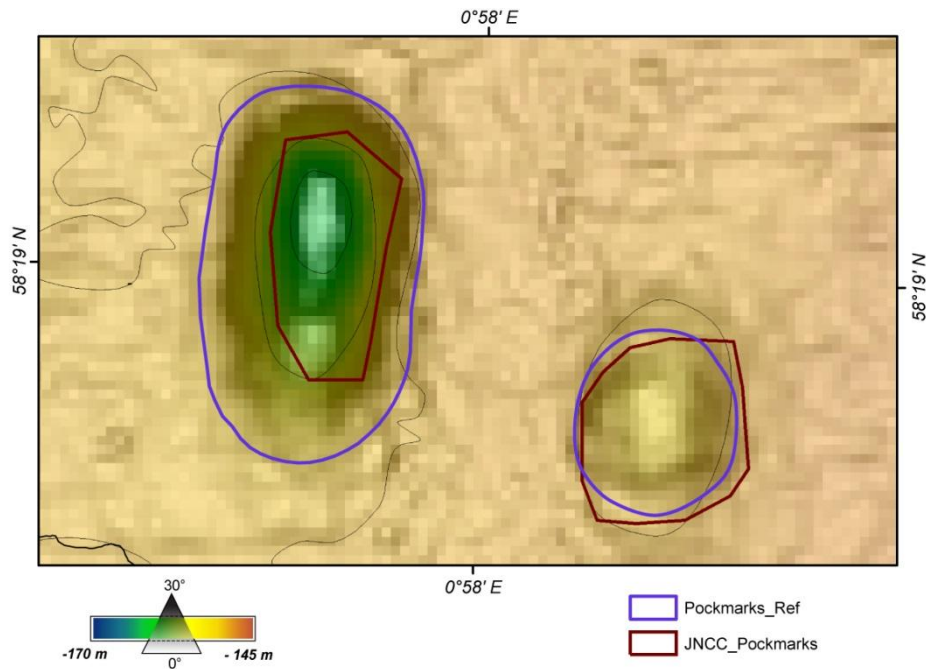


Figure 8. Detail view showing two pockmarks of different sizes (blue outline) that had previously been manually mapped as of similar size (red outline). This image exemplifies the consistency resulting from using an automated method to map seabed features.

Note that these pockmarks are located outside the SCI area but within the dataset collected during the CEFAS/JNCC cruise.

After visual assessment of the delineated polygons, overlaying the original bathymetric data and the derived surfaces such as the slope map, it was necessary to manually edit some of the polygons due to the spatial proximity of several pockmarks. When there is no marked ridge between two adjacent pockmarks or it is present but deeper than the value defined for the *Minimum Pockmark Depth*, the pockmarks are delineated as one single feature. In the study area, the outline of both the Scanner and Scotia Pockmark complexes had to be drawn manually and their attributes recalculated.

Using this method, 67 pockmarks were mapped within the close-look study area (defined by the minimum bounding rectangle containing the Scanner SCI Boundary). Figure 9 shows the outline of the mapped pockmarks whereas Figure 10 also shows the location of their deepest point and the polygon centroid. The morphologic attributes of each pockmark are compiled in Appendix 2, Table 3.

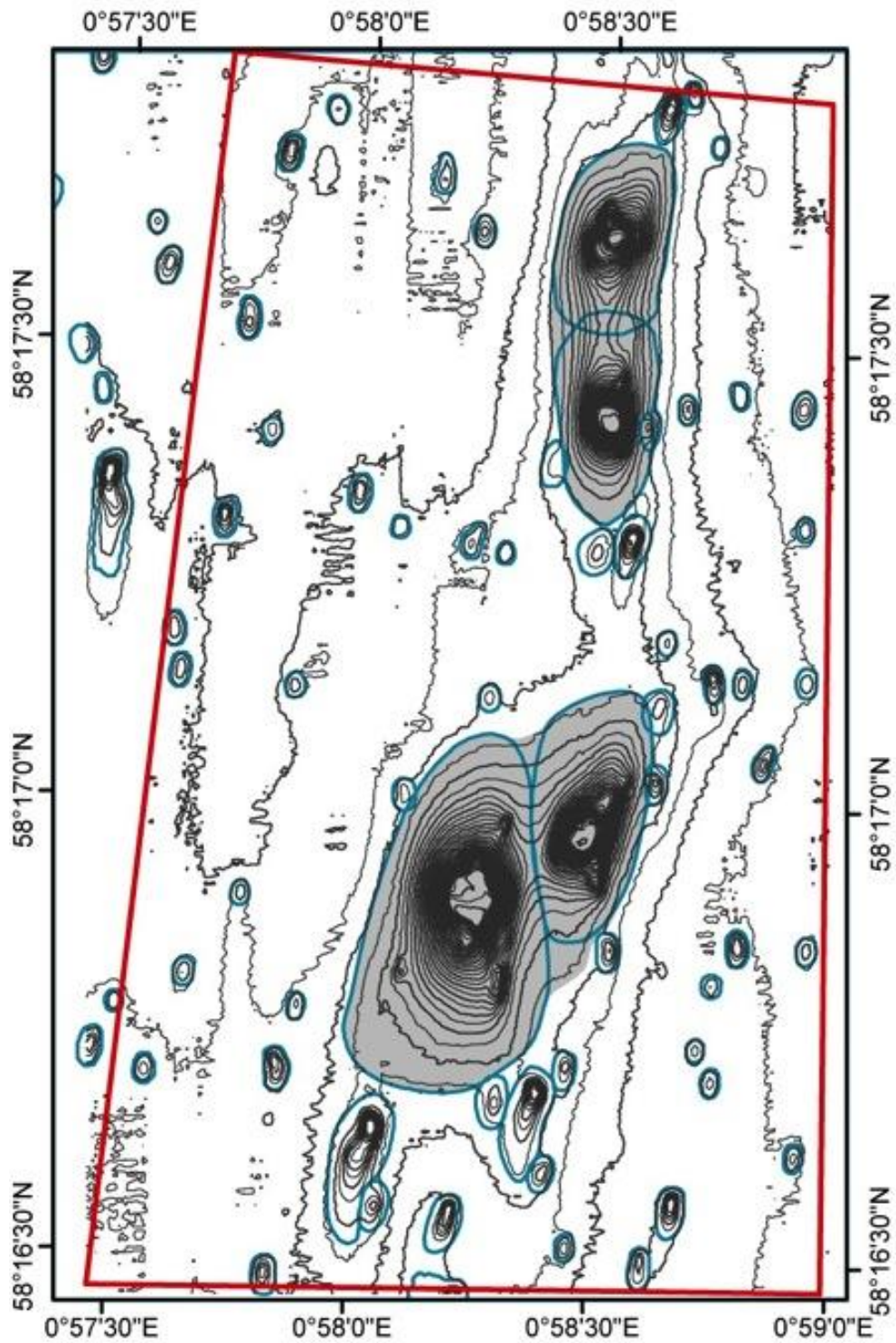


Figure 9. Outline of the 67 pockmarks mapped with the pockmark semi-automated mapping method.

The grey shading on both the Scanner and Scotia pockmark complexes shows the area initially mapped that was then manually split.

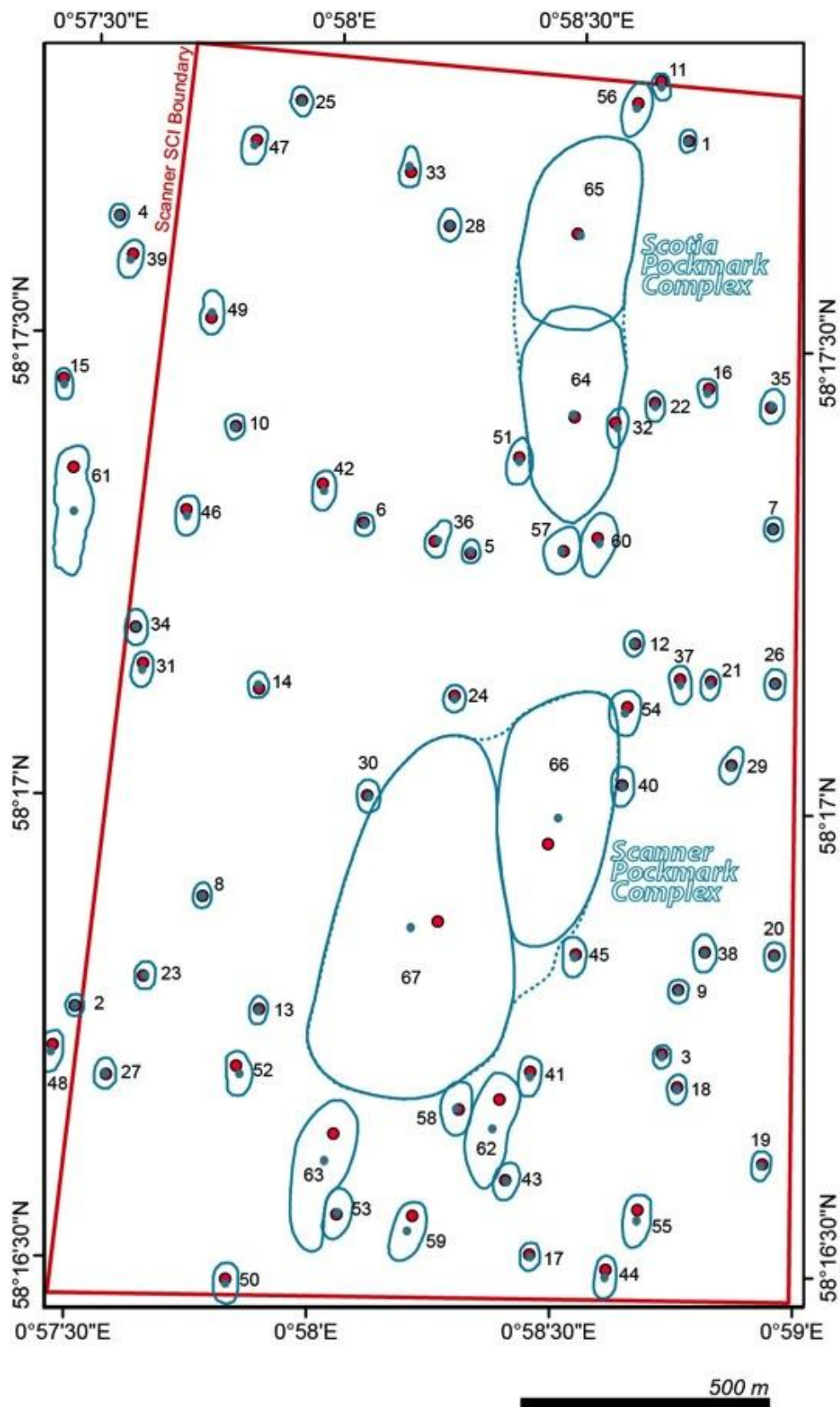


Figure 10. Outline of the 67 pockmarks mapped within and surrounding the Scanner Pockmark SCI showing their identification number and both their deepest point (red dot) and the polygons centre (blue dot).

4.2 Scanner Pockmark Complex

The Scanner Pockmark Complex (ScnrPC) comprises two main pockmarks (pockmarks 66 and 67), both with unusually large dimensions, which will be referred in this study as Eastern and Western Scanner respectively (Figure 11). The deepest parts of these two pockmarks are approximately 265 m apart and combined cover an area of nearly 320,000 m². These large pockmarks present quite distinct geometry in cross-section, mainly ‘U’- and ‘W’-shaped instead of the typical ‘V’ shape. That is the result of the presence of a marked flat bottom at the centre of both pockmarks (the outcropping Coal Pit Formation below the Witch Ground Formation sediments).

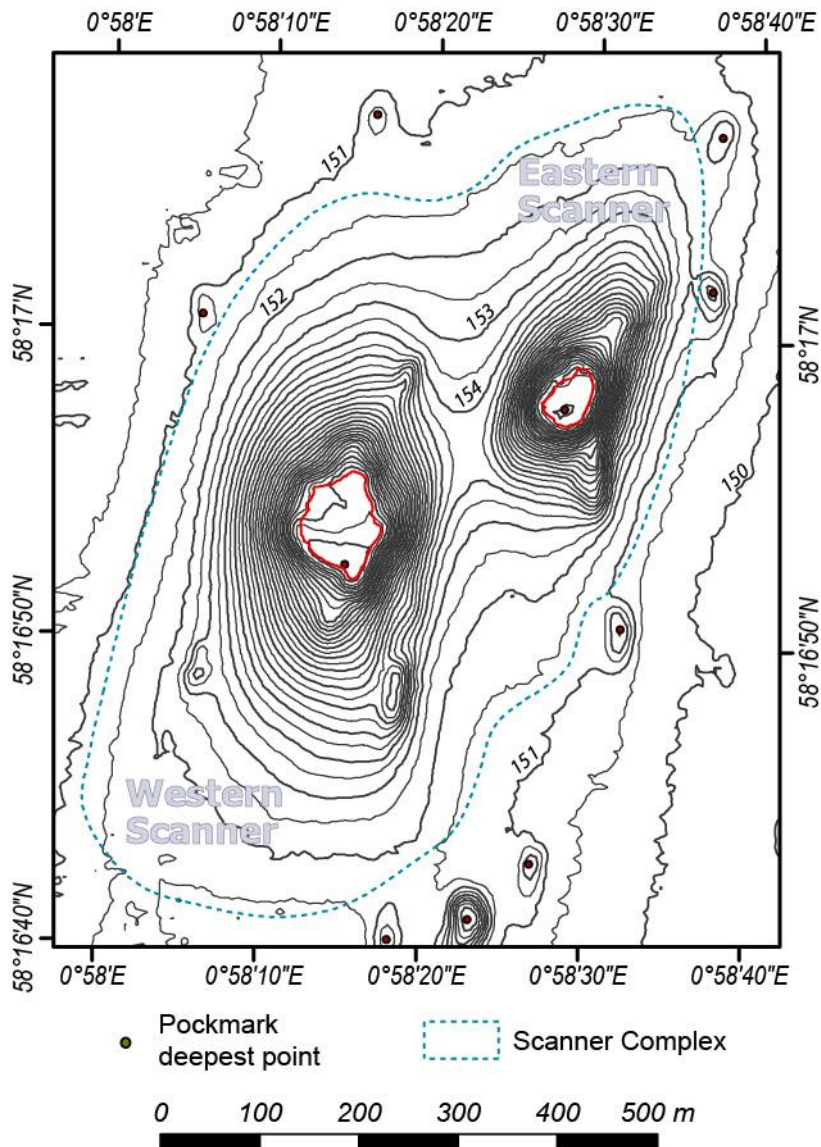


Figure 11. Bathymetry of the Scanner Pockmark Complex area (contour lines at 0.5m intervals).

Outline of the pockmarks as defined by the semi-automated method with the exception of the ScnrPC that had to be split manually into Western and Eastern Scanner. The dashed blue line gives the outline first picked by the semi-automated method. The limits of the flat bottom of both ScnrPC’s pockmarks are outlined in red.

The Western Scanner is the larger of the two, and the largest pockmark of the full study area, covering an area of more than 221,000 m². It is 16.7 m deep (Figure 11), with water depth

ranging from 150.8 m depth around the edge of the pockmark to 167.4 m depth at its deepest point (58.2812°N, 0.9708°E).

The slope angles within this feature reach 19.1° and have a mean value of 3° (Figures 12 and 13). However, the mean value is influenced by its large flat bottom with a rhomboidal shape (in plan-view) and an area of more than 5,500 m². The limits of this flat area were defined by using mainly the curvature map (Figure 14), since the floor of the pockmark presents a marked break of slope that can be precisely mapped by using the curvature values. Within this area the slope angle mean value is 1.5°.

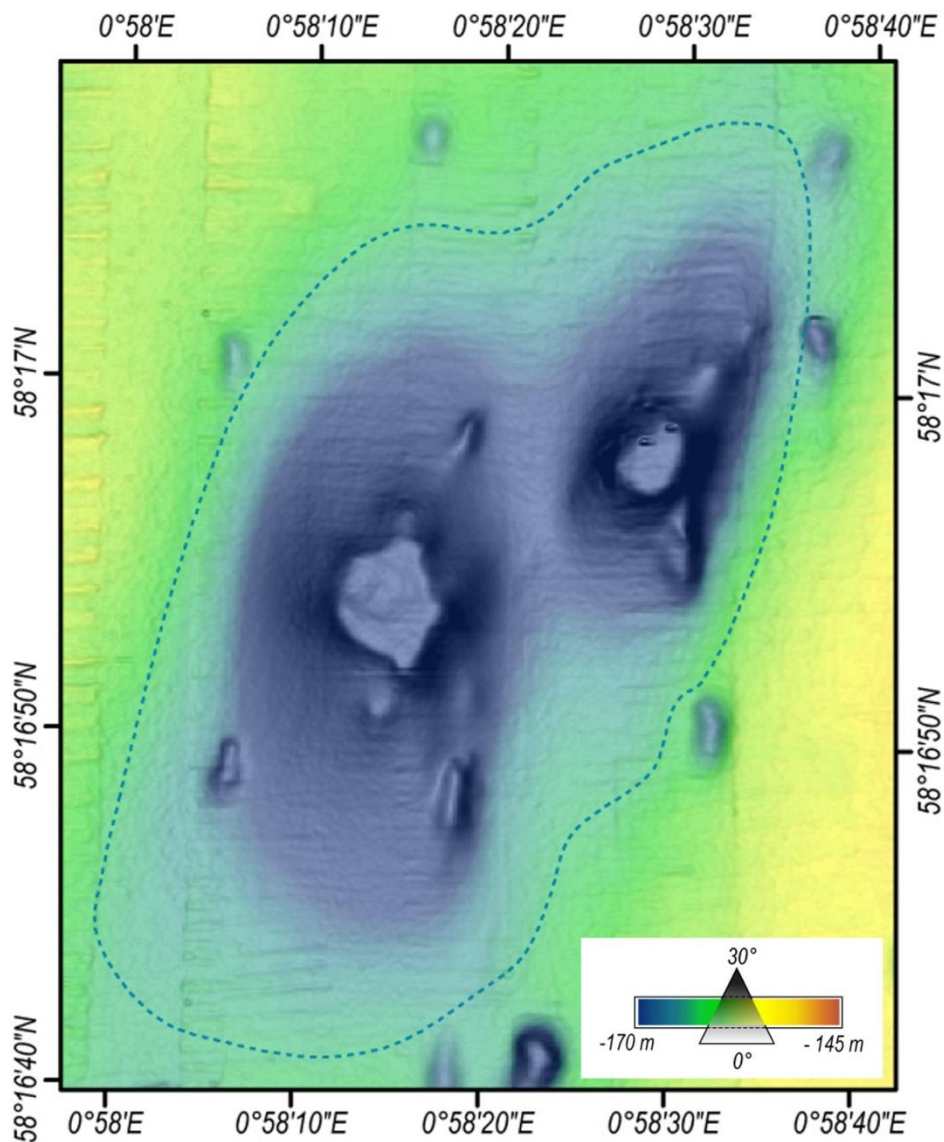


Figure 12. Slope angle and depth map of the Scanner Pockmark Complex area.

The brightness shows the slope angle (with low slopes in white and the steeper slopes in black) and the colour-scale shows the depth in metres.

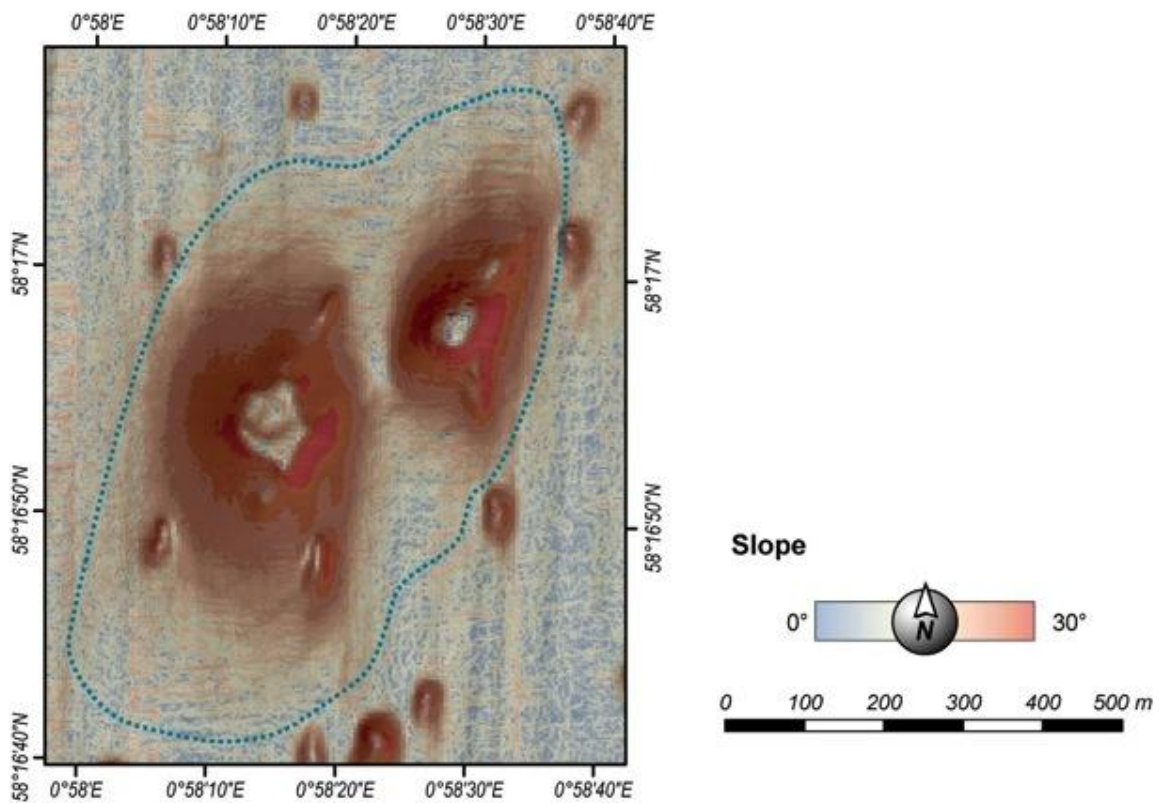


Figure 13. Slope angle map of the Scanner Pockmark Complex area overlying the shaded-relief map.

Note that the steeper slopes ($>12^\circ$) on the Western Scanner are located preferentially on the south-eastern sidewall.

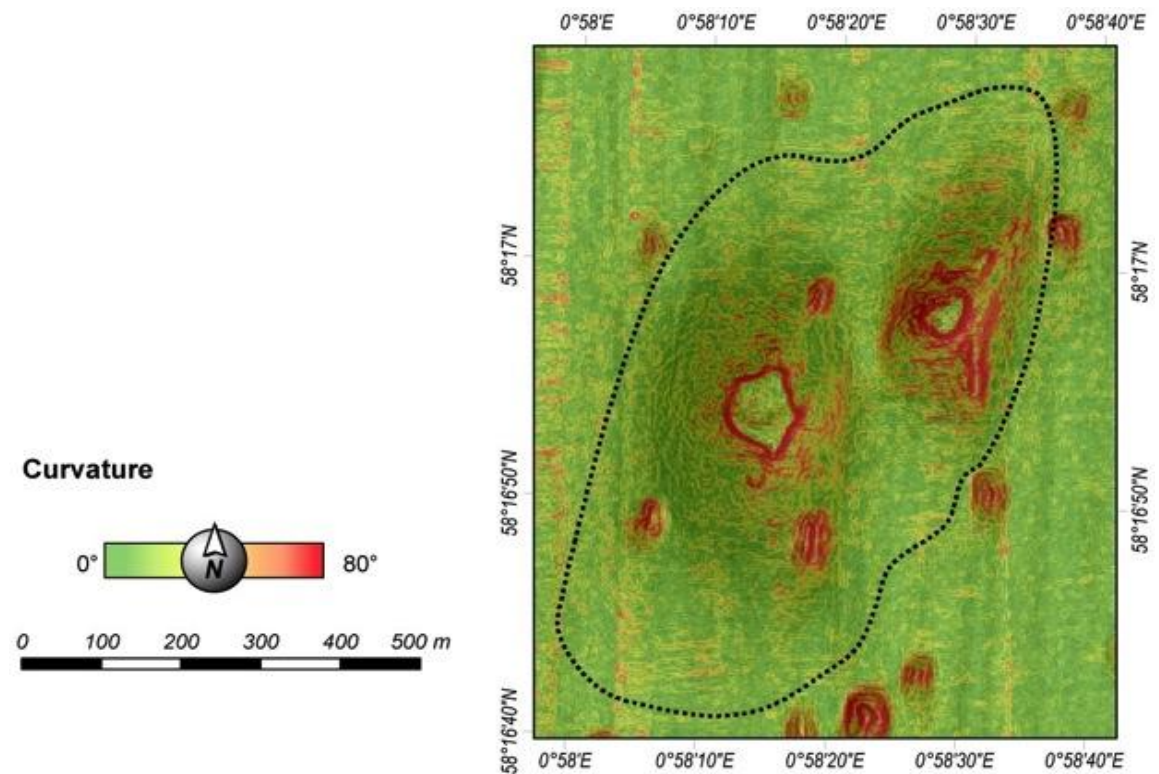


Figure 14. Curvature map of the Scanner Pockmark Complex area overlying the shaded-relief map.

The Curvature map displays the second derivative of the surface, *i.e.* the angle of the seabed slope, which highlight areas of rapid change in slope.. Note that in both pockmarks there is an abrupt change of slope gradient at the edge of the flat bottom.

The Eastern Scanner is, in plan-view, approximately only half the size of the Western Scanner. However, it is just 1.4 metres shallower than the Western Scanner. This pockmark covers more than 98,000 m² and is 15.3 m deep (Figure 11), with water depth ranging from 150.8 m depth around the edge to -166.1 m at the deepest point (58.2827° N, 0.9745° E).

The sidewalls of this pockmark reach slopes of 23.4° and the full pockmark has a slope angle mean value of 3.9° (Figures 12 and 13), almost a degree more than what observed on the Western Scanner Pockmark. This difference results in part from the fact that the Eastern Scanner Pockmark has a more complex geometry, with a N-S trough (30 m wide and 80 m long) south-east of its centre. This N-S trough may have been created by an alignment of smaller faults along a fault for example. However the limits of the flat area at the base of the pockmark, with an area of 1,880 m², can still be accurately define by using the curvature map (Figure 14).

Both Eastern Scanner and Western Scanner pockmarks include small associated pockmarks. These pockmarks, which occur within the large main pockmarks, have similar dimensions to the pockmarks outside the pockmark complexes, being no more than a few 10s of metres in diameter. These pockmarks can be referred to as 'unit-pockmarks' (e.g. Hovland *et al.*, 2010, 2012) within a major pockmark.

4.3 Scotia Pockmark Complex

The Scotia Pockmark Complex (SctPC) also comprises two main pockmarks (Figure 15), both with unusually large dimensions, which will be referred to as Northern Scotia (Pockmark 65) and Southern Scotia (Pockmark 64). These two pockmarks are approximately 370 m apart and combined cover an area of almost 150,000 m².

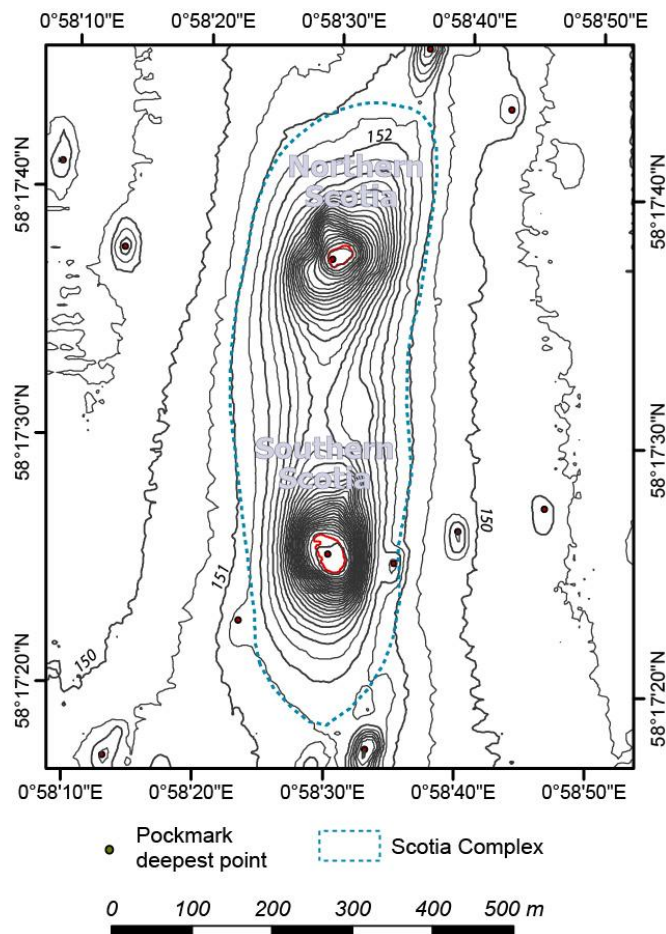


Figure 15. Bathymetry of the Scotia Pockmark Complex area (contour lines at 0.5 m intervals).

The dashed blue line gives the outline of the SctPC as defined by the semi-automated method. The limits of the flat bottom of both SctPC's pockmarks are outlined in red.

Both pockmarks cover similar extents of the seabed, Northern Scotia covers an area of 76,000 m² and Southern Scotia covers an area of more than 72,400 m². The Southern Scotia pockmark is the deeper of the two, with a depth of 14.6 m below the surrounding seabed, whereas the Northern Scotia pockmark has a depth of 12 m (Figures 15 and 16). The water depth within the Southern Scotia pockmark is 165.4 m at its deepest point (58.2904° N, 0.9750° E) compared with a water depth of 162.8 m at the deepest point (58.2937° N, 0.9749° E) of the Northern Scotia pockmark (Figure 15).

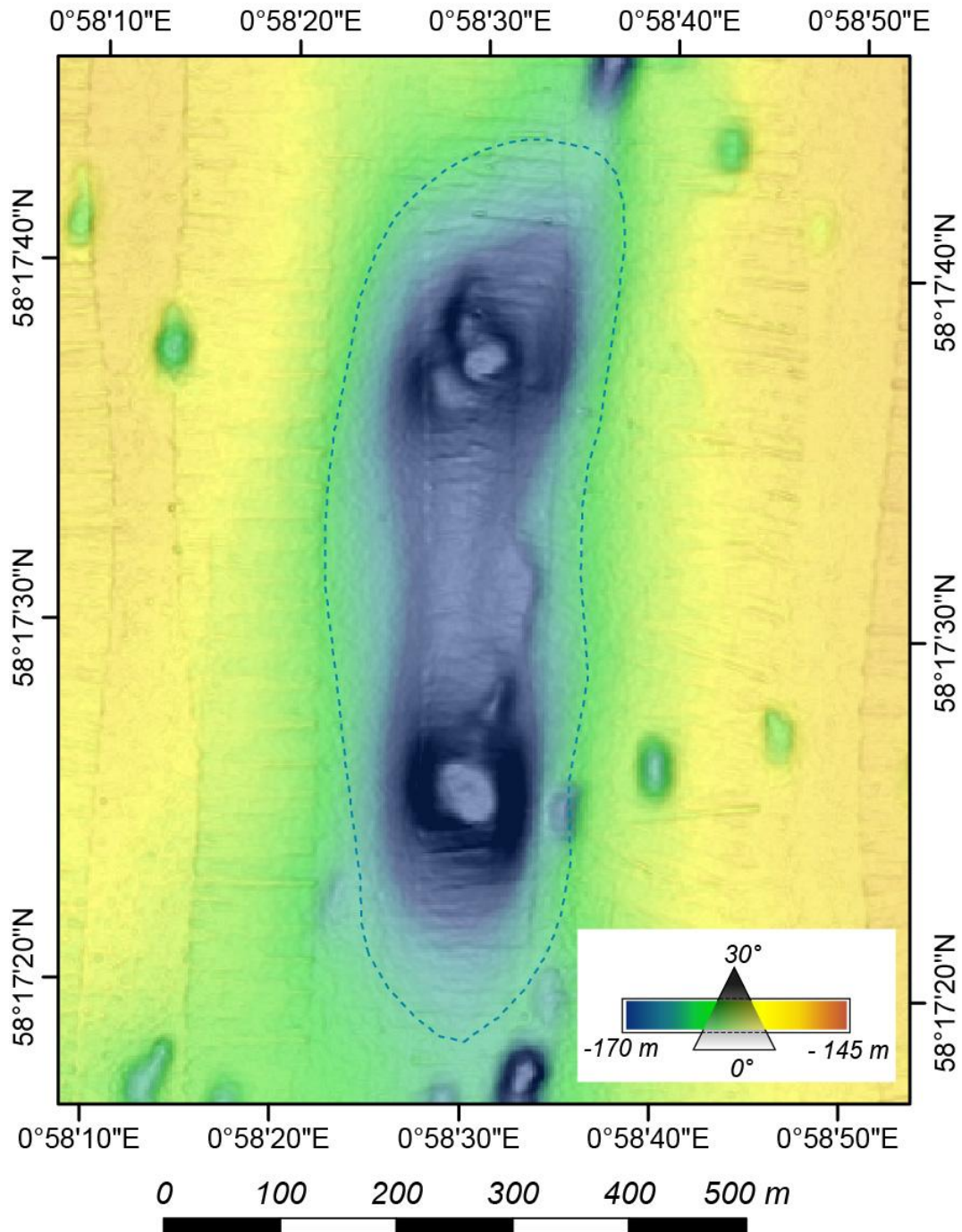


Figure 16. Slope angle and depth map of the Scotia Pockmark Complex area.

The brightness shows the slope angle (with low slopes in white and higher slopes values in black) and the colour-scale shows the depths in metres.

Although similar in size and elongated shape, in plan-view, these pockmarks are quite distinct in cross-section. Southern Scotia pockmark presents a consistent ‘U’-shaped profile independent of the orientation of the profile, whereas the profiles extracted from the Northern Scotia pockmark show quite varied geometries. Some of the profiles extracted from the Northern Scotia (especially from the north-west and south-west sidewalls) present several breaks in slope and lower slope values before reaching the flat bottom at the base of the pockmark (discussed in greater detail in the next section). Northern Scotia presents lower slope angles (max. slope 20.05° and mean slope 3.59°) than the values observed on the Southern Scotia (max. slope 30.20° and mean slope 4.4°) (Figures 16 and 17). The base of this pockmark as defined by the curvature plot (Figure 18) shows the smaller area of only 540 m^2 , less than half of the area of the flat base of the Southern Scotia that covers an area of nearly 1200 m^2 . The Southern Scotia is the pockmark with the steepest slopes from the four unusually large pockmarks studied (Figure 17). Southern Scotia also contains a small associated pockmark, on its NNE sidewall, but this is not very well developed.

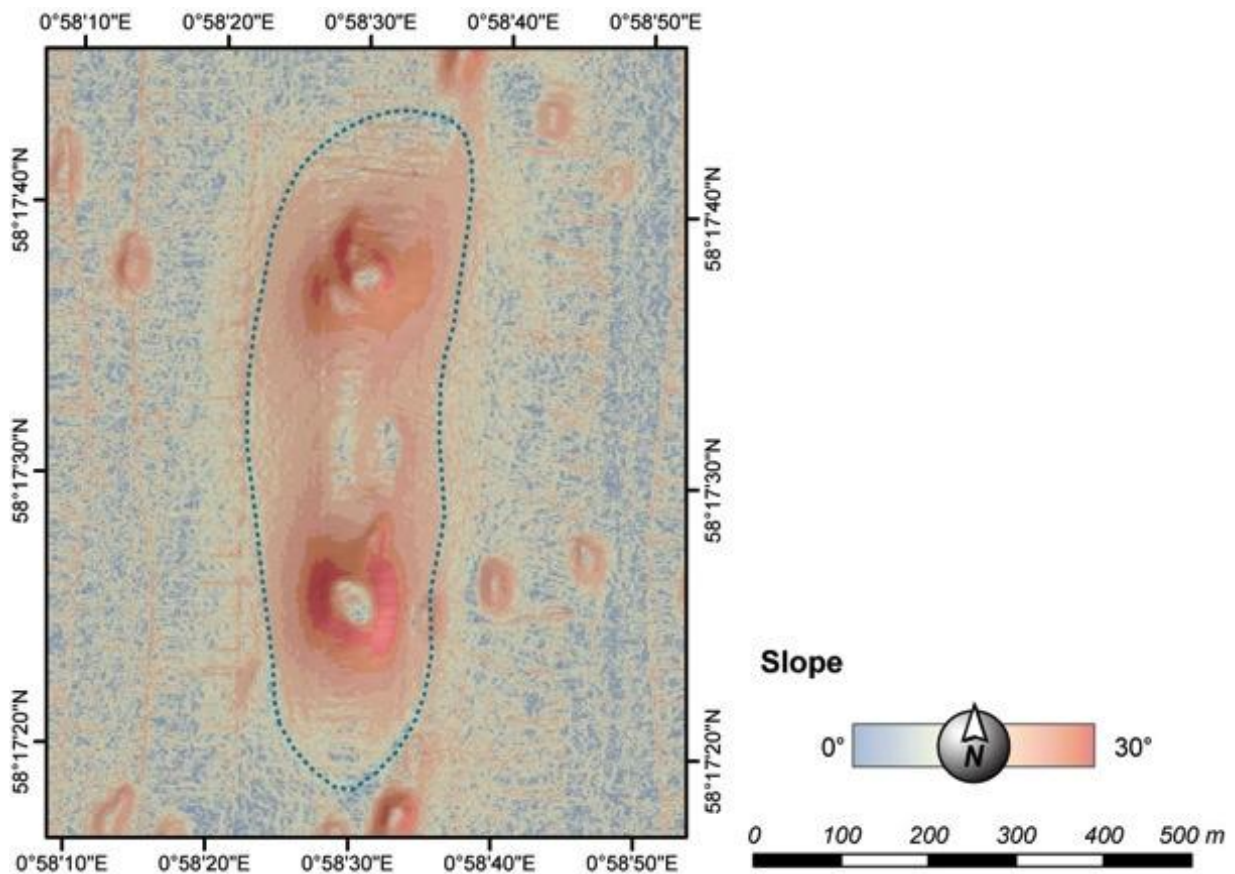


Figure 17. Slope angle map of the Scotia Pockmark Complex area overlying the shaded-relief map.

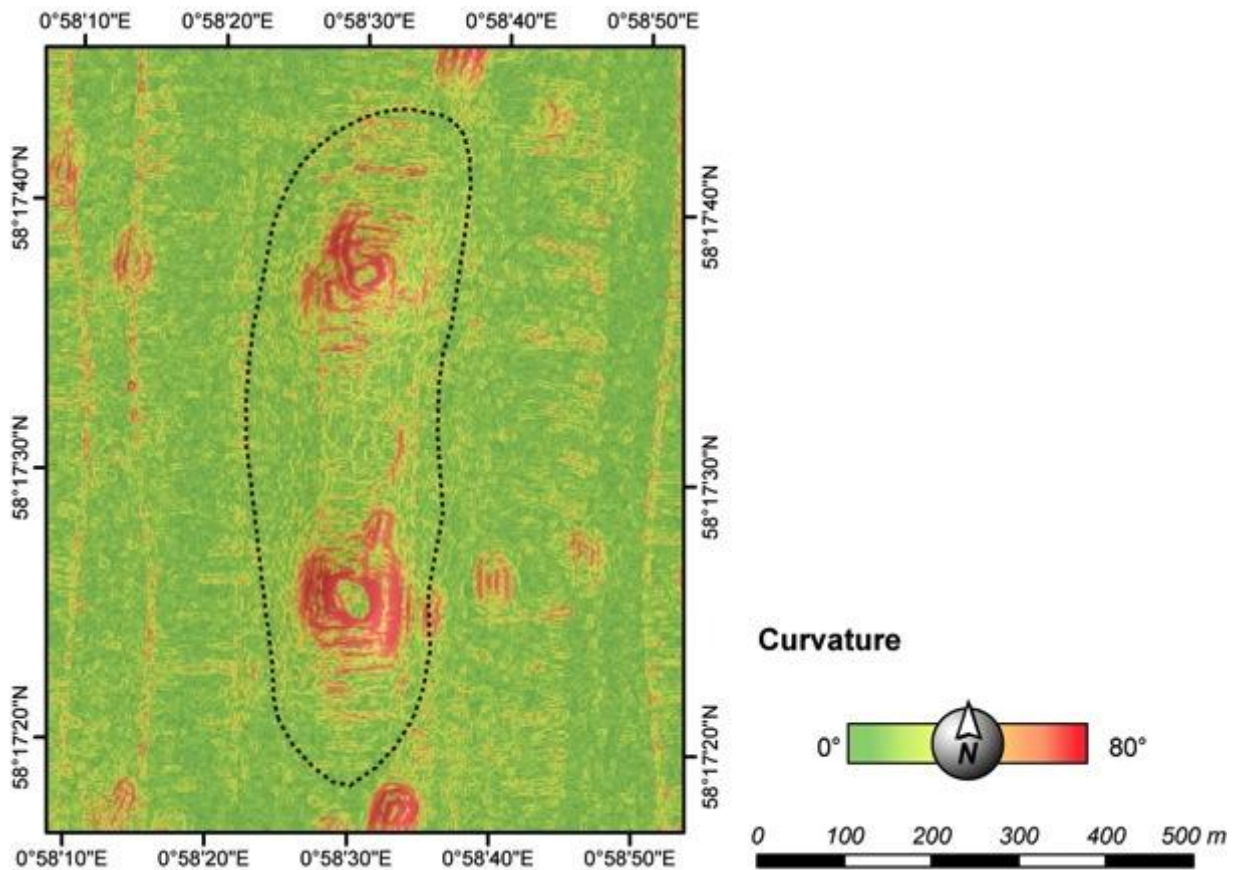


Figure 18. Curvature map of the Scotia Pockmark Complex area overlying the shaded-relief map.

The Curvature map displays the second derivative of the surface, *i.e.* the angle of the seabed slope, which highlight areas of rapid change in slope. Note that in both pockmarks there is an abrupt change of slope gradient at the edge of the flat bottom.

4.4 Unit pockmark morphology

The vast majority of the pockmarks found within the study area are much smaller than the pockmarks within the Scanner and Scotia pockmark complexes described above, with an average pockmark depth of 1.61 m and an average area of approximately 3,500 m². The 63 smaller pockmarks mapped in this study represent approximately 30% of the total area of the seabed disrupted by pockmarks in the study area, covering an accumulative area of approximately 222,100 m². These are referred to as unit pockmarks. Unit pockmarks “*occur as circular depressions in the seafloor (diameter < 5 m) either as singular features, as strings, or as clusters*” (Hovland *et al*, 2010). Hovland *et al* (2010) concluded that unit pockmarks represent the most recent and most active local seep locations.

These pockmarks are in cross-section mainly ‘V’-shaped, with a few ‘U’-shaped and very rarely ‘W’-shaped. The pockmarks mean slope angle varies between 1.26° and 4.76°, with an average value of 2.98°, whereas the maximum slope angle varies between 3.50° and 21.51°, with an average value of 7.78°. In plan-view, these pockmarks are generally circular to elliptical in shape; however three are unusually large and elongated (pockmark 61, 62 and 63; Figure 10). The largest of them, pockmark 63, is found southwest of the ScnrPC and presents a vertical relief of 6.12 m and covers an area of almost 26000 m².

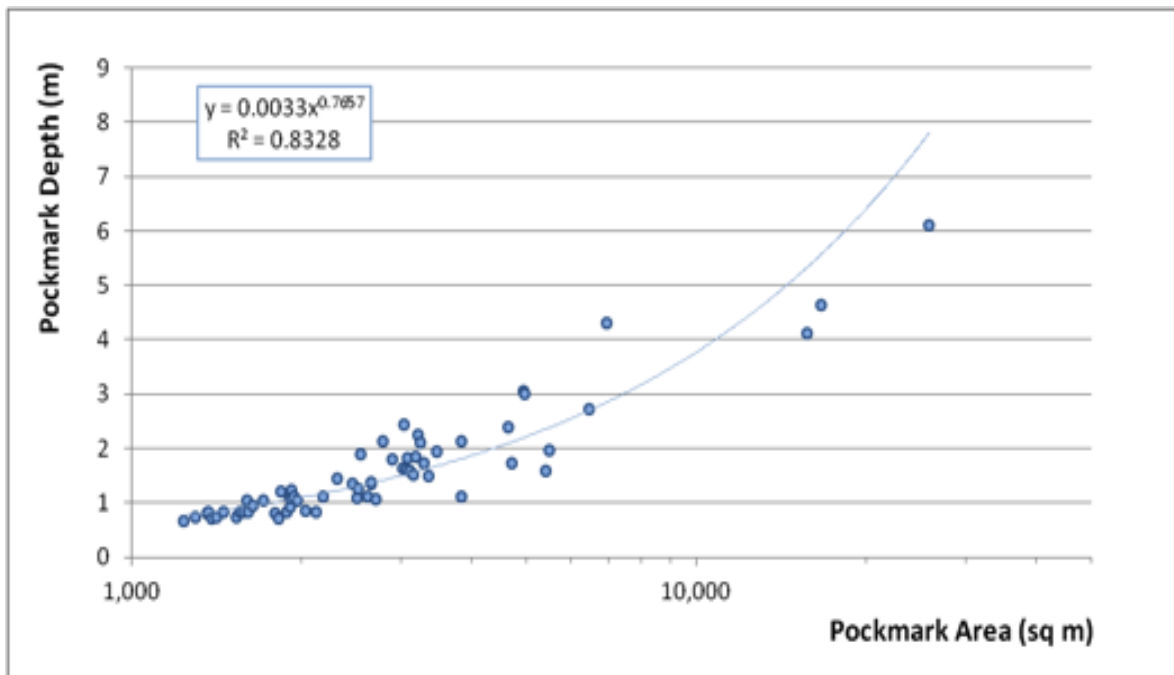


Figure 19. Relationship between the Pockmark Depth and Pockmark Area for the 63 unit pockmarks mapped within the Scanner SCI area.

Note the logarithmic horizontal scale used for the *Pockmark Area* axis. The four very large pockmarks (Eastern Scanner, Western Scanner, Northern Scotia and Southern Scotia) are not included in this graph.. They would be outwith the display area of the graph.

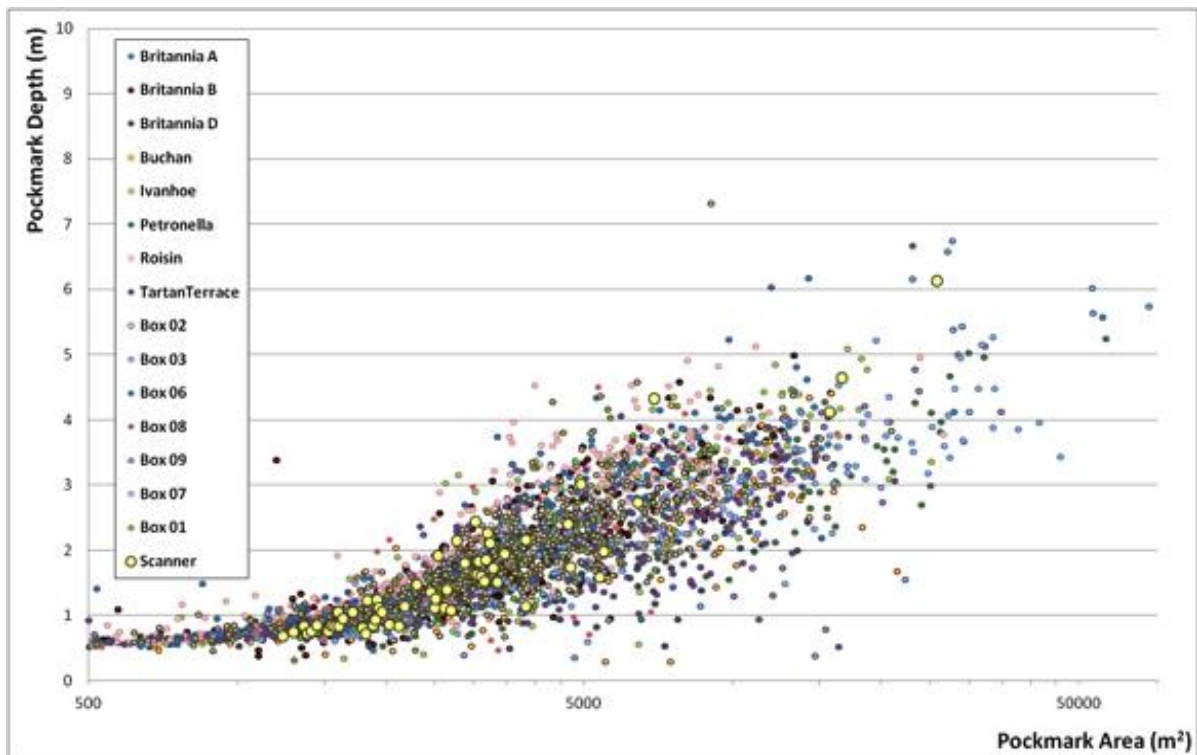


Figure 20. Relationship between Pockmark Area and Pockmark Depth for the unit pockmarks mapped within the Scanner SCI area (yellow dots) compared to the relationship found in 15 other sites within the Witch Ground Basin (Gafeira *et al.*, 2012).

Note the logarithmic horizontal scale used for the X-axis, and that deep pockmarks (e.g. Scanner, Scotia and Challenger) lie off the Y-axis.

Other than the Scanner and Scotia pockmark complexes the pockmarks from the study area present dimensions comparable to the pockmarks found in the rest of the Witch Ground Basin (WGB). The pockmarks of the WGB have an average pockmark depth of ~ 2 m and an average area of $\sim 6,900$ m², based on the values extracted from 18 survey areas using the same methodology (Gafeira *et al.*, 2012). These values are larger than the values extracted in this study (when Scanner and Scotia are excluded) but it should be noted that they also include other unusually large pockmarks such as the Challenger Pockmark, which have a strong impact on the average values.

They also follow a similar relationship between the area of an individual pockmark and its vertical relief (Figure 19) as found for the other study areas within the WGB (Figure 20). The fact that the trendlines for each data set are similar suggests that there are similarities in the physical properties of the surficial sediments across the survey areas into which the pockmarks are developed.

4.5 Survey comparison

One of the tasks planned for this study was the comparison of the two bathymetric datasets available for the study area; the SEA2 dataset (Area 3, Box 4), acquired in 2001, and the most recently acquired dataset provided by JNCC, acquired in 2012. The purpose of this comparison was to identify if there had been any infilling or expansion of the pockmarks present in the area. For example, changes in the morphology of the pockmarks leading to an increase in pockmark size could indicate active seepage.

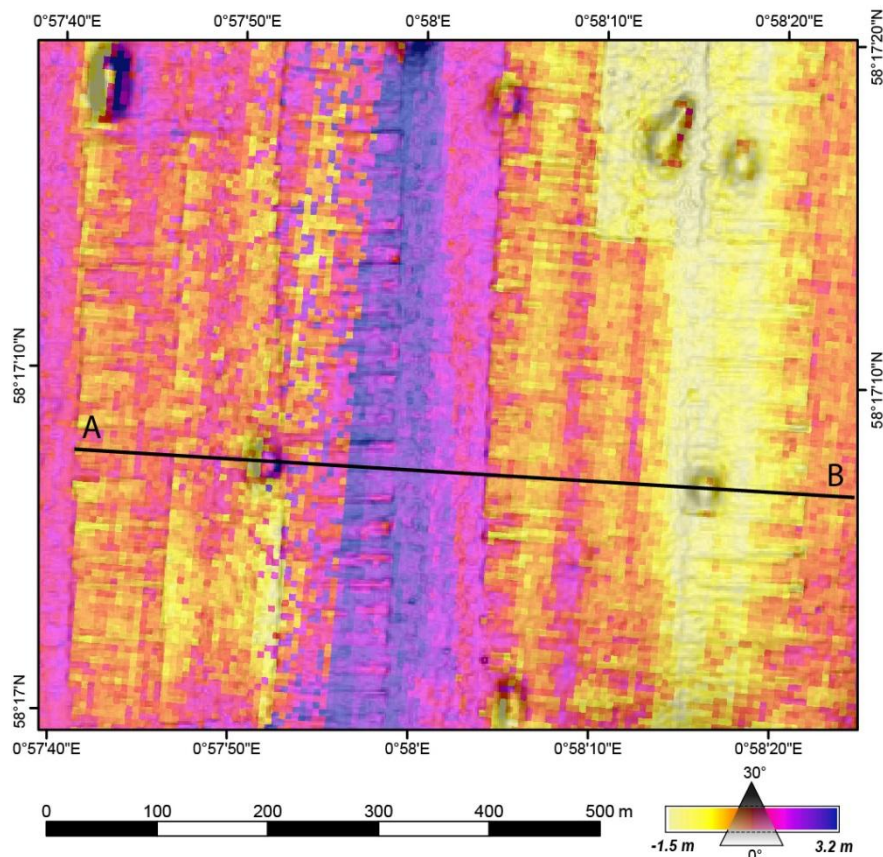


Figure 21. Detailed view of the raster generated by subtracting the depth values of the SEA 2, Box 4 dataset from the JNCC multibeam dataset values.

Due to strong acquisition artefacts the depth difference between both surveys can be more than 3 metres.

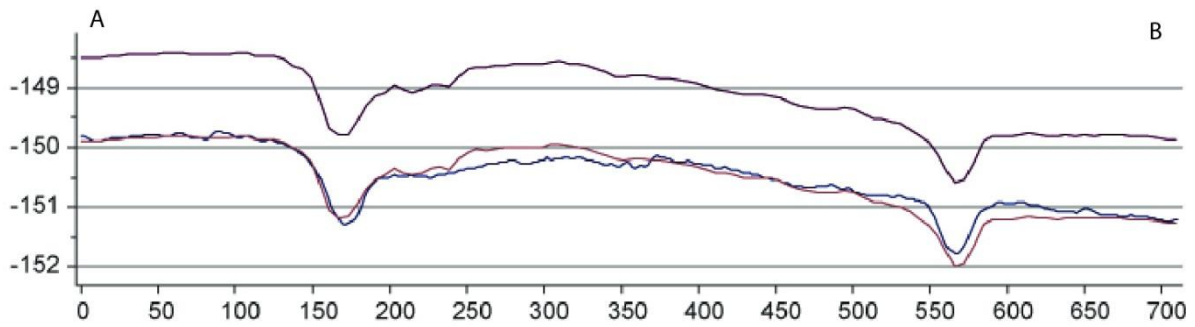


Figure 22. Profiles from A to B (on Figure 21) extracted from 1) the SEA2 dataset (in dark red), 2) the JNCC dataset (blue) and 3) the depth corrected SEA2 dataset (orange).

An analytical comparison was conducted using the ArcGIS 'Minus' tool, which subtracted the water depth value of the SEA2 raster from the water depth value of the JNCC raster on a cell-by-cell basis. However, the result of this subtraction revealed mainly the differences in the datasets' acquisition artefacts and the fact that there is a vertical shift between the two surveys of approximately 1.40 m (Figure 21 and Figure 22). To overcome the differences in water depth observed, derived rasters (sub-products of the pockmark automated mapping methods) were chosen. The rasters used for this comparison record only the pockmark depth. The result of the subtraction between these derived rasters is shown on Figure 23.

As shown on Figure 23 and Figure 24 there is an apparent infilling of the northern and eastern sidewalls and an apparent excavation of the southern and western sidewalls consistently throughout all the pockmarks. The absence of infilling outwith the pockmarks suggests that the effect is not due to sedimentation and is more likely to be the result from a horizontal shift between the two surveys. The current velocities measured nearby are considerably below the Hjulström curve values required to erode the fine grained sediments of the Witch Ground Formation.

When measuring the distance between the locations of the deepest point of the pockmarks in each survey, it was found that they varied from 1 m up to 20 m apart. And, more significantly, the displacement can be observed in all directions. Therefore there is not a standard transposition and so it is not practical to use this information to correct the positioning of the data.

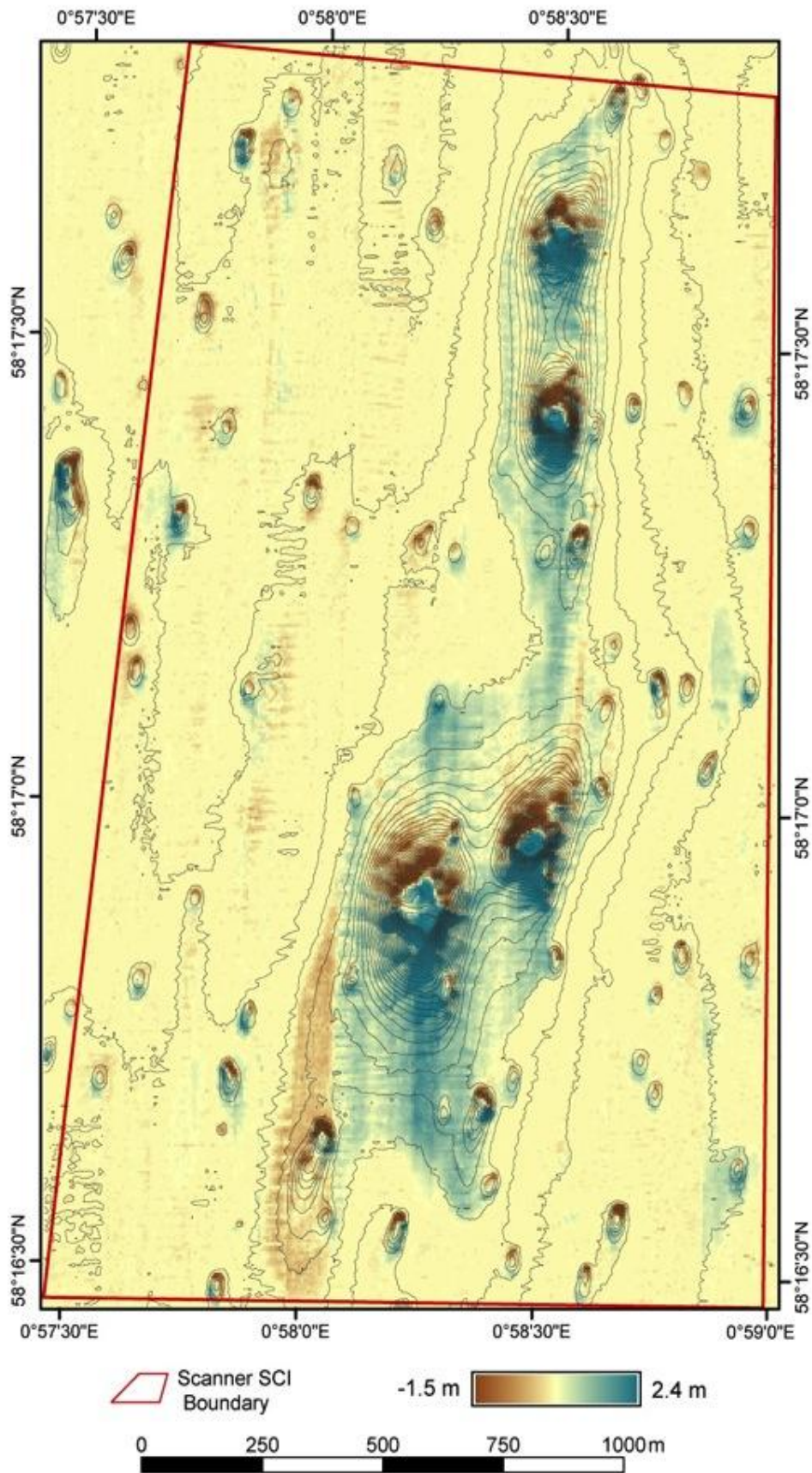


Figure 23. The difference of pockmark depth derived for the JNCC survey and the SEA2 survey, box 4.

Positive values would indicate an increase in water depth between 2001 and 2012, whereas negative values would indicate a decrease in water depth between the two datasets.

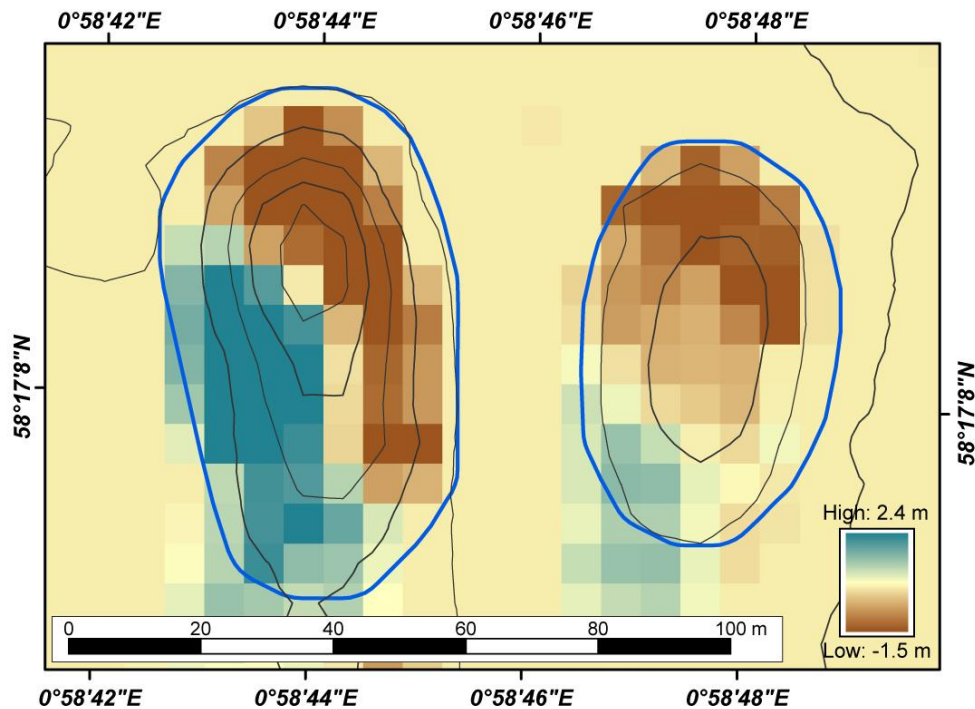


Figure 24. Detailed image showing the difference between pockmark depths extracted from the two surveys compared in this study.

Note that in both pockmark 37 and pockmark 21, as in almost all the other pockmarks, the northern and eastern areas show negative values (in brown) and the southern and western areas show positive values (in blue).

Therefore another approach was taken and the values of maximum water depth of each individual pockmark, extracted from both datasets, were compared. The value of the pockmark maximum water depth should not be affected by the dataset horizontal shift. The difference between the pockmark maximum water depths measure from the two datasets ranges from -29 cm to 1 m (Figure 25). It was considered that perhaps variations between 20 cm and -20 cm were due to the differences in cell size and algorithms used to generate the DDMs. Whereas difference values of more than 20 cm but less than 40 cm were considered to be more likely due to artefact issues. However the largest differences of more than 40 cm, observed in six pockmarks (47, 61, 64, 65, 66 and 67), were considered worthy of further investigation to assess if they were the result of real changes at the seabed reflecting infilling or deepening of the pockmark during the 11 year time interval.

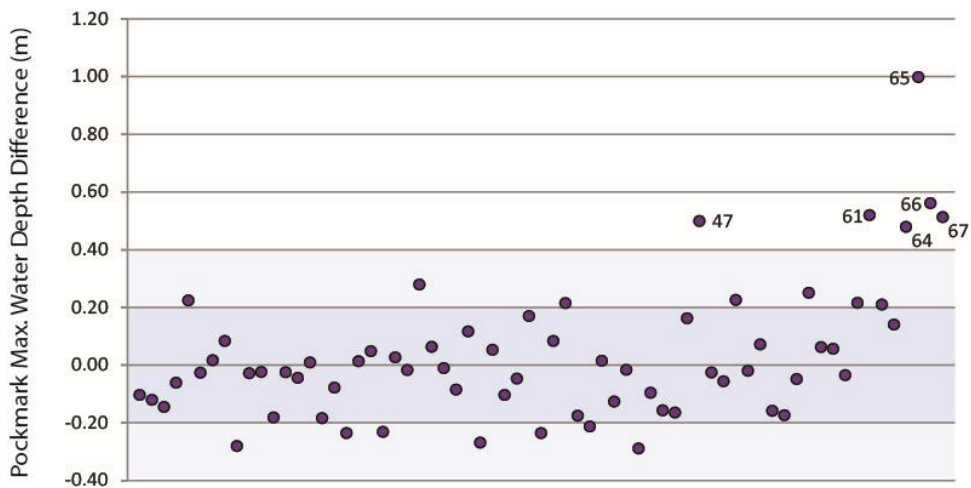


Figure 25. Difference values between the pockmark's Maximum Water depths extracted from the two datasets used in this study.

Negative values suggest that the pockmark was deeper in 2012; positive values suggest that it was shallower.

The horizontal distance between the deepest points of each pockmark extracted from the two datasets was also measured. Most of the pockmarks showed differences of less than 12.5 metres. That is within the range expected considering both the horizontal shift observed and differences resulting from the different cell sizes and algorithms used to generate the DDMs. However, there are four pockmarks (14, 46, 48 and 31) that present a greater distance between the deepest points extracted from the two datasets (Figure 26). These pockmarks were also the subject of further investigation.

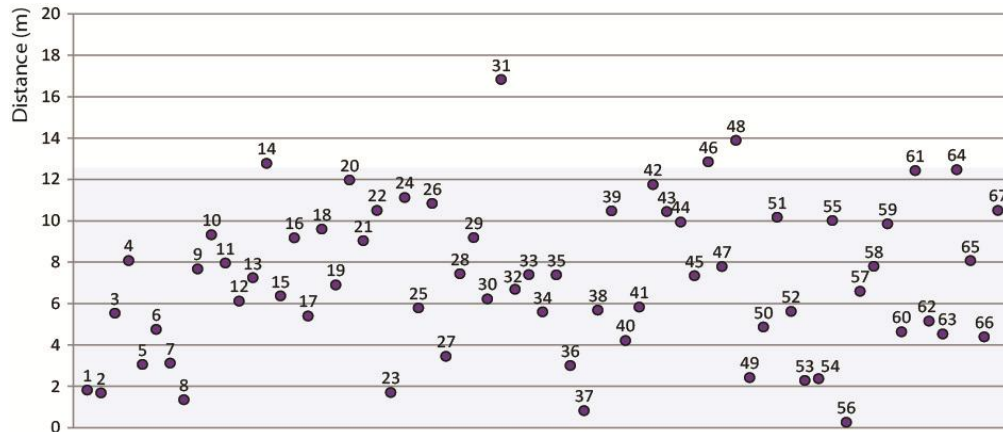


Figure 26. Horizontal distance between the positions of the deepest points of each pockmark, extracted from the SEA and JNCC datasets.

Pockmark 14 presents a distance of 12.8 metres between its deepest point extract from both surveys. However, this pockmark is located in an area where the data acquired for SEA2 is deeply affected by acquisition footprint, which makes the determination of its deepest point extremely sensitive to vertical shifts in the datasets.

Although Pockmark 31 is not in an area particularly affected by acquisition artefacts, it was not possible to identify why its deepest point is located 16.8 metres apart between the two surveys. No significant changes were noticed between profiles extracted, though, the N-S profiles are characterised by a marked U-shaped profile (broad flat bottom), which can lead to larger uncertainty in the identification of its deepest point.

The location of the deepest point of Pockmark 46 displays a displacement of 12.8 m between the two surveys, resulting of an apparent widening of the pockmark base towards the north, leading to an increase in the asymmetry of the N – S profiles across this pockmark (Figure 27).

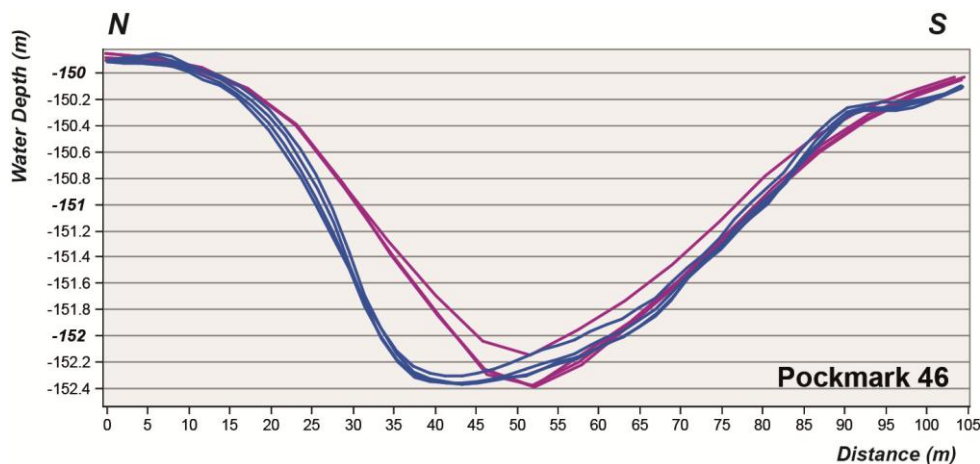


Figure 27. Bathymetric profiles extracted from both surveys across Pockmark 46, showing apparent erosion of the northern sidewall.

The purple profiles show the data from the SEA2 dataset, whereas the blue profiles show the data from the JNCC dataset extracted from an equivalent position, taking in account the horizontal shift between the two datasets.

The area where Pockmark 46 is located is not affected by significant artefacts in either of the two datasets. Therefore, the difference of 46 cm between the pockmark depths extracted for this pockmark is believed to be real. The profiles extracted from the most recent survey show that this pockmark presents a shallower and wider base. Local sedimentation rates cannot account for the infilling observed in this pockmark and it is proposed therefore that the infilling observed is the result of lateral collapse of a section of the pockmark sidewalls located in the southern area of the pockmark.

The Pockmark 48 deepest point shows a displacement towards the north-east of 13.9 metres between the two surveys. The bathymetric profiles extracted show that the location of the deepest point in 2001 is currently shallower and support the interpretation that sidewall collapse of the southern edge may have occurred.

The multibeam data from the Southern Scotia Pockmark (Pockmark 64) indicate the pockmark was 48 cm shallower in 2012 than recorded in 2001. The floor area, nearly 1200 m², shows apparent infilling of more than 30 cm over much of the area (Figure 28). That implies the remobilization of a significant volume of material; however no single lateral collapse was identified that could account for all the material found. It may be assumed that this marked infilling results from the cumulative effect of several events. In addition to any material remobilised by slope instability, some material may have been sourced by seepage activity within satellite pockmarks. The profiles presented in Figure 28 show not only the infilling of the base of the Southern Scotia Pockmark but also the excavation of the satellite pockmark situated on the north-northeast sidewall of the Southern Scotia Pockmark. Sediments set into suspension by pockmark activity could have been transported downslope and contributed to the infilling observed.

The pockmark that displays the highest vertical relief difference is the Northern Scotia Pockmark (Pockmark 65). This pockmark was 1 metre shallower in 2012 than in 2001. However, the infilling of the base of this pockmark required less material than that estimated for Southern Scotia, due to the fact that the area affected is considerably smaller (540 m² compared with 1200 m²). This pockmark presents a complex geometry marked by the presence of several areas where the hummocky profile is indicative of slope collapse. Several profiles extracted from both surveys strongly suggest that the infilling results mainly from slope instability (Figure 29).

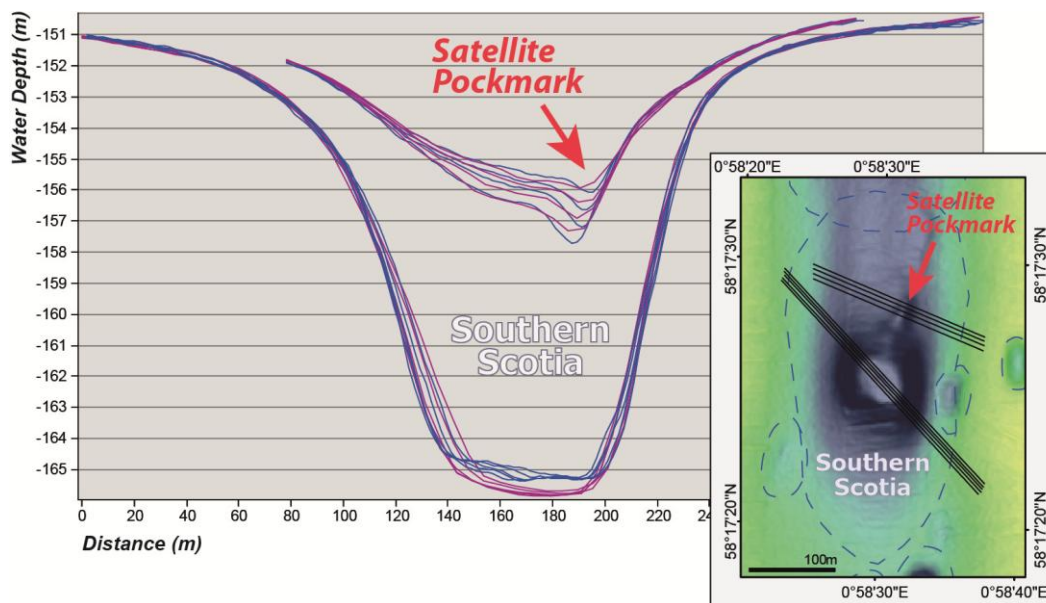


Figure 28. Bathymetry profiles extracted across Southern Scotia from both surveys.

Left: The dark red profiles show the data from the SEA2 dataset, whereas the blue profiles show the data from the JNCC dataset. These profiles suggest the infilling at the base of the pockmark and erosion on the satellite pockmark located to the NNE.

Right: Map showing the location of the 2012 profiles extracted. The 2001 data had to be translated horizontally to accommodate the offset in datasets.

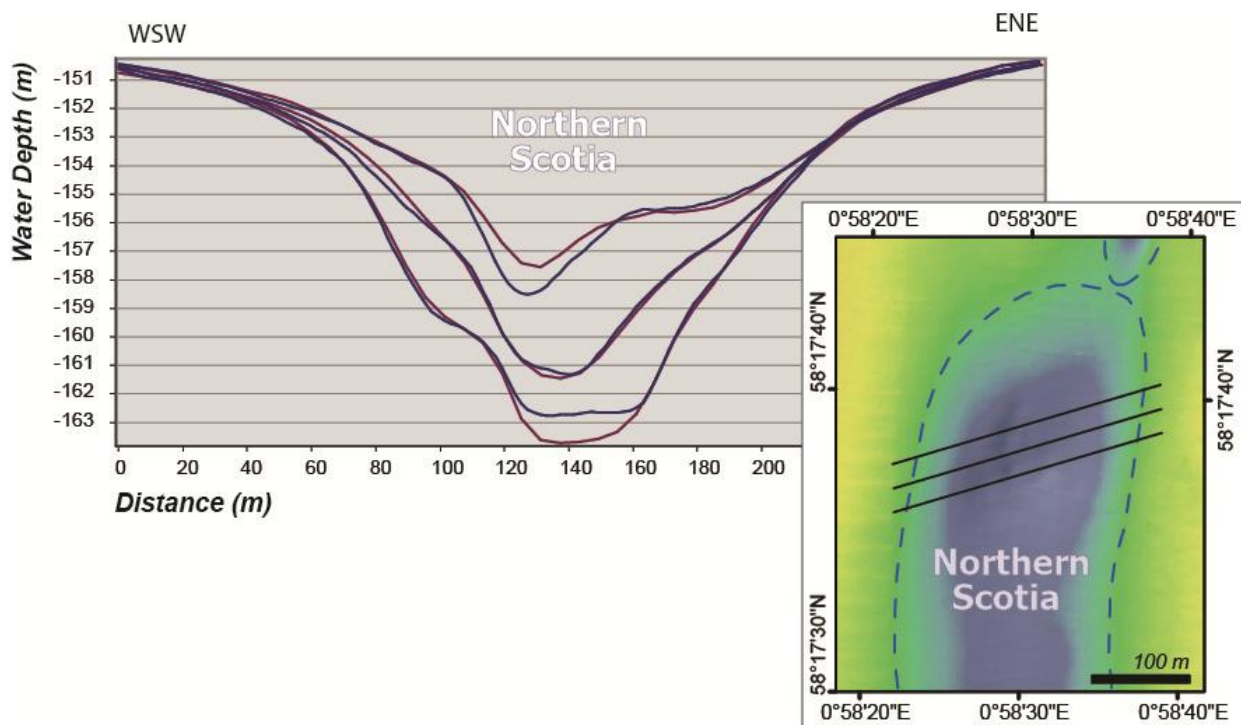


Figure 29. Bathymetry profiles extracted from both surveys across the Northern Scotia pockmark.

The dark red profiles show the data from the 2001 SEA2 dataset, whereas the blue profiles show the data from the 2012 JNCC dataset. These profiles suggest the infilling at the base of the pockmark and erosion of the sidewalls, mainly on the western sidewall.

Both the Eastern Scanner Pockmark (Pockmark 66) and the Western Scanner Pockmark (Pockmark 67) display significant infilling, of up to 56 cm and 51 cm respectively. However the distribution of the infilling material is quite distinct. Eastern Scanner presents an even

distribution resulting in a smooth and generally flat surface (Figure 30). The infilling observed on the Western Scanner Pockmark is mainly concentrated on the north-west edge of the base of this pockmark, where it is possible to recognise the toe deposits of an important slope failure. Nearly 85% of the bottom of this pockmark is covered by collapsed material, and only a small area of approximately 850 m², located on the southern edge of the base of the pockmark appears to be unaffected. The main volume of collapsed material was already deposited when the SEA2 dataset was acquired; however additional material seems to have collapsed during the gap between surveys.

A good example of apparent change at the seabed that was found to be the result of noise in the dataset can be found at the bottom of the Eastern Scanner Pockmark (Figure 30). On the JNCC dataset the presence of two topographic highs at the base of the pockmark was noticed. These highs were initially interpreted as artefacts due to the presence of gas bubbles within the water column. However, after reviewing the raw data in the CARIS project provided by JNCC the data did not corroborate this interpretation. The cause of the noise that causes these artefacts is still unknown.

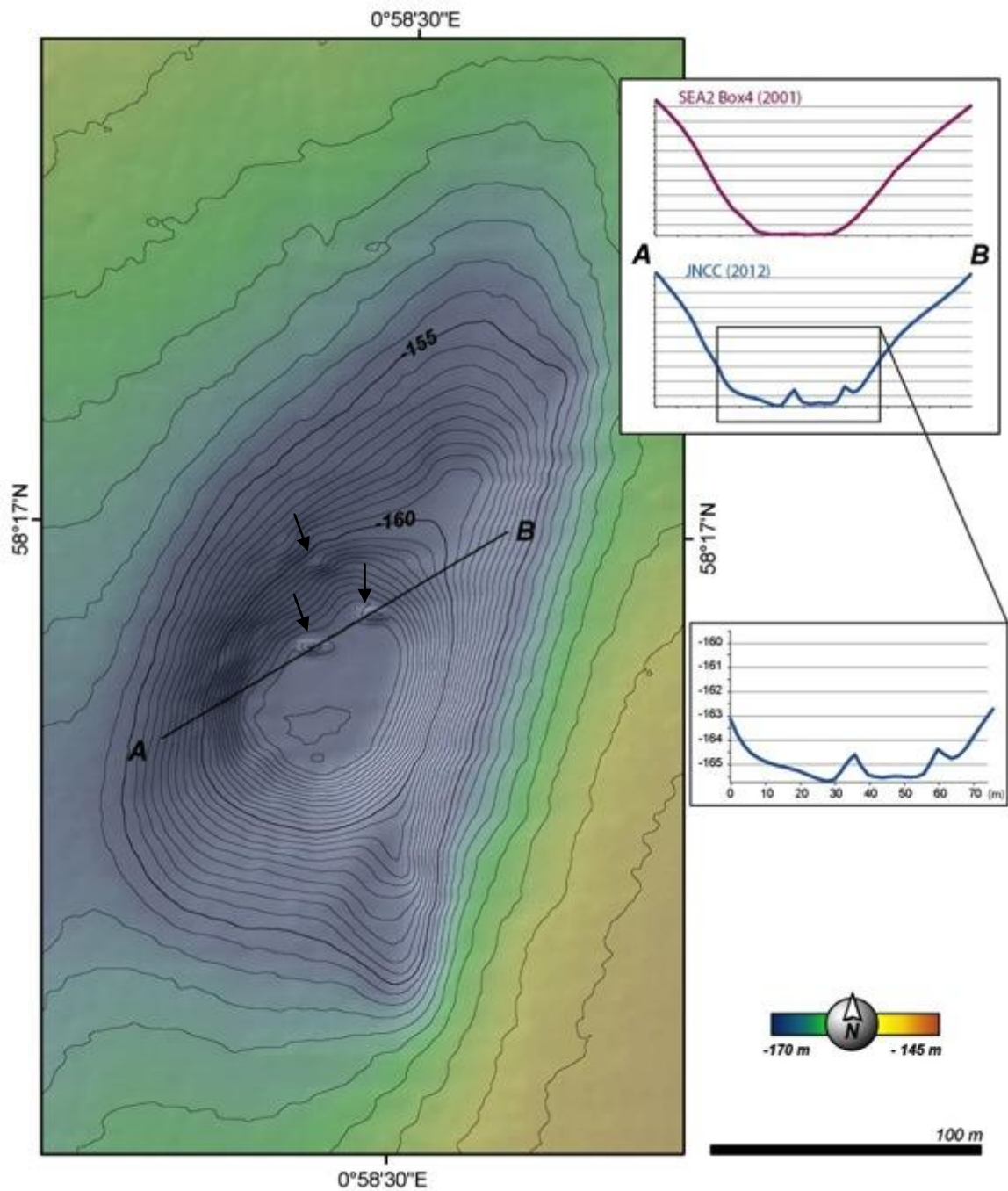


Figure 30. Shade-relief map (JNCC dataset) of the Eastern Scanner Pockmark, with contour lines every 50 cm.

Right: Bathymetric profiles extracted from both bathymetric datasets from A to B. Note the local highs detected on the JNCC dataset (shown by black arrows). Two of them are shown on the profiles. These are considered to be artefacts, not real topographic features.

5 Evidence of Gas Seepage

Present-day gas escape activity can be detected through direct evidence of gas seepage, either acoustic (*e.g.* mid-water high backscatter recorded on side-scan, or multibeam returns in the water column), geochemical (*e.g.* water column samples showing elevated concentrations of methane) or visual evidences of gas entering the water column.

However, as indicated by Judd (2001): “*the observations of actual seepage could be fortuitous, chancing upon an event that is part of an intermittent process*”. Therefore, the observation of other indirect evidence can play an important role in recognising areas of seepage. Various types of indirect evidence for gas seepage have been suggested (Hovland *et al.*, 2012). The most common are:

- presence of methane-derived authigenic carbonate (MDAC);
- presence of bacterial mats on the seabed;
- changes in the extent or character of the shallow gas accumulations.

The occurrence of MDAC is specific evidence of methane seepage at some point in the past, but does not necessarily imply active gas escape at the present time. However, it does imply that seepage has occurred over a prolonged time period. Likewise, the presence of bacterial mats is thought to indicate seepage that has been continuous for a period of time to allow a biological community to colonise the site (Judd and Hovland, 2007). Changes in shallow gas accumulations could be the result of either an isolated leakage event or from continuous seepage.

5.1. Direct evidence of gas seepage

5.1.1. Acoustic evidence

Bubbles emerging from the seafloor can be acoustically detected as mid-water column reflections. This is because the impedance contrast between gas and water is so high that the reflection will be strong at most seismic frequencies, except for low frequencies, where the wave-length is too large for bubble detection. In this instance, because gas bubble plumes have been observed coming from the seabed in the pockmarks (by ROV and manned-submersible), the interpretation of these water column targets as seepage plumes is justified. However, their composition is not certain. The acoustic targets may comprise gas bubbles, ‘hitch-hikers’ (mineral and/or organic matter lifted from the seabed by rising bubbles), upwelling water, or some combination of the above (see Leifer and Judd, 2002).

The first acoustic evidences of seepage within the Scanner Pockmark Complex were acoustic flares noted on hull-mounted echosounder, deep tow sparker and towed side-scan sonar data, during a CONOCO site survey in July 1983 (Geoteam, 1983). During this cruise, gas seepage was identified in both the Western and Eastern Scanner pockmarks, all within areas of exposure of firm clay (Coal Pit Formation) at seabed (Figure 31). Although considered possible, no seepage was detected in either the Southern or Northern Scotia pockmarks. Since then acoustic evidence of seepage has been provided by numerous surveys at both the Scanner and Scotia pockmark complexes.

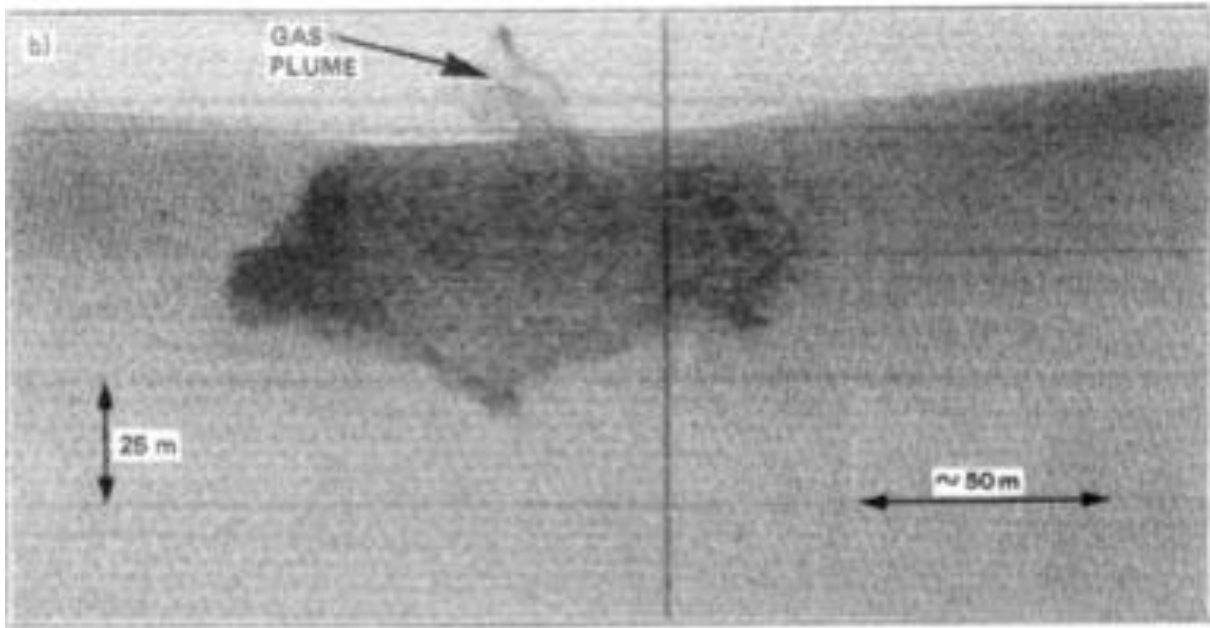


Figure 31. Towed Sidescan sonar image across the Western Scanner Pockmark.

Data collected in July 1983 during the Geoteam site survey showing gas seepage from the seabed into the water column. Note also the high reflective area inside the pockmark which is probably exposed Coal Pit Formation. Image extracted from Hovland and Sommerville (1985).

The Statoil survey in 1985 ran the ROV *Solo* at 130m water depth across the Scanner Pockmark Complex (Figure 32). The ROV-mounted side-scan sonar recorded some diffuse ‘noise’ either side of the vehicle suggesting small pockets of water with contrasting acoustic reflectivity (Hovland, 2012). The survey vessel *Lador*, following the ROV *Solo* identified a strong acoustic target with its hull-mounted 38 kHz echosounder (and also the ROV, as a dashed line on Figure 32). Although the large acoustic target centred over the pockmark (Figure 32) was interpreted as gas escape no bubbles were seen on the ROV-acquired video from the water column in front of the ROV (Hovland, 2012).

Scanner Pockmark Complex was explored again in August 1990 using the manned submersible *Jago* during the RRS Challenger Cruise 70 (CH70). The data collected especially with the deep-towed boomer was of a high standard, giving resolution and penetration never before seen with this system. Gas plumes were observed in all four pockmarks that comprise the Scanner and Scotia pockmark complexes, including twenty-one gas plumes just within Scanner Pockmark Complex (Dando, 1990). Unfortunately, the vessel positioning system available makes comparisons with modern mapping difficult (Figure 33 (Left)).

Figure 33 shows the only map presented in the CH70 cruise report (Dando, 1990) with the location of the gas plumes observed combined with the pockmark outlines and the most recent multibeam dataset acquired by JNCC. It is immediately evident that the position of the gas plumes is incorrect since the location of the Scanner Pockmark Complex is north-west of where it should be. Utilising the position of the well as shown by Dando (1990) to realign the gas plume plot does not align the bathymetry so a manual alignment has been made (Figure 33 (Right)).

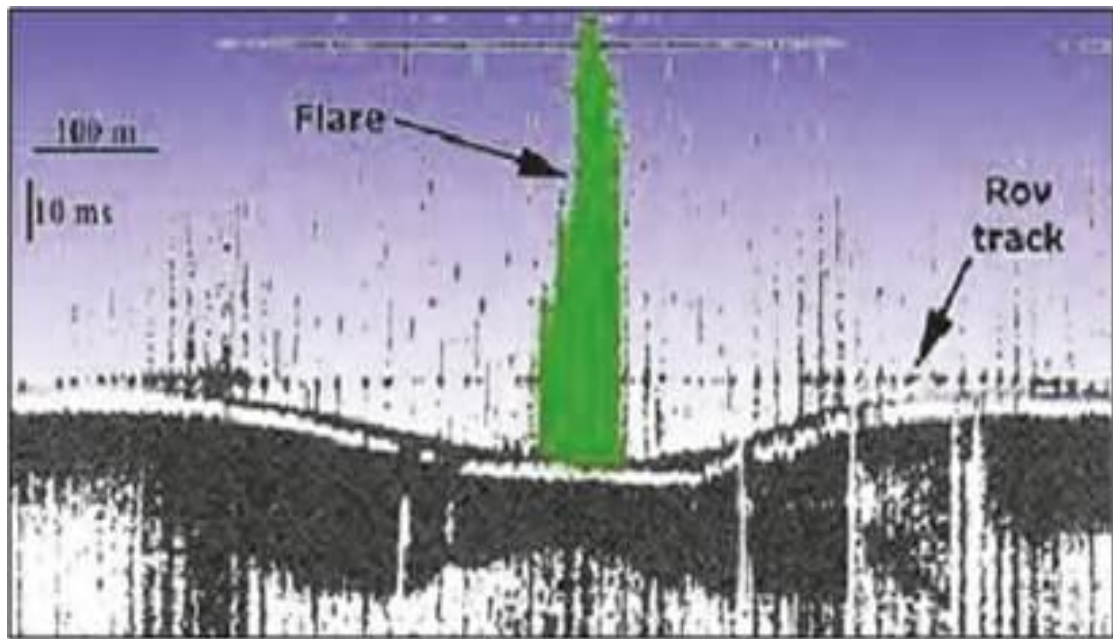


Figure 32. Single beam echosounder record acquired over the Scanner Pockmark Complex by the vessel Lador as the ROV Solo surveyed the pockmark at a constant depth (~130 m). Image extracted from Hovland (2012).

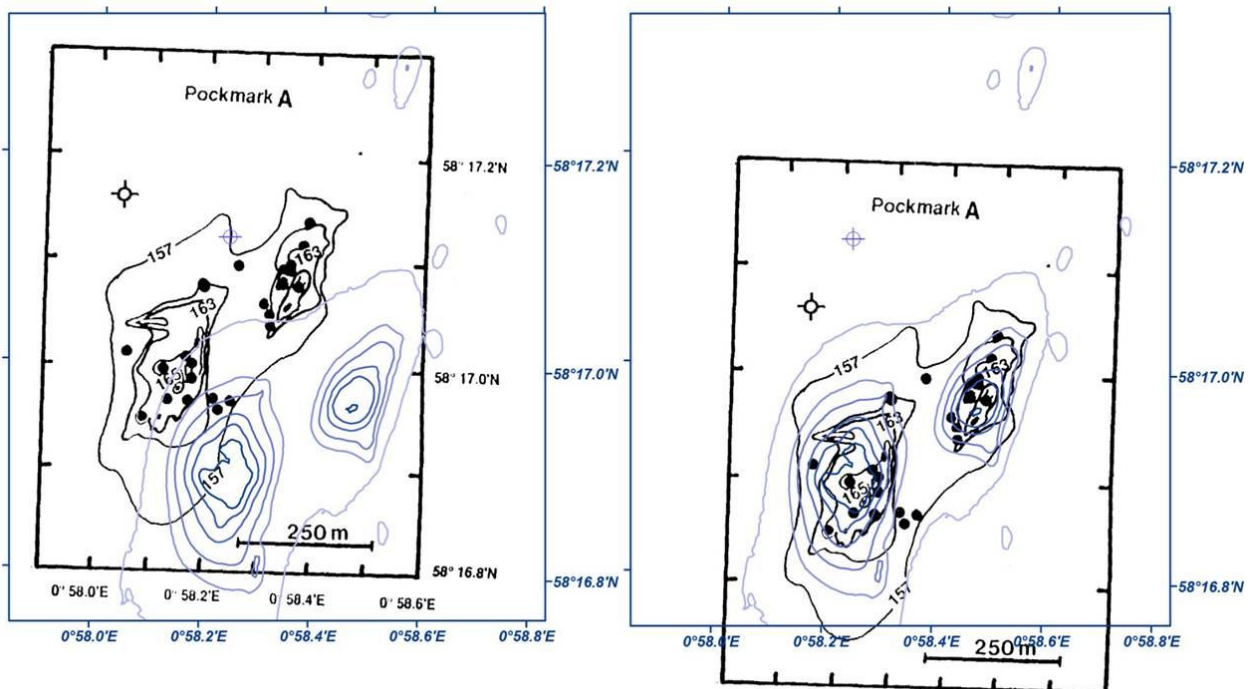


Figure 33. Data collected during the RRS Challenger Cruise 70 (Dando, 1990), overlying the pockmarks outlines (JNCC, 2012).

The black dots indicate the location of observed gas plumes. Note that the Scanner Pockmark Complex is misplaced on the 1990 data, appearing approximately 250 metres northwest of the presently known position, even after converting from spheroid ED50 to WGS84. Translating the plot with respect to the well 15/25b-1a does not align the bathymetry, so manual migration is made to get best fit to display location of gas plumes.

In July 1991, during the RRS Challenger cruise 82 (CH82), gas plumes were observed on the echo-sounder *Simrad EA 500* records in all the large pockmarks within the study area and individual gas seeps were imaged with the *Waverly* side-scan sonar in some of the pockmarks (Dando, 1991). However, the location of the gas plumes is not provided with the cruise report. Figure 34 shows a side-scan sonar record (BGS 91/03, Line 22) across Southern Scotia Pockmark.

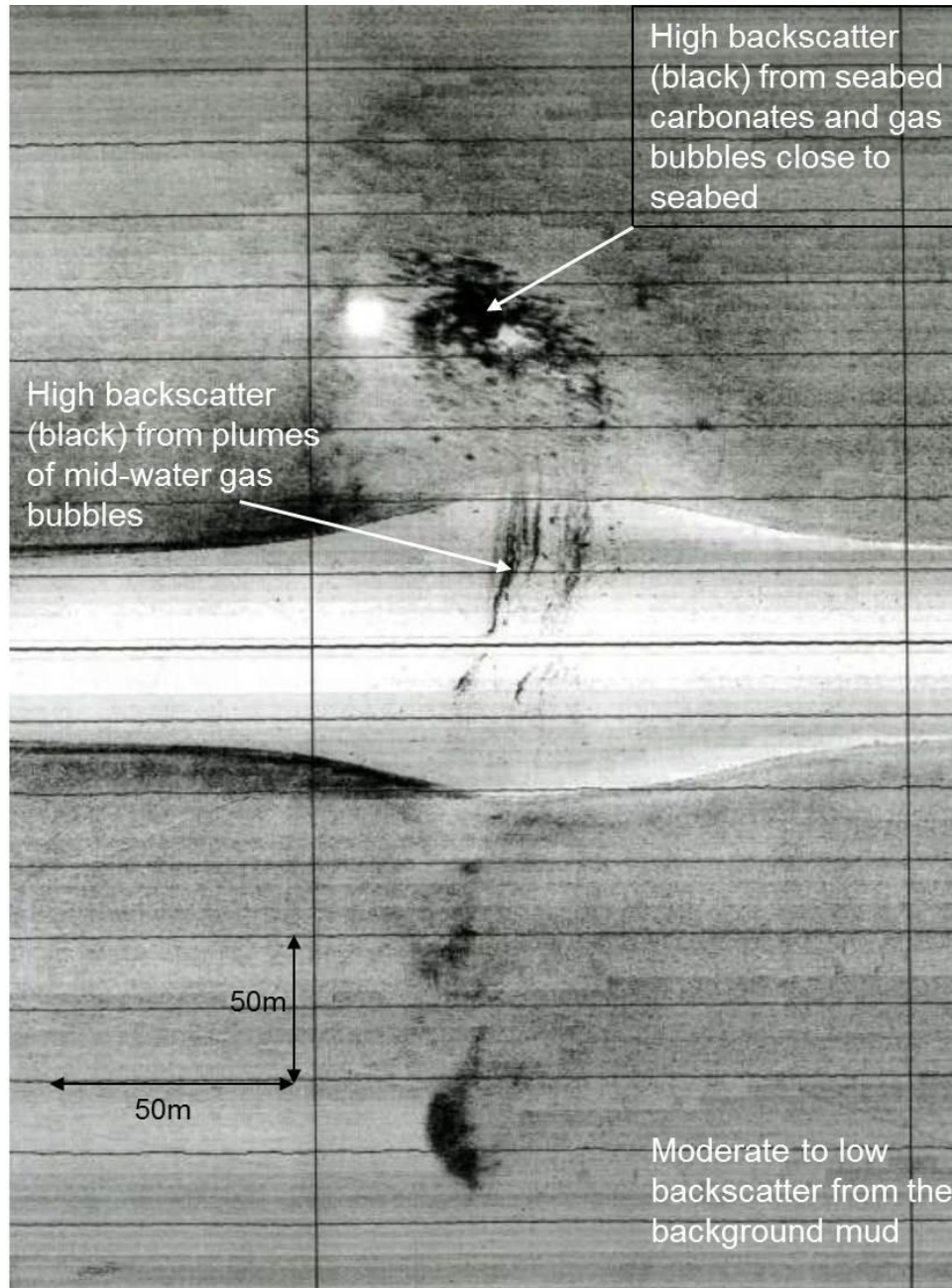


Figure 34. 1000 kHz side-scan sonar record (BGS 91/03 Line 22) across Southern Scotia Pockmark.

Here it is possible to detect gas plumes within the water column and backscatter anomalies due to the presence of carbonates at seabed. For location see Figure 35.

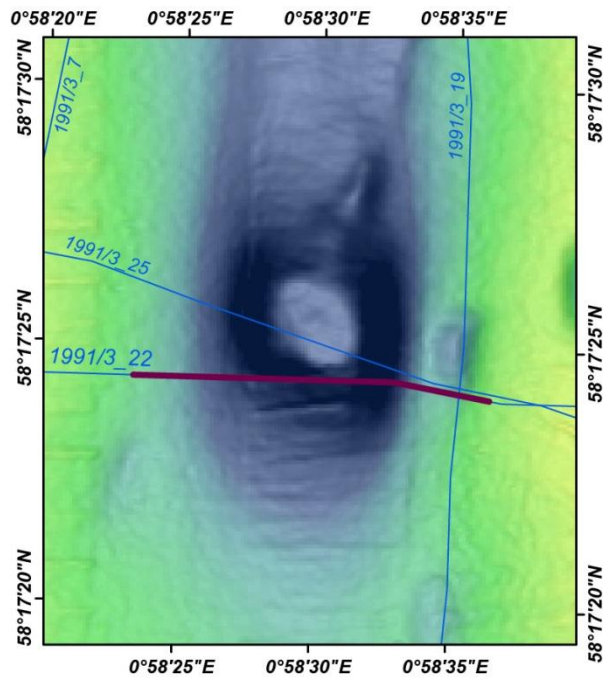


Figure 35. Shade-relief map of the Southern Scotia pockmark showing the location of the side-scan sonar (BGS 91/03, Line 22) shown in Figure 34 (purple line).

An uncorrected sidescan sonar image acquired in 2001 during the OSAE cruise, onboard the *SV Kommandor Jack*, shows gas plumes rising from the pockmarks (Judd, 2001). Also relatively weak gas flares were detected in both the Scanner and Scotia pockmark complexes with the 38 kHz echo sounder. However, the cruise report does not present any example nor provide the location of the referred gas plumes.

In October 2002, during the cruise HE 180 (RV *Heincke*), and in May 2004, during the cruise HE 208, the area was revisited and data collected across the main UK 15/25 pockmarks (Scanner, Scotia and Challenger). In both cruises, gas flares were detected using the parametric sediment echosounder system (SES-2000DS) developed at Rostock University, Germany (Boetius, 2004). During both cruises, all 5 pockmarks showed active seepage of methane from the deepest part of each depression (Figure 36). The highest gas flares were observed to reach up to 80 m below sea surface.

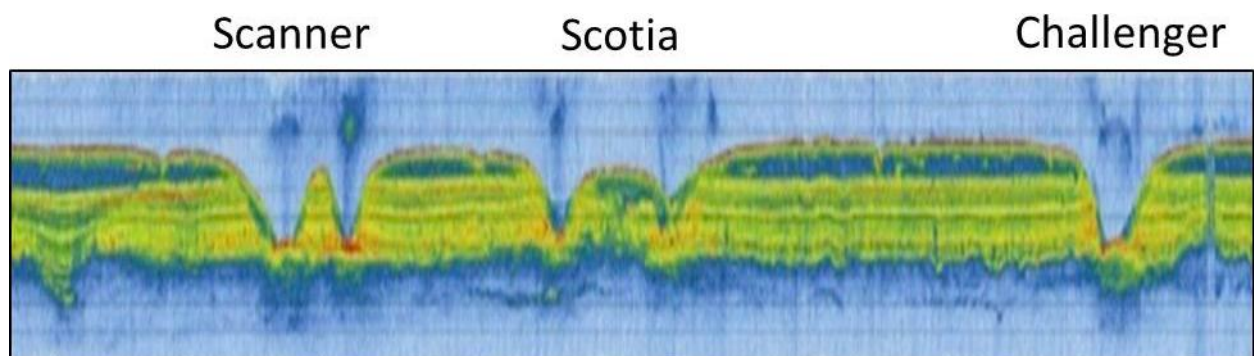


Figure 36. Scan image showing seep plumes from the major pockmarks in the Witch Ground Basin collected by the Heincke 180 cruise in 2002.

Figure adapted from Judd and Hovland (2007).

In June 2005, during the cruise ALKOR 259, a relatively weak gas flare was detected in both the Scanner and Scotia pockmark complexes with the 38 kHz echo sounder (Pfannkuche, 2005). No data on water column targets identified in the 2012 JNCC survey have been provided for this review.

5.1.2. Geochemical evidence

Seepage can be identified by geochemical anomalies in the sediment pore-water system and in the water column above, such as elevated levels of dissolved gases. Within the sub-surface sediments, there will be a concentration gradient in the pore-water surrounding the conduits transporting gas through the sediments. This gradient will be dependent on the porosity and permeability of the sediments (Hovland *et al.*, 2012). When the free gas migrates into the water column bubbles start to dissolve into the surrounding water through molecule exchange (Leifer and Patro, 1992) and may cause a strong concentration gradient of the leaking gases, with highest concentration adjacent to the stream of bubbles and reducing outwards in a radial aureole pattern. Because the rising plume of bubbles is influenced by currents, this chemical concentration anomaly will be highest down-current (Hovland *et al.*, 2012). Sediment porewater collected by the submersible *Jago*, during Challenger cruise 70, directly above a gas seep in the Western Scanner Pockmark had methane concentrations 3-4 orders of magnitude above the background (Dando, 1990). Additionally, dissolved CO₂, from a sample within the Scanner Pockmark Complex, had a $\delta^{13}\text{C}$ of -25.9‰, compared with -15.2‰ for a sediment sample from outside the pockmarks, suggesting oxidation of methane in the upper sediment leading to carbonate cementation as the $\delta^{13}\text{C}$ of the methane in the seep and within the sediments is -73 - 79.0‰ (Clayton and Dando, 1996; Judd and Hovland, 2007). Additionally, according to Jones (1993), the sample collected by *Jago* from the unconsolidated surface sediment around an active seep site within the Eastern Scanner Pockmark presented sediment methane concentration of 149 $\mu\text{mol}/\text{dm}^3$.

During the Challenger Cruise 82, 13 CTD casts with a water sampling rosette were taken and samples analysed to detect the presence of methane and hydrogen, within the Witch Ground Pockmark study area, including one at the southern edge of the Southern Scotia Pockmark (sample station 31: 58° 17.39' N, 0° 58.48' E). Although the results for that particular sample are not presented in the report, it states that: *“there is an approximate correspondence between the regions of high hydrogen and high methane concentrations and the presence of a ‘plume’ of dissolved gas at 110-130 m water depth”*. There is a steady reduction in methane concentration above this level (Leifer and Judd, 2002). It is also remarked that the depth at which some of the bubble traces disappear from the echo sounder and probably corresponds to a major area of gas solution (Dando, 1991).

At least two of the ten gravity cores collected in this study area during the He208 cruise, in 2004, show an increase of methane concentration in the sediment with depth. Figure 37 shows the methane profile of the gravity cores collected respectively from Eastern Scanner (Station 713: 58° 16.92' N, 0° 58.46' E) and from Southern Scotia (Station 717: 58° 17.42' N, 0° 58.51' E). Similar concentrations and increases with depth were shown in many of the cores from the Challenger cruise 82 (Dando, 1991).

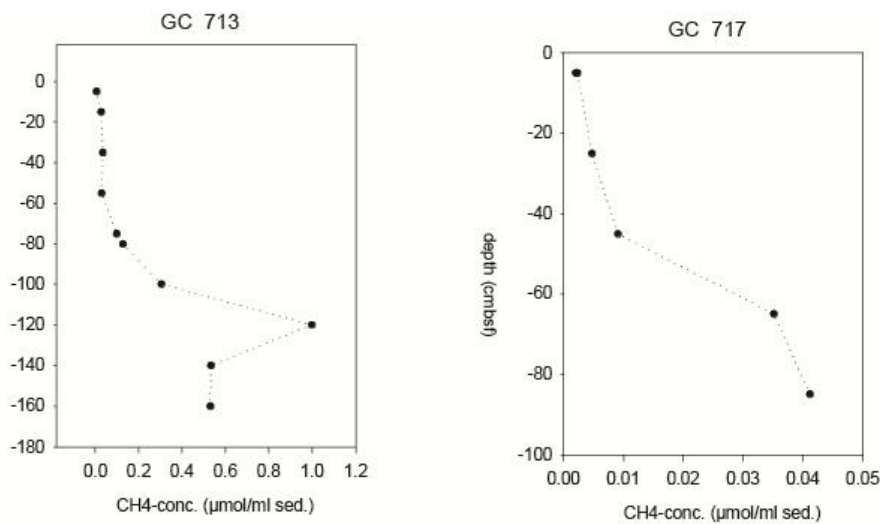


Figure 37. Methane profiles of the gravity cores collected during the He208 cruise from Eastern Scanner (St 713) and Southern Scotia (St 717).

5.1.3. Visual evidence

Statoil's 1985 survey detected gas plumes acoustically and then attempted to confirm them visually with the ROV. However, compared to the acoustic flares, the bubble streams are disappointingly small and feeble. Only three bubble streams were found inside the Scanner Pockmark Complex and one of them, located adjacent to a protruding MDAC block, was sampled (Figure 38). The maximum gas production (by bubble streams) was estimated to be 1 m³ per day from the entire pockmark (Hovland and Sommerville, 1985).

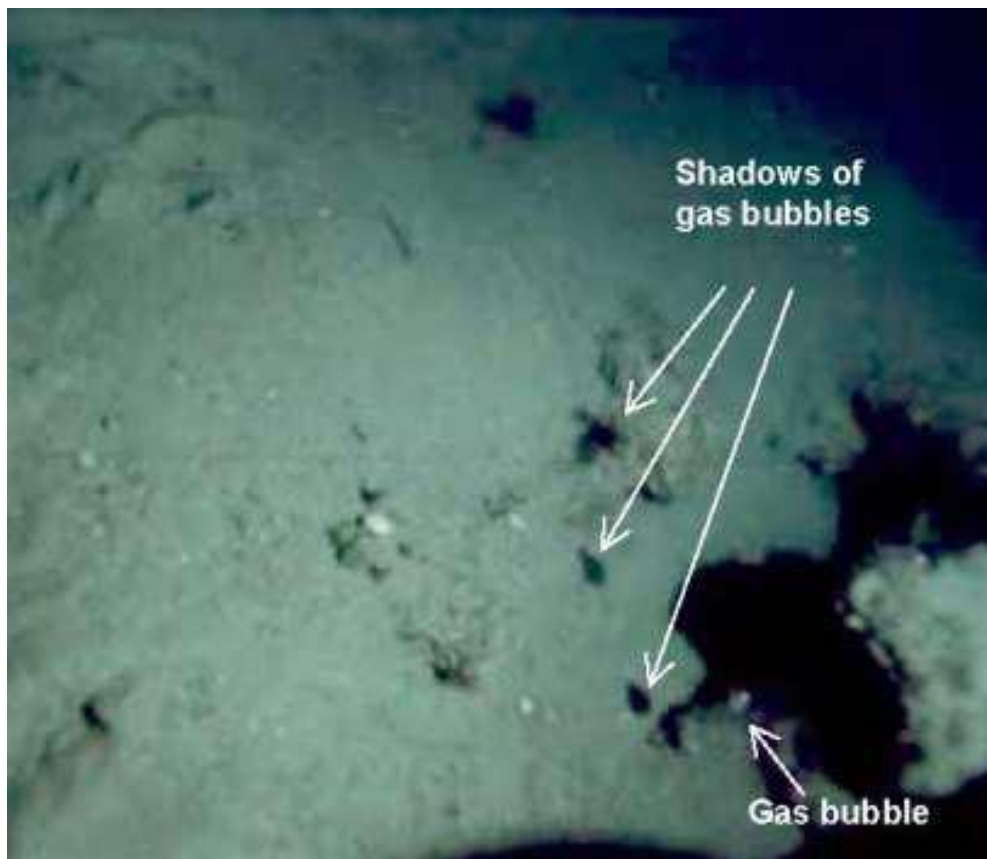


Figure 38. Image of bubbles escaping from Scanner pockmark collected by Statoil 1985.

During the dives with the submersible *Jago* that took place in August 1990, at least 27 individual gas seeps were counted. These were described as either continuous or intermittent streams of gas bubbles of up to 1 cm diameter. It was noted that although most streams of bubbles had dissolved before they had reached 60 m water depth, some large bubbles appeared to reach the sea surface. These large bubbles were derived from under a rock overhang (presumably carbonate) where gas accumulated before being released (Dando, 1990).

5.2. Methane-Derived Authigenic Carbonate

Methane-Derived Authigenic Carbonate (MDAC) has been described from continental shelves around the world at sites of gas seepage (Judd and Hovland, 2007). MDAC generally comprises carbonate minerals (high-Mg calcite, dolomite and aragonite) which cement the normal seabed sediment to form a hard substrate. MDAC was first identified in the North Sea in 1983 (Hovland and Sommerville, 1985; Hovland *et al.*, 1987). These carbonate cements result from inorganic and/or biologically mediated aragonite and/or calcite (CaCO_3) precipitation at seepage locations. This results from the anaerobic oxidation of methane (Boetius *et al.*, 2000) that usually takes places just below the seabed surrounding the gas seepage conduit (Hovland *et al.*, 2012). However, fluid escape remobilizing the seabed sediment can expose the carbonate.

Due to its hardness in contrast to the normal, uncemented seabed sediments, MDAC may be detected in side scan sonar records or multibeam backscatter datasets since these deposits will produce a strong acoustic reflection. Almost half of the mapped pockmarks present at least some area of high backscatter response, these are pockmarks: 10, 14, 15, 16, 23, 28, 31, 32, 34, 36, 38, 40, 41, 42, 43, 44, 47, 48, 50, 52, 54, 55, 56, 59, 60, 61, 62, 63, 64, 65, 66 and 67. However, ground truthing provided by visual observation or seabed samples is more reliable evidence of the presence of MDAC exposed at seabed, as a change in sediment particle size or the presence of shell hash, both characteristic of pockmarks, could also produce higher backscatter, albeit not as strong as that from cemented sediments. If samples are collected then the presence of MDAC can be confirmed by mineralogical, chemical and isotopic analysis.



Figure 39. A large slab of MDAC found by Statoil near the centre of the Western Scanner pockmark in UK Block 15/25. Taken from Judd (2001).

During the Statoil survey, the ROV *Solo* captured images of MDAC within the Western Scanner for the first time. These first images of the floor of the pockmark show that it is not flat but hummocky, and that MDAC occurs at seabed, sometimes partially covered by sediments but often as isolated protruding blocks (Figure 39). Several large slabs of MDAC were observed with the largest believed to measured approximately 2 m x 1 m and 20-50 cm thick. These slabs were generally oval discs which in at least some cases appeared to be supported centrally by a pillar or pedestal (Hovland and Judd, 1988). Samples collected showed the cement to be aragonite and calcite (CaCO₃). During the RRS *Challenger* Cruise 70 the *Jago* submersible dive, once again, revealed the complexity of the base of the Scanner Pockmark Complex and the presence of slabs of carbonate-cemented sediment (clay, sorted sand and gravel).

In 2004, during the cruise HE 208, exposed carbonate cements at the base of the pockmarks were observed as carbonate outcrops populated with benthic organisms, mostly sea anemones.

During the 2012 JNCC cruise, a total of 16 video clips and 402 stills were acquired within the Scanner study area; three across Western Scanner Pockmark (1, 2, 3), two across Eastern Scanner Pockmark (6, 14), two across Southern Scotia Pockmark (5, 13) and two across Northern Scotia Pockmark (4, 15). The remaining videos were collected across Challenger Pockmark (12) and across some smaller pockmarks. None of these videos captured images that show clearly the presence of MDAC (Envision, 2013). The PMPA Video Analysis Report (Envision, 2013), highlights the possibility of visual evidence of carbonates at seabed; one observed at 13:55:45 in the video for station SCDC06 and the other at 03:30:19 in the video for station SCDC08. Only station SCDC06 is within the Scanner Pockmark SCI area, near the rim of the Eastern Scanner Pockmark. An image from this video is shown in Figure 40. The deposits at seabed could indeed be interpreted as accumulation of MDAC. However, considering its position near the rim of the pockmark, 100 metres northwest of the pockmark centre and 12 metres above its floor, this accumulation is unlikely to be *in situ*. If it was formed at the main leakage site then this sample implies subsequent transportation to the edge of the pockmark or if *in situ* it implies formation at a side vent and not the main seepage site.

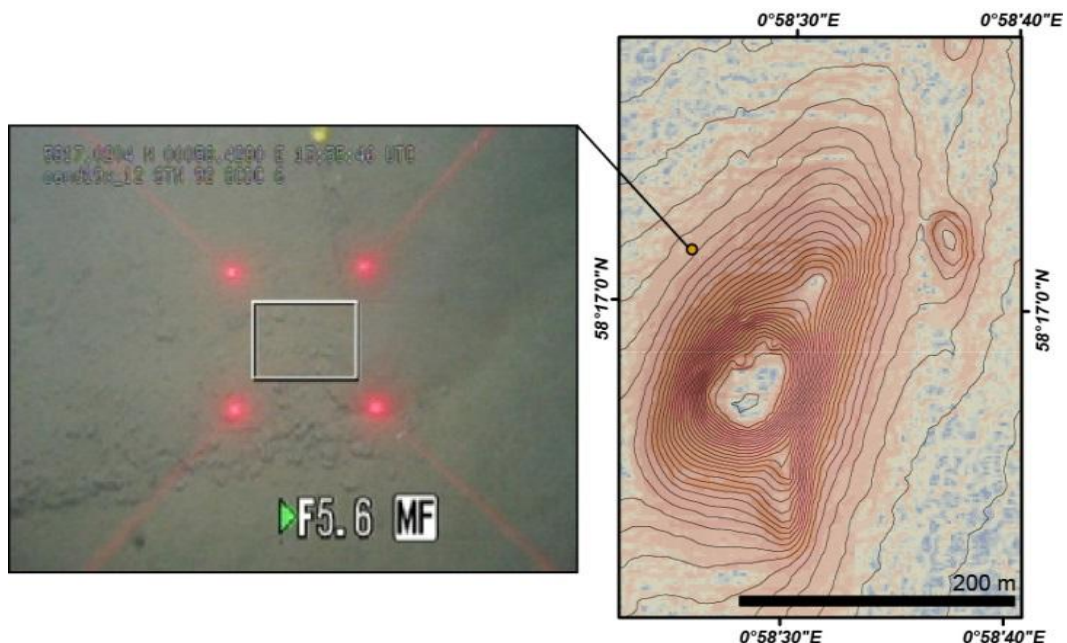


Figure 40. Image extracted from STN92 video SCDC06 at 13:55:46 UTC, located near the rim of the Eastern Scanner Pockmark.

This image shows accumulation of deposits interpreted as possible MDAC.

Additionally, within the Word file named *ScannerImagesForPublishing* provided by JNCC, the still image Stn92 026 is described as possibly showing an MDAC ledge (Figure 41). Taking into

consideration the image and its location this interpretation is not supported. The apparent ledge does not present any light deposits, typical of cemented carbonates, and appears to be comprised of the same surrounding material. This small relief could be instead related to slope instability on the steep slopes of the pockmark sidewall.

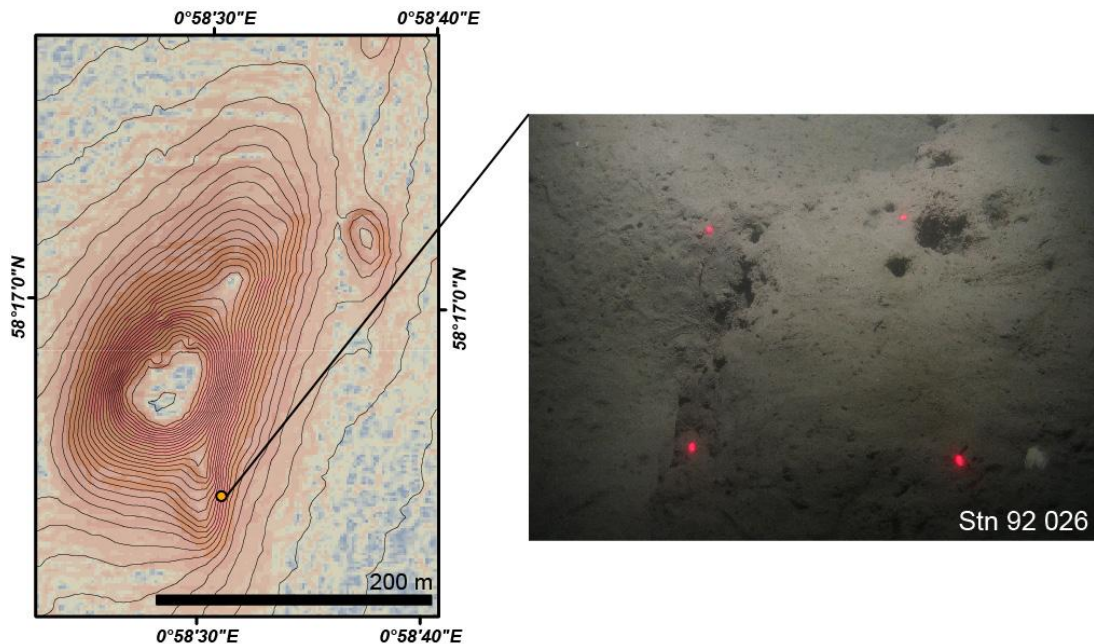


Figure 41. Left: Location of Stn 92 026, on the southern edge of the Eastern Scanner Pockmark. Right: The still image extracted at Stn 92 026, described as possible MDAC ledge.

Geochemical analysis of the carbonate cements from Block 15/25 show that the carbon-isotope values ($\delta^{13}\text{C}$ -52.0‰) lie within the range (-60 to -20‰) rather than that of normal marine carbonates (-7 to +7‰) (Judd and Hovland, 2007; Figure 5.7).

5.3. Bacterial Mats

As a result of strong chemical gradients at seepage locations communities of the sulphide oxidising microbes can flourish at such sites. The most common visible microbe found at marine methane seep sites is the thiotrophic bacterium *Beggiatoa sp.* (Hovland *et al.*, 2012). This and also many other types of bacteria can produce thick bacterial mats on the seafloor that may be considered as evidence of seepage. However, their presence can only be confirmed by visual observation, sampling and subsequent culturing of specimens. Therefore they will be limited to areas covered by either the submersible dive or ROV surveys; none were observed during the JNCC study of Scanner pockmark SCI (Figure 42).

White bacterial mats were observed from the ROV during the Statoil survey of 1985 (Figure 42). In 1990, during the *Jago* dives which were part of the Challenger Cruise 70, several bacterial mats were observed where gas was in contact with the rocks and in one area rings of bacteria were reported on the sediment surface (Dando, 1990). In 2005, during the ALKOR 259 cruise, no traces of *Beggiatoa* mats were observed (Pfannkuche, 2005).

5.4. Seep-associated fauna

Within the Scanner and Scotia Pockmark Complexes the mouthless and gutless nematode *Astomonema southwardorum sp.* was the dominant species of meiofauna (Austen *et al.*, 1993). This nematode depends on their endosymbiotic bacteria, which thrive on sulphides or methane available in the sediments.

The macro-fauna in these pockmarks described by Dando (1991) was similar to that of the surrounding area with only one species exclusively found within pockmark sediments, the bivalve *Thyasira sarsi*. Additionally, a dead specimen of *Lucinoma borealis* was recovered attached to a fragment of MDAC, during the CH70 Cruise's *Jago* dives (Dando, 2001). Both these bivalves are known to be symbiont-hosting species containing thiotrophic microbes. Later Dando (2010) also mentions the presence of the bivalves *Axinulus croulinensis* and *Thyasira equalis* under a list of chemosynthetic organisms reported at the Scanner Pockmark Complex. The presence of these organisms could also be considered as indirect biological evidence of seepage. However Dando (2010) notes that none of these shallow-water seep symbiont-containing species are restricted to seep sites but can all be found in other reducing environments.



Figure 42. Seabed photograph showing anoxic sediments (black) and bacterial mat (white) adjacent to MDAC at area of gas seepage in UK Block 15/25.

Photographed during the Statoil (1985) survey; extracted from Judd, 2001. No exact location given.

5.5. Shallow gas accumulations

BGS's regional mapping involved the acquisition of shallow seismic data in the area (Figure 4) that showed the presence of acoustic blanking within the shallow sediments (Figure 7). This is typically located within the top of the Aberdeen Ground Formation, where it has not been eroded by the Ling Bank Formation (Andrews *et al.*, 1990). The acoustic blanking is commonly caused by gas concentrations in the sediment pore water being greater than the maximum solubility for the water depth resulting in bubbles of free gas being of sufficient size to absorb the seismic signal. The JNCC survey did not collect any shallow seismic profiles that might have shown changes in extent but the BGS data shows that gas is available to leak to the seabed (see also Section 3).

6. Sedimentation

The environmental history of the area has been controlled by climatic changes since the last glacial maximum about 18,000 years ago. At that time the area was buried under ice many hundreds of metres thick however, as warming began the ice sheet started to melt away and eventually allowed a marine incursion from the north to occur (Bradwell *et al.*, 2008). Before 15,000 years ago, the area was probably a small shallow sea with a near permanent sea-ice cover. The sea was probably no larger in extent than the present Witch Ground Formation. The sea ice, together with small icebergs, transported sediment from the flanks of the basin in to the central area. The seabed was continually being re-worked by the ploughing of ice keels, and locally, ice loading, causing overconsolidation of the underlying sediments. During periods of low temperature it is likely that permafrost occurred, creating lenses of ground ice extending from adjacent land areas (Long, 1991).

As the temperature began to rise, about 15,000 years ago, sea level rose slightly, the sea ice became thinner, and the seabed ceased to be disturbed by the ice keels. This transition is represented by the irregular base of the Witch Ground Formation where the last sea ice plough marks are preserved (Stoker and Long, 1984). Between about 15,000 and 13,000 years ago, rapid sedimentation beneath a cover of seasonal sea ice took place, forming the acoustically well-layered Fladen Formation (Long *et al.*, 1986, Long, 1992).

About 13,000 years ago, the cold polar front was moving rapidly northwards past Britain, permitting the entry of warmer North Atlantic waters into the North Sea. Palaeontological evidence (Long *et al.*, 1986) suggests a rapid rise in temperature with only limited sea ice. Such a rise in bottom water temperatures is also likely to have rapidly melted any sub-surface lenses of ground ice.

Marine sedimentation continued, with the short-term return of sea ice during the Younger Dryas (Loch Lomond) period (circa 11,000 to 10,000 years ago; Long *et al.*, 1986). Radiocarbon dating of seabed sediments in the Witch Ground Basin suggests that there has been virtually no sediment input since the early Holocene, about 8,000 years ago (Erlenkeuser, 1979 & pers. comm. 1988; Johnson and Elkins, 1979). Sedimentation today is restricted to the formation of the Glenn Member through re-working of the Witch Member during pockmark formation. Gas escape during pockmark formation sorts the near-surface sediment in such a way that a very thin layer of very well-sorted silt forms, increasing in thickness into individual pockmarks (Stoker *et al.*, 1985; Andrews *et al.*, 1990).

Early attempts at dating sediments in the central North Sea involved whole sediment radiocarbon analyses (Holmes, 1977), which has the potential to incorporate 'old carbon' thereby generating an inaccurate age. There have been only a few actual radiocarbon datings to calibrate the geological model created for the Witch Ground Formation. These include a series of dates from a core (58+00/111VE) taken near the centre of the basin, 58°35'N 00°30'E (Hedges *et al.*, 1988). Although the dates are not in sequence, they suggest very rapid sedimentation around 13,600 years ago (D. Long comment *in* Hedges *et al.*, 1988). They underlie a horizon (0.4 – 0.6 m depth) containing shards of volcanic glass correlated with the Vedde Ash event of ~10.6 ky. This site and site BH81/26 (58° 08.34'N, 0° 10.63'W) which has shards from the same event (Long and Morton, 1987) indicate that there was a sudden change in sedimentation rates following the Younger Dryas episode and the onset of the Holocene at 10,000 years ago, giving a greatly reduced sedimentation rate of ~5 cm/ky for the last 10,000 years. This is supported by a gastropod at 27 cm depth with an age of 4780±130 years BP giving a sedimentation rate of 5.6 cm/ky (Johnson and Elkins, 1979) for a core located at 58°25.5'N, 0°40'E (Elkins, 1977). Similar radiocarbon ages have been obtained at similar depths in a couple of cores analysed by

Erlenkeuser (1979) supporting a reduced sedimentation rate during the Holocene (the last 10,000 years) but suggesting sedimentation ceased around 2000 years ago (Figure 43 and Figure 44).

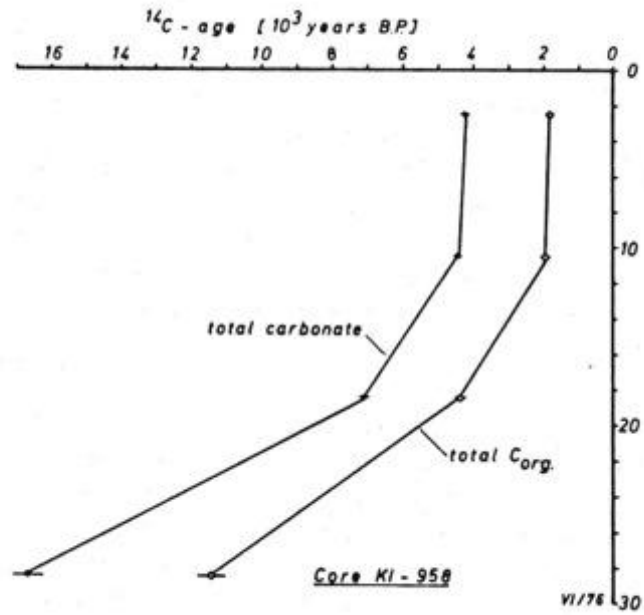


Figure 43. Profile of core KI-958 in 146m water depth, Witch Ground Basin (Erlenkeuser, 1979).

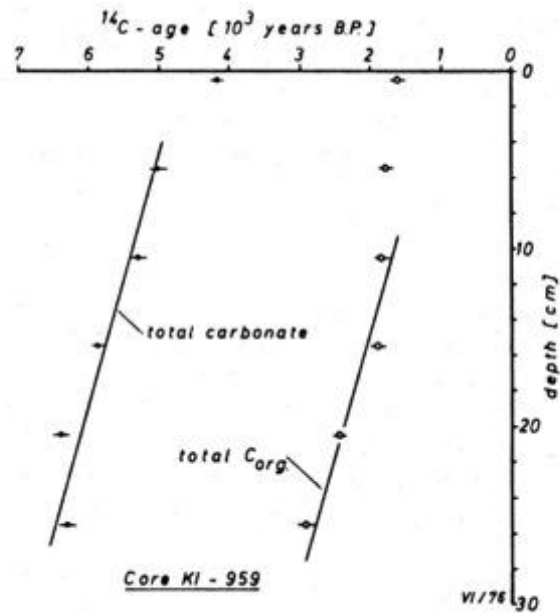


Figure 44. Profile of core KI-959 in 125m water depth, Witch Ground Basin (Erlenkeuser, 1979).

7. Anthropogenic Activities

The main potential sources of human physical disturbance to the seabed and foreseeable effects are summarised below, followed by considerations as to whether these could adversely affect the integrity of the Scanner Pockmark SCI and the designated features within.

7.1. Oil and Gas Exploration and Production

The Scanner SCI is located in an area of oil and gas exploration (Figure 45). Several activities associated with oil and gas exploration and production can lead to physical disturbance, damage, alteration or contamination of seabed habitats and geomorphological features, with consequent effects on benthic communities. According to the environmental assessment published by DECC (2013) prior to the 27th Seaward Licensing Round, the main potential sources of physical disturbance of the seabed from oil and gas activities near the Scanner Pockmark SCI are:

Anchoring of semi-submersible rigs: Semi-submersible rigs use anchors to hold position, typically between 8 and 12 in number at a radius depending on the water depth. The use of anchors and chains or cables can cause seabed disturbance and some re-suspension of sediments, and ‘anchor mounds’ could be left after their retrieval in cohesive sediments. The water depths in the area of the SCI are considered too deep for a jack-up rig to be used.

Drilling of wells: The top-hole sections of exploration wells are typically drilled riserless, producing a localised (and transient) pile of surface-hole cuttings around the surface conductor pipe. The installation of the surface casing and blowout preventer may result in physical disturbance of the immediate vicinity (a few metres) of the wellhead. Once the casing has been installed the drilling of wells is unlikely to be a source of sediment or disturbance to the seafloor.

Production platform jacket installation: Limited physical footprint similar to a drilling rig, but present on site for a longer period.

Subsea template and manifold installation: Limited physical footprint at seabed, smaller than a drilling rig and production platform, but present on site for a longer period.

Pipeline, flowline and umbilical installation, trenching and potentially, placement of rock armour: Large pipes (greater than 16 inches in diameter) do not have to be trenched according to a general industry agreement as they will not be moved by fishing gear, but they may still need to be trenched for reasons of temperature loss or upheaval buckling (due to buoyancy). Smaller pipes will need to be trenched to avoid interaction with fishing gear dragged along a seafloor. Trenches may require several passes before they are of the required depth of burial. Or if it is impossible to achieve the required depth due to obstructions, in which case rock is usually placed on the pipeline (rock dump) to protect and stabilise it. Rock dumping may also alleviate the hazard of free-spanning within the pockmark.

The south-eastern corner of the Scanner Pockmark SCI overlies part of the Blenheim oil field (Figure 45), which is a small Palaeocene oil field located in UK block 16/21b and extending into UK block 15/25c. The Blenheim field was discovered in 1990 and production started five years later and lasted until April 2000. During peak production a total of 1.36 million tonnes of oil were recovered per year. The field was developed by *Talisman North Sea Ltd.* (90.0%) with *Premier Pict Petroleum Ltd* (7.5%) and *Croft Exploration Limited* (2.5%) as partners. During production three subsea wells were tied back via individual risers to a Floating Production,

Storage and Offtake (FPSO) system. Within five kilometres from the Scanner Pockmark SCI there are two other oil fields - Bladon (Status: *Ceased in 2000*) and Balmoral (Status: *Producing since 1986*). In 1984, *ConocoPhillips UK Ltd.* completed two exploration wells (15/25-1 and 15/25-1A) within the Scanner Pockmark SCI area, north of the Western Scanner Pockmark (Figure 45). After almost thirty years have passed, acoustic anomalies can still be seen at the well sites in both backscatter and sidescan sonar data. The acoustic anomaly, no bigger than one thousand square metres, is most likely due to the deposition of cuttings and anchoring of the rig. The preservation of this evidence of man-made activity demonstrates the low sedimentation rate in the area.

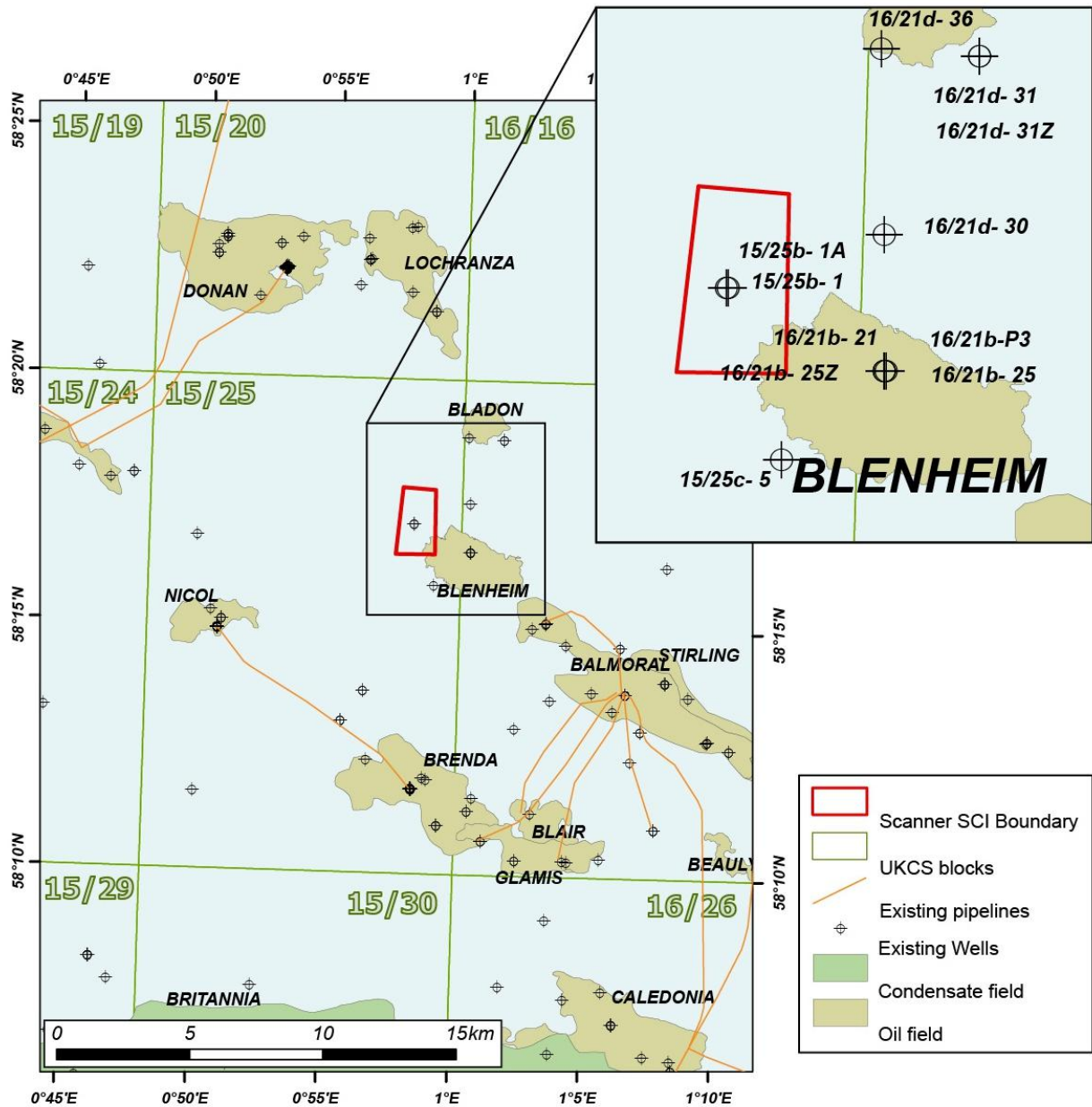


Figure 45. Oilfields and subsea infrastructure features on the vicinity of the Scanner Pockmark SCI.

Oil and gas exploration and production activities can cause marine discharges that include produced water, sewage, cooling water, drainage, drilling wastes and surplus water-based mud, which may contain remnant particulate oil (in droplet form), dissolved oil, organic acids, phenols, metals, production chemicals, and radioactive material. The produced water is the

largest-volume marine discharge for offshore oil and gas production activities. However, several produced water toxicity studies (*e.g.* Berry and Wells, 2004) have concluded that the necessary dilution to achieve a *No Effect Concentration* (NEC) would be reached at <10 to 100 m and usually less than 500 m from the discharge point depending of the currents and water stratification.

The elevated hydrocarbon readings in seabed sediments surveyed in October 2000 around the Blenheim oilfield after it ceased production, provide a useful analogue for sediment movement near the Scanner Pockmark SCI. Hydrocarbons are presumed to be mainly spread with the drill cuttings discharged during the drilling of wells and from other chemicals used in drilling. Figure 46 and Figure 47 show that the high concentrations of hydrocarbon are only found up to 200 m from the site, which suggests that sediment migration is relatively limited in this part of the North Sea. These data were extracted from the UK Benthos Dataset See http://www.oilandgasuk.co.uk/knowledgecentre/uk_benthos_database.cfm and are presented in Appendix 3. Equivalent environmental datasets if gathered for other wells in the area have not been deposited with UK Benthos.

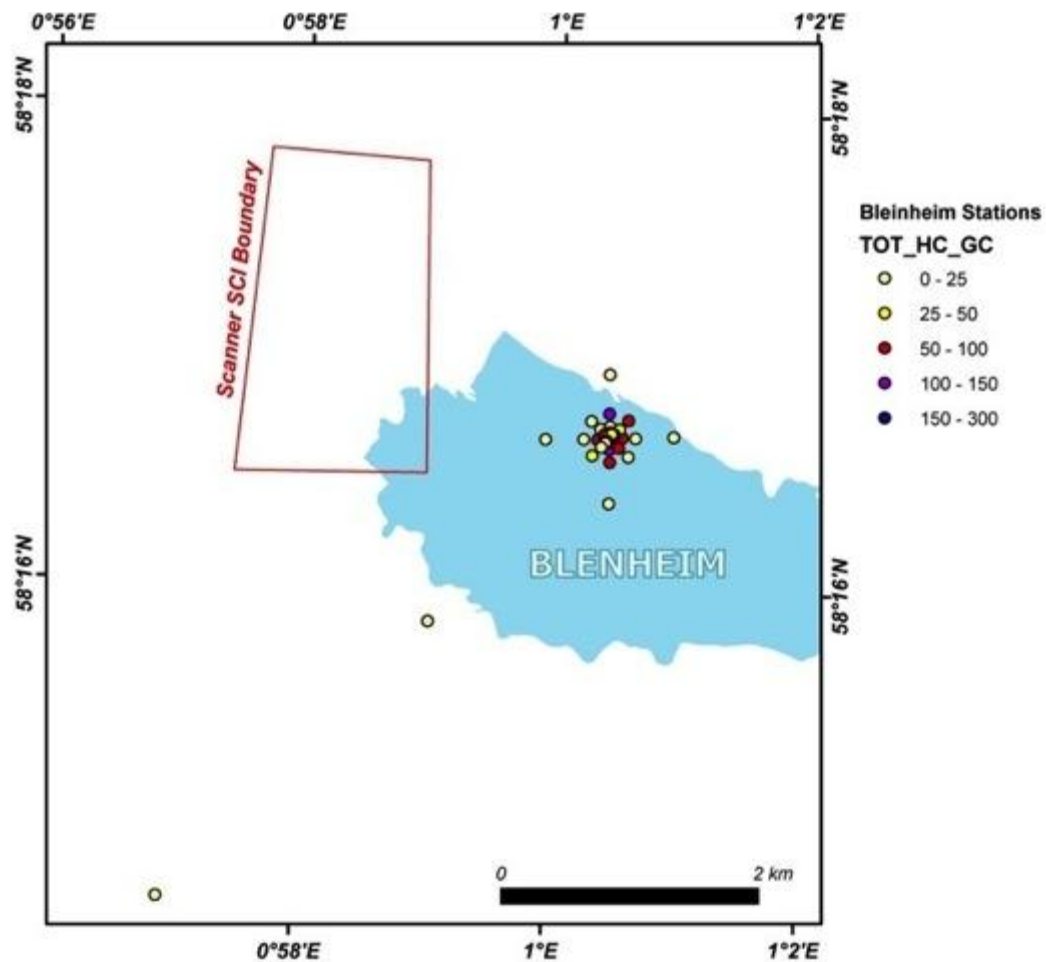


Figure 46. Spatial relationship between the Scanner Pockmark SCI Boundaries and the sample stations collected in the vicinity of the Blenheim platform.

Light blue polygon shows Blenheim field area and the sample points are colour coded according to the values (in µg/g) of hydrocarbon in the sediments determined by gas chromatography (TOT_HC_GC).

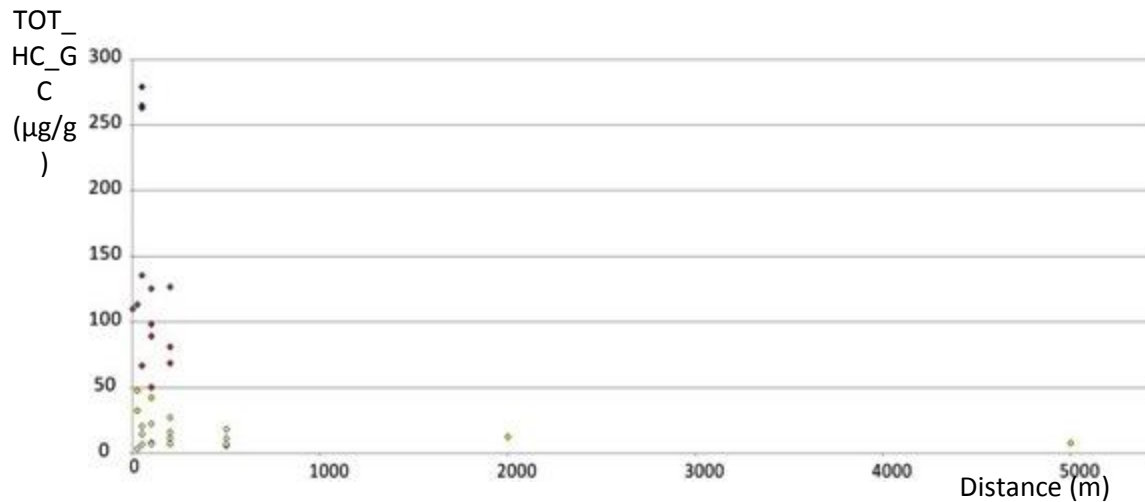


Figure 47. The concentrations of hydrocarbon in the sediments versus distance from the sample station to the Blenheim oil platform.

Data extracted from the UK Benthos dataset.

7.2. Fishing Activity

It is generally accepted that the principal source of human physical disturbance to the seabed and seabed features is bottom trawl fishing (Hall-Spencer *et al.*, 2002) and thus it is a major cause of concern with regard to conservation of shelf and slope habitats and species (Gage *et al.*, 2005). Direct, immediate effects include scraping and ploughing of the substrate, sediment resuspension, destruction of benthos, and dumping of processing waste. The magnitude of the effect depends on the type of gear employed, the depth of penetration of the gear into the sediment, the water depth, the nature of the substrate (mud, sand, pebbles, or boulders), the kind of benthic communities being impacted (*i.e.* epibenthic *vs.* infauna), the frequency with which the area is fished, the weight of the gear on the seabed, the towing speed, the strength of the tides and currents, and the time of year. The long-term effects of bottom fishing disturbance is less well understood due to the complex nature of the changes and the lack of pre-impact or control data (Bradshaw *et al.*, 2002).

The parts of a trawl that leave the most distinctive marks are the otter boards. Single otter-board tracks range in width from approximately 0.2 to 2 m and their depths can vary from 3 to 30 cm deep (Krost *et al.*, 1990). Sediment type is one of the more important factors. In sandy sediment, there is low penetration of the otter boards due to high mechanical resistance of the sediment and the seabed in sandy areas is more rapidly restored by waves and currents. Therefore, on sand dominated seafloors the tracks are short-lived, whereas on muddy bottoms the tracks will be deeper and will last longer (Krost *et al.*, 1990).

The particle size analyse (PSA) of the samples recovered during the CEFAS CEND19x/12 cruise from outside the pockmarks, show that the seabed in this area comprises mainly mud and sandy mud, comparable to that on the published maps (BGS, 1986). In such soft sediments, lineations recognised on both sidescan sonar and multibeam backscatter data are interpreted as fishing trawl tracks (Figure 48). This interpretation is supported by the direct observation of trawl marks on the seabed during the submersible *Jago* dives in 1990 as well as from sidescan sonar records on the JNCC survey in 2012 (Cefas and JNCC, 2013). Dando (2001) mentions trawl nets on rocks of carbonate-cemented sediment within the pockmark base but does not indicate in which pockmark this was observed. Two of the seafloor images collected by CEFAS (SCDC05_stn91_013 and SCDC09_stn103_008) noted plastic debris.

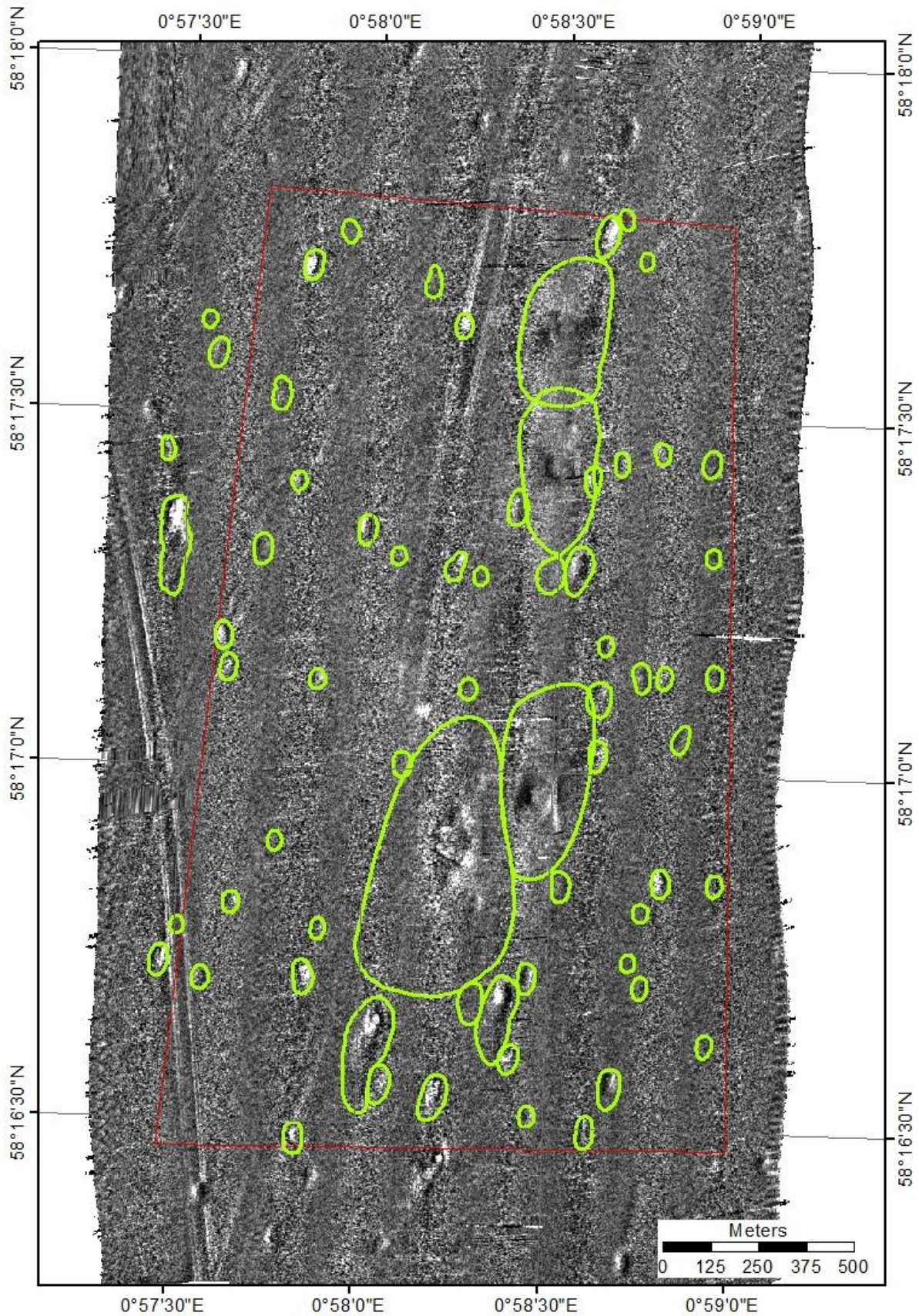


Figure 48. Multibeam backscatter from CEFAS cruise showing several pairs of trawlmarks (~50m apart) crisscrossing the Scanner SCI area (red outline).

Pockmarks are outlined in green, note the hard return from the floor of the Scanner Complex and Scotia Complex pockmarks where Cold Pit Formation is exposed.

As there are no bedforms indicative of sediment migration it is possible that these linear features are the accumulative record of several decades of fishing activity. The position of the sidescan sonar data is not precise enough to show if new scars were created by fishing activity in recent years or if old ones have been obscured by later sedimentation (Figure 46). Additionally, any apparent weakening or disappearance of these seabed features could also result from differences related to equipment used and orientation of data acquisition. The low current velocities in the area suggest that fishing scars would not be degraded quickly. The nearest current meter (BODC reference 10995, see Appendix 2) recorded a mean current speed of 0.12 m/s, 10 m above the seafloor and even maximum currents would not erode. Degradation due to reworking by subsequent fishing activity is likely to be the only mechanism to remove a trawl scar.

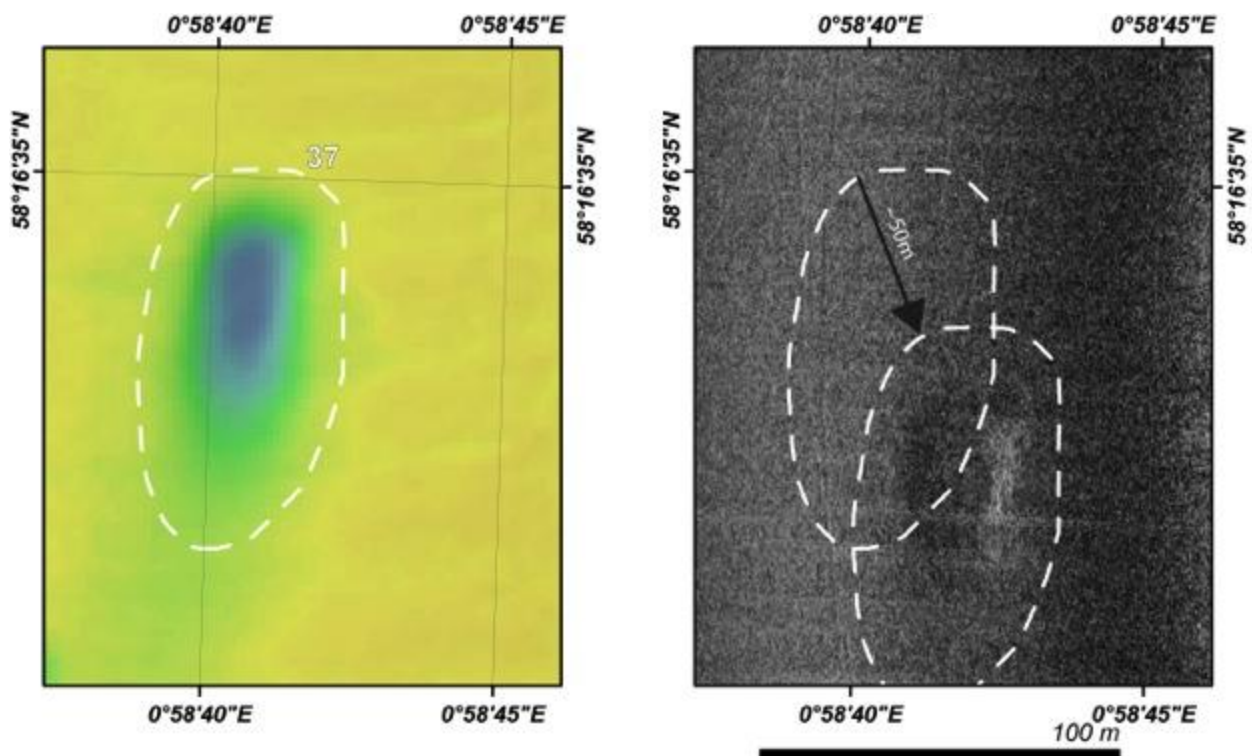


Figure 49. Comparison between the positions of Pockmark 37 within the two acoustic datasets acquired during the cruise CEND19x/12, multibeam on left and sidescan sonar image on the right.

Note that the sidescan sonar dataset is affected by the layback (which can be corrected for), and thus pockmark 37 appears ~50 m distant from its equivalent on the multibeam backscatter data.

8. Comments

Pockmark designation and sample location:

One of the main challenges of this study was to determine which pockmarks were being described in previous studies. Several articles and reports refer to the studied pockmarks as the UK Block 15/25 pockmarks or merely 'a' large North Sea pockmark, without providing any indication whether the description or data provided relates to the Scanner Pockmark Complex, Scotia Pockmark Complex or Challenger Pockmark. When there is an intention to specify the pockmark in question, the terminology used is not consistent. For instance, the Western Scanner Pockmark is referred to as SE Pockmark throughout the CH 70 cruise report (Dando, 1990), whereas Challenger Pockmark is named in that report as NW Pockmark. This inconsistency is combined in some cases with a lack of awareness that both the Scanner and Scotia pockmark complexes are comprised of two main depressions (see Appendix 5: Figure 55, Figure 59 and Figure 60).

With a few exceptions, descriptions of evidence of gas seepage is often provided without any information relative to its location, and it is often unclear in which pockmark this evidence was observed. When the location is given, it must also be considered that most data collected in the 1980s and 1990s were frequently collected with inaccurate positioning. For example, the given location for Scanner Pockmark by Dando *et al.* (1991) is 58° 16.95' N, 0° 59.20' E, situated more than 950 metres east of the correct location of this pockmark.

However, it should be noted that the nomenclature and location fixes of individual pockmark features have progressively improved over the last 30 years since the discovery of the Scanner Pockmark Complex, particularly since the development of MBES and GPS.

Gas escape:

Gas escape can either be continuous or intermittent over extended time periods. However, pockmark formation is most likely due to vigorous release of gas which lifts fine-grained sediments into the water column. According to the conceptual model proposed by Hovland and Judd (1988) cyclic pockmark activity can occur, with relatively strong gas escape occurring at the start of each cycle, followed by a gradual reduction in the flow rate as gas overpressures dissipate.

The Scanner Pockmark SCI area has been intensively surveyed since Scanner Pockmark Complex was first discovered in 1983. Over more than 30 years, repetitive observation of acoustic evidences of gas plumes supported by visual evidences and the presence of both bacterial mats and MDAC, support the interpretation that gas seepage is an enduring process within the studied pockmark complexes.

There is also evidence, however, that the activity of these pockmarks may not be constant. In 2005, during the cruise ALKOR 259, an unusually large pockmark (named Alkor Pockmark, 58° 19.58' N, 0° 55.47' E) approximately 5.5 kilometres northwest of Scanner Pockmark Complex (Figure 50) was detected with the largest gas flares of that cruise's study area, which included the Scanner, Scotia and Challenger pockmarks (Pfannkuche, 2005). However, during the ALKOR 290 cruise in the following year, the Alkor pockmark was revisited and no gas flares were detected (Pfannkuche, 2006).

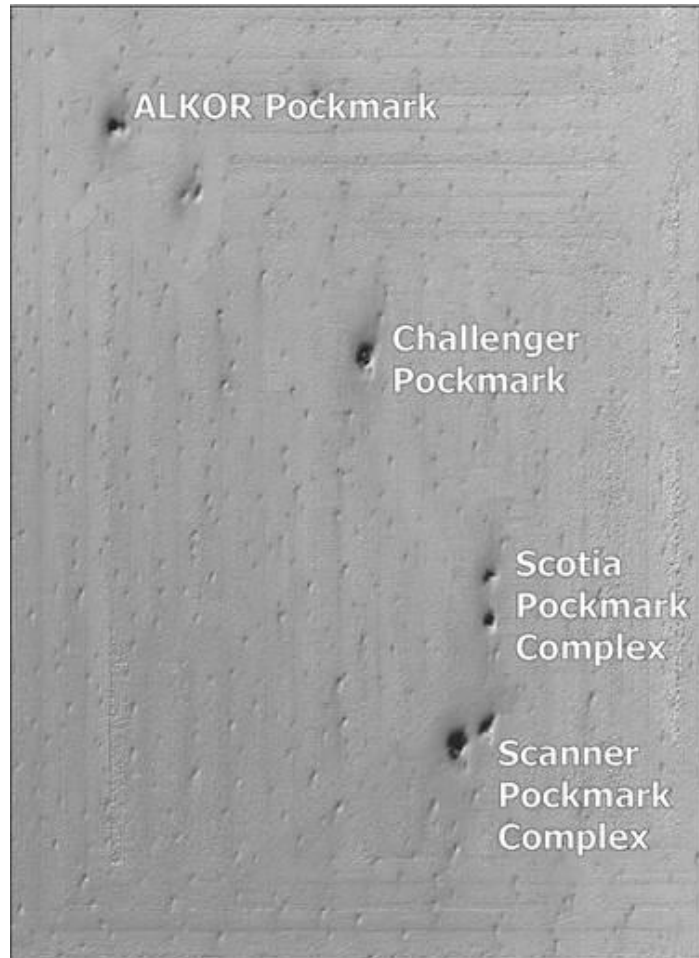


Figure 50. Bathymetric imaged collected during the ALKOR 259 cruise, showing the location of Scanner and Scotia pockmark complexes, Challenger Pockmark and Alkor Pockmark (that was first found during that cruise).

Sedimentation:

The Scanner Pockmark SCI is located in an area of negligible erosion or sedimentation since the climatic conditions stabilised after the last ice age. Consequently, any changes in individual pockmarks are likely to be due to processes associated with pockmark development, slope stability, and/or anthropogenic activities.

Anthropogenic Activity:

In the most recent (27th) Hydrocarbons Licensing Round, none of the blocks that overlap the site (Block 15/25c) or are situated within 10 km of the site (Blocks 15/20f, 15/24a and 16/16) were awarded. Site conservation objectives may be undermined by future licensing of oil and gas exploration activities through physical damage, smothering by drilling discharges, or from interruption or alteration of gas supply to the pockmarks, therefore requiring mitigation strategies.

Loss of shallow gas from the gas-charged interval at approximately 280-300 ms two-way time would cut off the supply of shallow gas to the active pockmarks. The dry well 15/25b-1A drilled in 1984, located immediately to the north of the Scanner Pockmark Complex (58°17'08.1"N, 0°58'15.3"E), appears to have been drilled on the margin of the shallow gas reservoir, presumably located beyond the zone of shallow gas for safety reasons.

Fishing activity occurs across the pockmark complexes as evidenced by scars seen on sidescan sonar records, however difficulties in positioning these datasets means that it is not possible to confirm 1) the presence of new trawling scars created between the SEA2 and JNCC surveys, or 2) the weakening or disappearance of old scars.

Geomorphological changes:

Comparative studies of seabed morphology have been used to infer pockmark activity. The comparative study of the pockmarks within Belfast Bay (Maine, USA) presented by Gontz *et al.* (2001) demonstrated that new pockmarks were formed while older, less active pockmarks were infilled over a period of time of only two years.

However the ability to detect and quantify morphological changes is significantly restricted by the quality of the data used, and the differing modes of data acquisition. The presence of marked artefacts, primarily the acquisition footprint, and the different resolution between the two surveys used in this study, limited our ability to differentiate real morphological change from artificial change. Therefore, changes up to 40 cm were not considered reliable.

Slope instability is the primary cause of changes in pockmark morphology detected in this study. Within the Witch Ground Basin, the seabed outside of the pockmarks is typically flat and the average seabed slope in some areas is less than 0.2° . In contrast the side walls of some pockmarks have slopes of $>20^\circ$. In the soft sediments of the Witch Ground Formation these slopes are most likely unstable.

Only in one pockmark, pockmark 46, was there evidence of expansion of the pockmark volume. For this pockmark, evidence suggests the steepening of the northern sidewall and the migration of its deepest point towards the north; this erosion may be the result of gas escape.

Triggers for geomorphological change:

The WGF sediments are very soft and could be disturbed by fishing activity. Several trawl scars were recognised on both sidescan sonar and MBES backscatter. If trawling impacted on the flanks of the pockmark it may lead to the gravitational relocating sediment downslope. However there is no conclusive evidence that human activity has triggered slope failure, leading to the potential burial of MDAC, bacterial mats or other ecosystems dependent on gas seepage.

Alternative triggers for slope collapse include a build-up of pore pressure due to methane gas migration within the side wall away from the main vents on the floor of the pockmark. Pore pressure change during ground acceleration triggered by an earthquake is another possible trigger for slope failure. Earthquakes are detected instrumentally in the North Sea and are typically of low magnitude (Musson, 1996). Three such events have occurred near the Scanner SCI (Figure 51), with two events less than 10km away (Table 2). Although small magnitude they may have been sufficient to change pore pressures briefly to trigger sediment failure on the flanks of the pockmark.

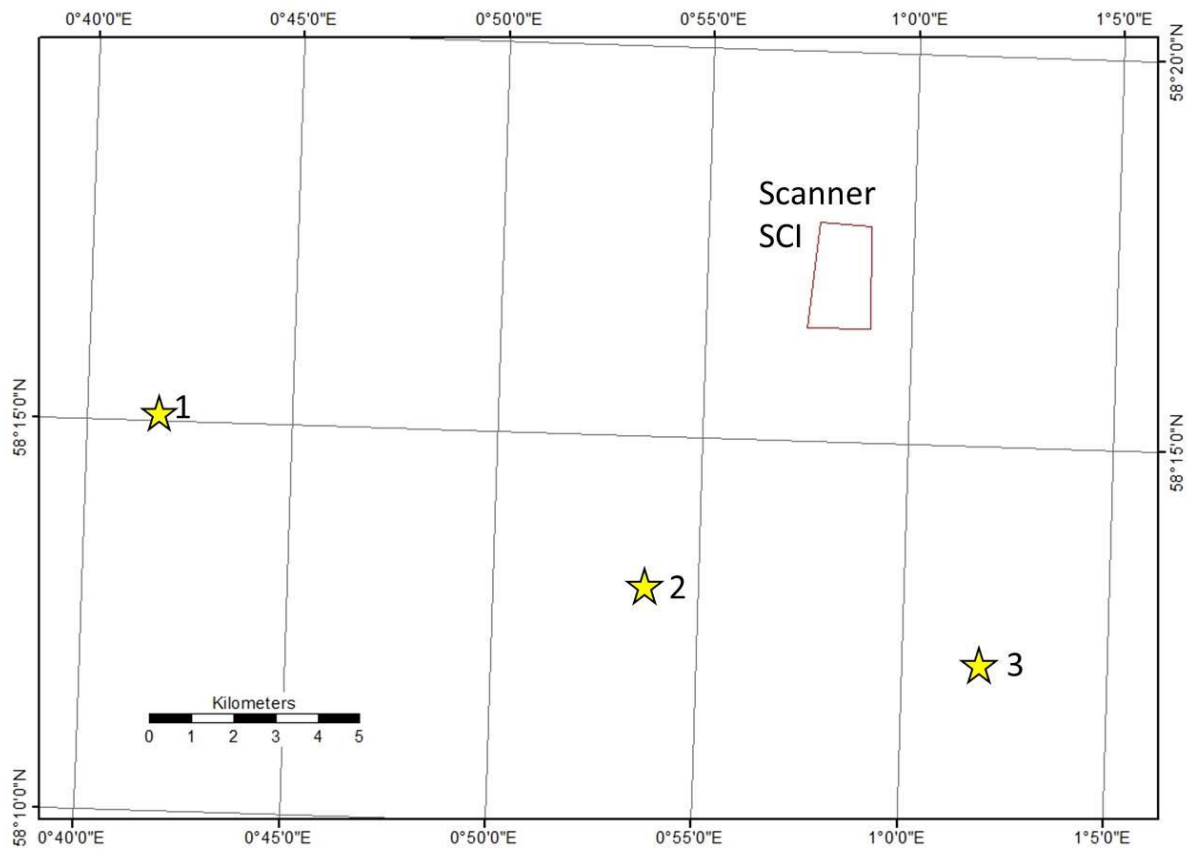


Figure 51. Earthquake epicentres between 2000 and 2014 located near the Scanner SCI.

Details of earthquake events are given in Table 2.

Table 2. Details of earthquakes located near Scanner SCI recorded between 2001 and 2014

Event	Year	Month	Day	Hour	Minute	Second	Latitude	Longitude	Depth	Local magnitude
1	2001	3	14	22	20	43.3	58.252	0.6948	19.5	3.4
2	2004	4	21	21	53	34.5	58.218	0.896	12.1	2.7
3	2008	1	9	22	39	4.66	58.204	1.032	20.2	3.1

Data from: <http://www.earthquakes.bgs.ac.uk/earthquakes/dataSearch.html>

Choice of sampling sites:

On the JNCC survey in 2012, only 9 seabed samples, out of a total of 59, were collected from within three individual pockmarks: Western Scanner, Eastern Scanner, and Southern Scotia (Cefas and JNCC, 2013). These 9 samples were all collected from the floor of the pockmarks.

All samples exhibit highly uniform particle size analysis (PSA) results, with mud percentage varying between 79.9% to 86.2%, sand percentage varying between 13.7% and 20.1% and gravel percentage not exceeding 0.2%. Surprisingly, no significant difference was observed between the PSA results from seabed samples collected within or outside of pockmarks areas. It was expected to see a greater distinction due to the gas escape, as observed in the Braemar Pockmarks SCI area. Conceptual models predict that finer material is preferentially re-suspended and dispersed by bottom currents leaving coarser material. Additionally, at the Scanner and Scotia pockmark complexes, reported outcropping of Coal Pit Formation at the base of the pockmarks should also

lead to a higher variability between the particle size analysis results from the distinct areas of the seabed sampled. It should be noted that the seabed samples taken in the base of the Scanner pockmark were of stiff clay (Dando *et al.*, 1991), part of the Coal Pit Formation.

Future sampling locations should be more representative of the features of interest and should take account of the presence of collapsed material. A more extensive sampling campaign should help to define if the infilling observed in the multibeam bathymetry dataset (within the Scotia Pockmark Complex – see Section 1.5) is generalised, and whether the events of lateral collapse are the cause of the apparent homogenisation of seabed sedimentary cover.

Lateral collapse implications:

The absence of significant increases in methane concentration in the box core samples collected from the bottom of the Western Scanner Pockmark and the similar rates of aerobic methane oxidation shown within and out of this pockmark, may imply that the methane is reaching the surface through discrete channels in the underlying clay and is not, in general, diffusing out into the bottom muds (Dando, 1990). If that is the case, the infilling observed within this pockmark could have interrupted the previously used channels of gas migration, leading to the need to develop new conduits through the recently deposited material. Additionally, the extensive infilling observed in some of the pockmarks could obscure features previously present at the seabed such as MDAC or bacterial mats.

Limits of the SCI:

Pockmarks outside of Scanner Pockmark SCI were not mapped during this study, but the existence of a vast number of pockmarks with vertical relief of 1 to 2 metres and an average area of approximately 3500 m² is already known. Two other large pockmarks of comparable size to Scanner and Scotia and having evidence of gas seepage albeit intermittent are known to occur in the proximity of the Scanner Pockmark SCI, namely the Challenger and Alkor pockmarks (Figure 50).

Future surveying

In the eleven years between the SEA2 and the JNCC surveys morphologic changes have occurred on the seabed, due to slope instability and pockmark development. However, these observations are affected by a high level of uncertainty, resulting from the different survey resolutions, positional issues, and dataset artefacts. It would be relevant to conduct a third multibeam survey to minimize these uncertainties, preferentially using equivalent settings as used during the JNCC survey. By increasing the similarity between the multibeam surveys, smaller seabed changes could be detected and it should not be necessary to have such a long time lapse between surveys. It may also be worth considering collecting data from the large pockmarks outside the Scanner SCI to contrast with the designated SCI.

High resolution seismic profiles may be able to distinguish whether slope failure within the pockmarks occurs as a single or multiple events and define the real thickness and distribution of the collapsed material. However this would probably require a deep tow seismic system to have the decimetre resolution need.

Single-beam echosounding data is mainly used to detect the seafloor depth and it would be a useful addition to the multibeam as it is capable of detecting objects in the water column to a finer resolution. Due to the high impedance contrast between water and free gas, this system could be used to detect gas bubble streams emerging from the seafloor and assess the level of gas escape.

The JNCC survey in 2012 cruise collected visual imagery. However as the drop camera frame moved along the transect above the seabed, it often struck the seafloor disturbing sediment and obscuring the field of view (ENVISION, 2013). Future surveys should aim to collect geographically referenced video and/or stills photography from ROVs or other horizontally moving units (such as AUVs) to improve the mapping of gas-related features such as MDAC, bacterial mats and gas bubbles.

To provide longer term monitoring of the site a lander could be considered with a range of sensors including temperature, pressure, current, video camera and hydrophone. This could be positioned over a suspected seepage site within any of the large pockmarks. Although the field of view of a camera may be limited, gas seepage over a wider area may be detectable with a hydrophone. Monitoring bottom water conditions may show correlations with gas flow.

9. Conclusions

A total of 67 pockmarks were identified, mapped and characterized during this study. Of the mapped pockmarks, 61 are within the Scanner Pockmark SCI.

The water depths over which the pockmarks are found varies from -149.32 to -150.75m. Most pockmarks are small to medium sized; however there are four pockmarks with an area unusually larger than the others (with over 72,000 m²). In total, more than 468,000 m² of the studied seabed were disrupted by these gas escape features. This represents 14% of the area of the Scanner Pockmark SCI. The majority of the pockmarks have a relief of between 1 m and 2 m; there are only 17 pockmarks of vertical relief >2 m, 6 with a vertical relief between 3 and 6.5 m and just 4 with a relief greater than 12 m.

The smaller pockmarks have dimensions comparable to the unit pockmarks found in other parts of the Witch Ground Basin. Besides their dimensions they also tend to present a similar geometry to what was observed in other areas, characterised by typical circular or elliptical shape in plan-view and 'V'-shaped or 'U'-shaped profiles. However, the 6 pockmarks with a vertical relief between 3 and 6.5 m present markedly elliptical shapes in plan-view with high values of eccentricity and a NNE orientation. They also present more complex profiles, the NNE-SSW profiles present asymmetric 'V'-shaped profile marked by steeper gradients in the northern segment and more gentle gradients in the southern segment.

The four unusually large pockmarks in the Scanner Pockmark SCI constitute two pockmark complexes, Scanner Pockmark Complex and Scotia Pockmark Complex, and both are comprised of two main pockmarks. Scanner Pockmark Complex includes Western Scanner (pockmark 67) and Eastern Scanner (pockmark 66), both with unusually large dimensions. These two pockmarks are approximately 265 metres apart and combined cover an area of nearly 320,000 square metres. They present quite distinct geometry in cross-sections, mainly 'U'- and 'W'-shaped instead of the typical pockmark's 'V' shape. That is the result of the presence of a marked flat bottom at the centre of both pockmarks, due to the presence of outcropping Coal Pit Formation below the Witch Ground Formation sediments. The Western Scanner is the larger of the two and the largest pockmark of the full study area, disrupting an area of the seabed of more than 221,000 m² and with a vertical relief of 16.67 m with water depth dropping from -150.75 m depth around the edge of the pockmark to -167.42 m depth at its deepest point (58.2812°N, 0.9708°E). The Eastern Scanner, in plan-view, is less than half the size of Western Scanner; however, it is only 1.35 metres shallower. This pockmark covers an area of more than 98,000 m² and presents a vertical relief of 15.32 m, with water depth dropping from -150.75 m depth around the edge of the pockmark to -166.07 m depth at its deepest point (58.2827° N, 0.9745° E).

The Scotia Pockmark Complex includes Northern Scotia (pockmark 65) and Southern Scotia (pockmark 64), which are approximately 370 metres apart and combined cover an area of almost 150,000 m². Both pockmarks cover similar areas of the seabed; Northern Scotia covers an area of 76,000 m² and Southern Scotia covers an area of more than 72,400 m². The Southern Scotia presents the greater vertical relief of the two, of 14.63 m, whereas the Northern Scotia has a vertical relief of 12.04 m. The seabed within the Southern Scotia drops to -165.38 m at its deepest point (58.2904° N, 0.9750° E) while it drops to -162.79 m at the deepest point of the Northern Scotia (58.2937° N, 0.9749° E). The Southern Scotia pockmark has the steepest slopes (max. slope 30.20° and mean slope 4.4°) of all the pockmarks studied.

Since 1983, when the Scanner Pockmark Complex was first found, a total of 11 known cruises have surveyed the area, collecting a large and varied volume of data on this seabed feature. Most cruises observed direct evidence of seepage, confirming gas release at seabed continually or recurrently for a period of more than 30 years. The occurrence of seepage over a prolonged

period of time was also confirmed by the observation of MDAC and bacterial mats at seabed. However, no gas escape activity was detected during the cruise CEND19x/12.

The overlap of multibeam data coverage between the dataset collected in 2001 and the dataset collected in 2012 allowed the study of morphological changes at seabed revealing pockmark evolution within the Scanner Pockmark SCI. Only one pockmark (pockmark 46) showed an increase in depth of the deepest point between the two surveys that appears to be due to expansion of the pockmark base towards the north (Figure 25), which may be explained by gas escape activity.

The most marked difference observed was the infilling of the some of the pockmarks. Pockmarks 47, 61, 64, 65, 66 and 67 showed infilling greater than 0.45 m and up to 1 m in thickness. Local sedimentation rates due to sediments from outwith the area cannot account for the degree of infilling measured and it is therefore believed that the pockmark infilling is the result of lateral collapse of the pockmark sidewalls. In some cases it is possible to identify the source of the material and also the distribution of the displaced material. Such extensive infilling of the base of pockmarks must have obscured features previously present at the seabed such as MDAC or bacterial mats. It could even have interrupted the pathways for fluid flow previously established.

Based on the interpretation of both sidescan and multibeam backscatter and the presence of patches of high backscatter (that have been correlated to seabed exposures of authigenic carbonates), it is believed that several pockmarks in the study area could have MDAC at or near seabed. The pockmarks with the most extensive cover of high backscatter patches are pockmarks 28, 47, 56, 59, 61, 62 and 63. Further investigation would be required to confirm the presence or absence of MDAC at these pockmarks.

The main potential sources of human physical disturbance to the seabed are related to either oil and gas exploration or fishing activity. Evidence of both these activities is present in the Scanner Pockmark SCI, where acoustic anomalies due to two exploration wells (15/25-1 and 15/25-1A) and several trawl scars were recognised on both sidescan sonar and MBES backscatter. The latter activity (as well as E&P anchor handling operations) could modify the shape of existing pockmarks but there is no conclusive evidence that human activity has triggered slope failure, leading to the potential burial of MDAC, bacterial mats or other ecosystems dependent on gas seepage.

It is suggested that this area should be monitored regularly to check if the features of interest are being compromised by natural or anthropogenic processes and to assess if the limits of the protected area are the most appropriate.

Appendix 1. List of Cruises

Cruises												
Year	1983	1985	1989	1989	1990	1991	2001	2002	2004	2005	2006	2012
Name	Conoco	Stabil	Scotia 5/89	?	CH 70 Cruise	CH 82 Cruise	OSAE	He 180	HE 208	ALKOR 259	ALKOR 290	CEND19X/12
Ship	Geo-Scanner	Lador	FRV Scotia	MV Resolution	RRS Challenger	RRS Challenger	SV Kommandor Jack	RV Heincke	RV Heincke	RV Alkor	RV Alkor	RV Endeavour
Type of survey	Geophysics	Geophysics Groundtruthing	Geophysics Groundtruthing	Geophysics Groundtruthing Biological	Geophysics Gas & water sampling Groundtruthing	Geophysics Geochemical	Geophysics	Geophysics Groundtruthing Water sampling	Geophysics Groundtruthing Geochemica Water sampling	Geophysics Groundtruthing Water sampling	Geophysics Groundtruthing Water sampling	Geophysics Groundtruthing
Equipment	Echo-sounder, sidescan sonar, Deep-tow Sparker	Echo-sounder, ROV Solo , side-scan sonar (plus??)	Echo-sounder Smith-McIntyre corer, Gravity corer, Multiple corer, and Grab	Echo-sounder, Box corer, Bottom water sampler and Agassiz trawl	Echo-sounder, sidescan sonar, Deep-tow boomer and Pinger, bottom gas samples, stable isotopes and submersible Jago	Deep Tow Boomer Side Scan Sonar (plus??)	Multibeam echo-sounder	Echo-sounder, Sediment echosounder SES2000, multicorer, vibrocorer, Camtranise and CTD/Rosette water sampler	Echo-sounder, Sediment echosounder SES2000, Gravity corer, Rümohr lot corer, TV multicorer, CTD/Rosette water sampler, mini ROV 'Spy'	Multibeam echo-sounder, OFOS, Van Veen Grab, TV Multicorer, Gravity corer, CTD/Rosette water sampler, GasQuant, Bottom water sampler, Fluid flow observatory, van Veen grab, OFOS and submersible Jago	Multibeam echo-sounder, CTD/Rosette water sampler, GasQuant, Bottom water sampler, Fluid flow observatory, van Veen grab, OFOS and submersible Jago	Multibeam echo-sounder, sidescan sonar, Sidescan sonar, Drop camera, Day Grab, Hamon Grab with a HamCam
Large Pockmarks surveyed	Scanner PC and Scotia PC	Scanner PC (plus??)	Scanner PC and Scotia PC	Scanner PC and Scotia PC	Scanner PC and Challenger P	Scanner PC, Scotia PC, and Challenger P	Scanner PC, Scotia PC, and Challenger P	Scanner PC, Scotia PC, and Challenger P	Scanner PC, Scotia PC, and Challenger P	Scanner PC, Scotia PC, Challenger P, and Alkor P.	Alkor Pockmark	Scanner PC, Scotia PC, and Challenger P
Direct Evidences of seepage	Yes ¹	Yes ²	?	Yes ³	Yes ⁴	Yes ⁵	Yes ⁶	Yes ⁷	Yes ⁸	Yes ⁹	No (only Alkor P was surveyed)	No
MDAC		Observed and sampled		?	Observed	-	-	-	Observed	Not observed	Not observed	Not observed
Bacterial Mats	-	Observed	-	?	Observed	-	-	-	Not reported	Not observed	Not observed	Not observed

- Acoustic flares on hull-mounted echosounder, deep tow sparker and towed side-scan sonar data, in both Western and Eastern Scanner pockmarks.
- Strong large acoustic flare centred over the pockmark recorded by the hull-mounted 38 kHz echosounder. Plus, photographic evidence of release of gas bubble in to the water column.
- Acoustic "plume" seen on echosounder record.
- Gas plumes were observed on deep-towed boomer records from all four pockmarks (Scanner and Scotia pockmark complexes), including twenty-one gas plumes just within Scanner Pockmark Complex. Sediment samples presented methane concentrations 3-4 orders of magnitude higher than the background. At least 27 individual gas seeps were counted during *Jago* dives.
- Gas plumes were observed on the echo-sounder Simrad EA 500 records in all the large pockmarks within the study area and individual gas seeps were imaged with the Waverly side-scan sonar in some of the pockmarks. Water sampling detected the presence of methane and hydrogen in the water column above Southern Scotia.
- Gas plumes rising from the pockmarks on both sidescan sonar and 38 kHz echosounder record.
- Gas flares were detected in all the large pockmarks using the echosounder and parametric sediment echosounder system (SES-2000DS).
- Gas flares were detected in all the large pockmarks using the echosounder and parametric sediment echosounder system (SES-2000DS). Increase of methane concentrations in the sediments from the bottom of the pockmarks. Gravity cores show increase of methane concentration with depth.
- Relatively weak gas flare was detected in the Scanner pockmark with the 38 kHz echosounder. Alkor pockmark presented the higher levels of gas release activity.

Appendix 2. Pockmark attributes

Pockmarks attribute table (Table 3), generated by the semi-automated method. The given values for latitude and longitude correspond to the position of the deepest point of the respective pockmark. Area is in square metres; Perimeter, Pockmark depth (P_Depth), Maximum Water Depth (MaxWD) and Minimum Water Depth (MinWD) are in metres; Maximum Slope Angle (MaxSlope), Mean Slope Angle (MeanSlope), Longitude (Long) and Latitude (Lat) are in decimal degrees. The highlighted rows correspond to the four unusually large pockmarks that comprise both the Scanner and Scotia pockmark complexes. The pockmarks are numbered in order by area with the smallest pockmark numbered as 1 and the largest being pockmark 67. Locations are indicated on Figure 8.

Table 3. Scanner SCI survey area Pockmark morphological attributes.

<i>ID</i>	<i>Area</i>	<i>Perimeter</i>	<i>P_Depth</i>	<i>Max WD</i>	<i>Min WD</i>	<i>Max Slope</i>	<i>Mean Slope</i>	<i>Latitude</i>	<i>Longitude</i>
1	1236.42	128	0.7	-151.0	-150.3	4.79	2.17	58.295428	0.978649
2	1297.16	130	0.7	-151.3	-150.6	3.60	1.97	58.279525	0.958460
3	1361.09	133	0.8	-150.7	-149.9	4.51	2.33	58.278967	0.978667
4	1364.38	133	0.8	-150.6	-149.8	3.72	2.18	58.293791	0.959207
5	1384.12	134	0.7	-151.4	-150.7	3.66	2.05	58.287884	0.971580
6	1412.86	136	0.8	-150.9	-150.2	4.13	2.10	58.288382	0.967870
7	1452.5	138	0.8	-150.4	-149.5	5.30	2.59	58.288479	0.981943
8	1529.4	142	0.8	-151.3	-150.5	4.74	2.32	58.281568	0.962739
9	1552.23	141	0.8	-150.6	-149.7	5.63	2.18	58.280123	0.979147
10	1577.06	144	0.8	-150.7	-149.9	5.18	2.15	58.290052	0.963411
11	1597.03	148	1.0	-151.8	-150.7	7.75	3.10	58.296489	0.977634
12	1603.32	145	0.8	-151.6	-150.8	3.90	1.89	58.286342	0.977326
13	1638.97	150	1.0	-151.7	-150.8	4.76	2.41	58.279554	0.964797
14	1711.48	150	1.0	-151.3	-150.3	5.00	2.48	58.285330	0.964466
15	1788.29	161	0.8	-150.9	-150.1	4.74	2.57	58.290818	0.957435
16	1821.25	157	0.7	-150.5	-149.8	4.87	2.13	58.290973	0.979585
17	1834.36	156	1.2	-151.8	-150.5	6.79	3.27	58.275272	0.974312
18	1883.28	159	0.8	-150.7	-149.8	4.42	2.24	58.278365	0.979213
19	1896.42	161	1.1	-150.7	-149.6	6.03	2.89	58.277030	0.982219
20	1906.79	159	0.9	-150.3	-149.3	4.30	2.23	58.280803	0.982414
21	1916.26	162	1.1	-151.4	-150.3	6.36	3.04	58.285701	0.979953

ID	Area	Perimeter	P_Depth	Max WD	Min WD	Max Slope	Mean Slope	Latitude	Longitude
22	1920.41	163	1.2	-151.6	-150.4	6.58	3.34	58.290693	0.977760
23	1931.25	160	1.1	-151.5	-150.4	5.05	2.65	58.280101	0.960779
24	1962.45	159	1.1	-151.8	-150.8	4.08	1.97	58.285311	0.971182
25	2027.57	164	0.9	-150.6	-149.7	3.50	1.87	58.295953	0.965322
26	2121.28	169	0.8	-150.5	-149.7	4.66	1.88	58.285700	0.982169
27	2184.41	171	1.1	-151.7	-150.6	4.87	2.46	58.278305	0.959621
28	2311.62	176	1.5	-151.3	-149.9	7.57	3.29	58.293773	0.970527
29	2456.92	191	1.4	-151.2	-149.8	8.51	3.61	58.284206	0.980754
30	2510.13	182	1.1	-151.9	-150.8	5.22	1.94	58.283470	0.968288
31	2517.15	186	1.3	-151.4	-150.1	5.98	2.83	58.285732	0.960455
32	2545.43	197	1.9	-152.7	-150.8	8.41	3.12	58.290312	0.976418
33	2621.16	204	1.1	-150.6	-149.4	7.65	2.59	58.294721	0.969143
34	2656.16	190	1.4	-151.5	-150.1	6.20	2.78	58.286374	0.960179
35	2656.92	189	1.4	-150.8	-149.4	6.30	3.01	58.290666	0.981750
36	2705.05	202	1.1	-151.6	-150.5	5.67	2.64	58.288080	0.970342
37	2776.7	200	2.1	-152.9	-150.7	12.48	4.34	58.285720	0.978896
38	2887.73	200	1.8	-151.5	-149.7	8.31	3.91	58.280819	0.980027
39	3016.19	204	1.6	-151.4	-149.8	9.58	3.14	58.293098	0.959690
40	3030.47	208	2.4	-153.2	-150.8	11.93	3.51	58.283788	0.977029
41	3056.52	209	1.6	-152.4	-150.8	8.29	2.77	58.278572	0.974157
42	3073.71	208	1.8	-152.0	-150.1	10.61	3.80	58.289059	0.966433
43	3112.27	205	1.6	-152.3	-150.8	7.19	2.72	58.276604	0.973418
44	3152.7	216	1.5	-151.3	-149.8	9.77	3.15	58.275044	0.976948
45	3182.36	213	1.9	-152.6	-150.8	9.33	3.37	58.280713	0.975603
46	3205.24	212	2.3	-152.4	-150.1	11.90	4.61	58.288518	0.961794
47	3244.91	212	2.1	-151.8	-149.7	12.27	4.48	58.295211	0.963830
48	3294.52	217	1.7	-152.3	-150.6	8.79	3.11	58.278814	0.957751
49	3356.05	224	1.5	-151.2	-149.7	6.83	3.14	58.291993	0.962447
50	3475.42	220	2.0	-152.7	-150.8	9.09	3.41	58.274676	0.963919

ID	Area	Perimeter	P_Depth	Max WD	Min WD	Max Slope	Mean Slope	Latitude	Longitude
51	3827.25	236	1.1	-151.9	-150.8	3.54	1.26	58.289632	0.973150
52	3832.27	235	2.2	-152.9	-150.8	11.30	3.88	58.278520	0.964073
53	4651.6	260	2.4	-153.1	-150.8	9.66	2.46	58.275902	0.967665
54	4708.53	251	1.7	-152.5	-150.8	6.11	1.79	58.285189	0.977119
55	4936.23	270	3.1	-152.9	-149.8	13.96	4.42	58.276137	0.977976
56	4952.81	273	3.0	-153.8	-150.8	13.71	4.76	58.296082	0.976873
57	5396.03	268	1.6	-152.3	-150.8	4.77	1.41	58.287971	0.974779
58	5497.03	279	2.0	-152.7	-150.8	5.51	1.68	58.277852	0.971745
59	6454.99	309	2.7	-153.5	-150.8	14.27	3.40	58.275907	0.970254
60	6947.7	321	4.3	-155.1	-150.8	18.05	4.66	58.288222	0.975924
61	15716.16	597	4.1	-154.5	-150.3	21.51	3.48	58.289228	0.957867
62	16617.36	544	4.6	-155.4	-150.8	15.67	2.84	58.278053	0.973130
63	25848.44	715	6.1	-156.9	-150.8	21.23	3.21	58.277353	0.967479
64	72419.08	1069	14.6	-165.4	-150.8	30.20	4.40	58.290398	0.975015
65	76007.71	1053	12.0	-162.8	-150.8	20.05	3.59	58.293700	0.974929
66	98048.73	1261	15.3	-166.1	-150.8	23.41	3.85	58.282689	0.974535
67	221625.3	1864	16.7	-167.4	-150.8	19.08	2.96	58.281230	0.970836

Appendix 3. Current data provided by BODC

Modern bottom water current data held by the British Oceanographic Data Centre (BODC) near the Scanner Pockmark SCI (Table 4). Latitude and Longitude given in decimal degrees; duration in days; sea floor depth, series depth in metres and series height above seafloor in metres. Summary results are given in Figure 52.

Table 4. BODC data sets with bottom water data examined by Gafeira *et al.* 2012.

<i>BODC reference</i>	<i>Latitude</i>	<i>Longitude</i>	<i>Series duration</i>	<i>Sea floor depth</i>	<i>Series depth</i>	<i>Series height above seafloor</i>
10786	57.8899	-0.7116	16	90	80	10
10958	58.0179	-0.4894	57	115	105	10
10995	58.4271	1.3464	49	136	126	10
12965	57.9966	0.5116	23	148	121	27
26395	58.4267	0.0017	59	140	135	5
62138	58.6877	0.8048	121	140	126	14
430165	58.5363	0.0987	125	142	130	12

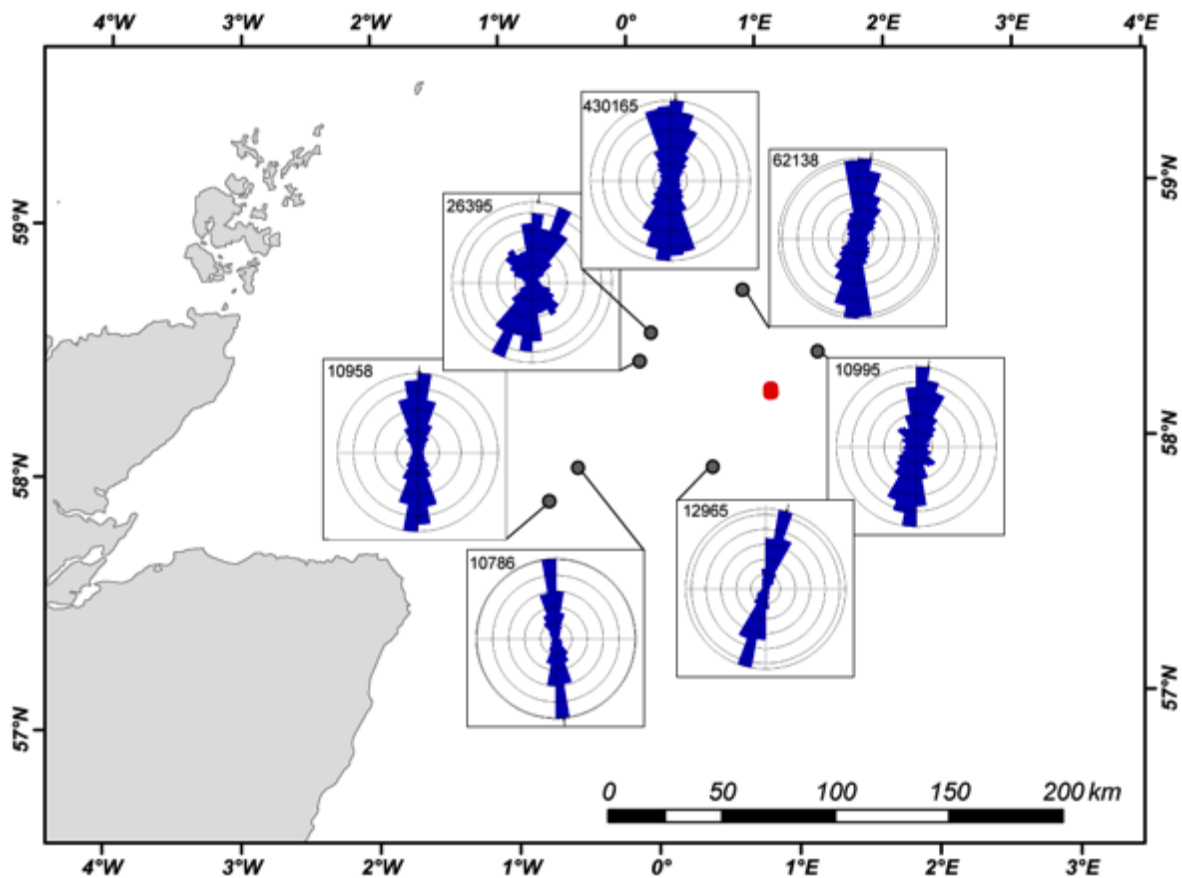


Figure 52. Rose diagrams showing the current direction of modern bottom waters (generally less than 15m above seafloor).

Data provided by the BODC. Red dot shows the location of the Scanner Pockmark SCI. Derived from Gafeira *et al.* (2012).

Appendix 4. UK Benthos data for the Blenheim Platform

UK Benthos is a database of offshore environmental benthic surveys, since 1975, in the UK sector of the North Sea. This data was brought together by oil companies that were members of the United Kingdom Offshore Operators Association (now Oil & Gas UK) and have made it accessible via the Internet.

See http://www.oilandgasuk.co.uk/knowledgecentre/uk_benthos_database.cfm.

The table below corresponds to an extract of this dataset with some of the information referred to the site near the Blenheim field. This gives the sample station unique code; station location in UTM; distance from the platform to the station and depth of sample in metres, the sediment median grain size in Phi units (MDO), the sediment silt/clay content (Silt/Clay), and the hydrocarbon content determined by gas chromatography in µg/g (TOT_HC_GC).

Table 5. Data extracted from the UK Benthos dataset for the sample stations collected in the vicinity of the Blenheim platform (58° 16.33'N, 01° 00.27'E).

<i>Station</i>	<i>UTM E</i>	<i>UTM N</i>	<i>Distance</i>	<i>Depth</i>	<i>MDO</i>	<i>Silt/Clay</i>	<i>TOT_HC_GC</i>
BLE0001	383140	6461804	500	0	5.42	83.5	18.7
BLE0002	383136	6461500	200	0	5.5	84.6	126.9
BLE0003	383139	6461400	100	0	5.18	79	22.8
BLE0004	383146	6461354	50	0	5.05	75.8	7.1
BLE0005	383140	6461308	0	0	5.12	70.6	110.2
BLE0006	383137	6461266	50	180	5.31	83.8	20.8
BLE0007	383134	6461218	100	180	5.23	80.4	125.6
BLE0008	383138	6461121	200	180	5.34	82.1	68.9
BLE0009	383128	6460800	500	180	5.4	83.2	11.7
BLE0010	382638	6461301	500	270	5.45	85.4	6.1
BLE0011	382935	6461300	200	270	5.37	82.9	11.8
BLE0012	383042	6461298	100	270	5.35	83.1	50.6
BLE0013	383095	6461312	50	270	5.34	83.3	135.7
BLE0014	383194	6461308	50	90	5.29	81.2	264.8
BLE0015	383234	6461309	100	90	5.42	84.1	98.5
BLE0016	383339	6461306	200	90	5.48	85.1	7.7
BLE0017	383633	6461315	500	90	5.35	83.1	7.2
BLE0018	382996	6461441	200	315	5.43	84.4	16.3
BLE0019	383067	6461380	100	315	5.29	82	8.2
BLE0020	383101	6461341	50	315	5.28	81	67
BLE0021	383122	6461324	25	315	5.3	84	3.7

<i>Station</i>	<i>UTM E</i>	<i>UTM N</i>	<i>Distance</i>	<i>Depth</i>	<i>MDO</i>	<i>Silt/Clay</i>	<i>TOT_HC_GC</i>
BLE0001	383140	6461804	500	0	5.42	83.5	18.7
BLE0002	383136	6461500	200	0	5.5	84.6	126.9
BLE0003	383139	6461400	100	0	5.18	79	22.8
BLE0004	383146	6461354	50	0	5.05	75.8	7.1
BLE0022	383152	6461298	25	135	5.51	77.1	32.8
BLE0023	383177	6461265	50	135	5.4	82.9	263.1
BLE0024	383208	6461233	100	135	5.36	82.6	89.4
BLE0025	383279	6461162	200	135	5.33	82.9	7.8
BLE0026	383284	6461447	200	45	5.44	85.2	81.3
BLE0027	383213	6461374	100	45	5.35	82	42.7
BLE0028	383175	6461340	50	45	5.25	81.9	279.2
BLE0029	383154	6461340	25	45	5.27	82.4	48.1
BLE0030	383118	6461289	25	225	5.99	87.8	113.5
BLE0031	383104	6461274	50	225	5.25	80.7	14.9
BLE0032	383070	6461240	100	225	5.24	81.2	7.5
BLE0033	383000	6461175	200	225	5.17	78.2	27.5
BLE0034	381722	6459893	2000	225	5.41	85.2	12.8
BLE0035	379606	6457770	5000	225	5.54	88.3	8.1
BLE0001	383140	6461804	500	150.6	5.42	83.5	18.7
BLE0002	383136	6461500	200	151.5	5.5	84.6	126.9
BLE0003	383139	6461400	100	150.4	5.18	79	22.8
BLE0004	383146	6461354	50	150.5	5.05	75.8	7.1
BLE0005	383140	6461308	0	150	5.12	70.6	110.2
BLE0006	383137	6461266	50	149.8	5.31	83.8	20.8
BLE0007	383134	6461218	100	150.4	5.23	80.4	125.6
BLE0008	383138	6461121	200	149.6	5.34	82.1	68.9
BLE0009	383128	6460800	500	149.4	5.4	83.2	11.7
BLE0010	382638	6461301	500	150.1	5.45	85.4	6.1
BLE0011	382935	6461300	200	148.8	5.37	82.9	11.8
BLE0012	383042	6461298	100	149.7	5.35	83.1	50.6
BLE0013	383095	6461312	50	149.6	5.34	83.3	135.7

<i>Station</i>	<i>UTM E</i>	<i>UTM N</i>	<i>Distance</i>	<i>Depth</i>	<i>MDO</i>	<i>Silt/Clay</i>	<i>TOT_HC_GC</i>
BLE0001	383140	6461804	500	0	5.42	83.5	18.7
BLE0002	383136	6461500	200	0	5.5	84.6	126.9
BLE0003	383139	6461400	100	0	5.18	79	22.8
BLE0004	383146	6461354	50	0	5.05	75.8	7.1
BLE0014	383194	6461308	50	148.9	5.29	81.2	264.8
BLE0015	383234	6461309	100	149	5.42	84.1	98.5
BLE0016	383339	6461306	200	149.1	5.48	85.1	7.7
BLE0017	383633	6461315	500	149	5.35	83.1	7.2
BLE0018	382996	6461441	200	150	5.43	84.4	16.3
BLE0019	383067	6461380	100	150.2	5.29	82	8.2
BLE0020	383101	6461341	50	150.3	5.28	81	67
BLE0021	383122	6461324	25		5.3	84	3.7
BLE0022	383152	6461298	25	150.8	5.51	77.1	32.8
BLE0023	383177	6461265	50	149.8	5.4	82.9	263.1
BLE0024	383208	6461233	100	150.2	5.36	82.6	89.4
BLE0025	383279	6461162	200	153.8	5.33	82.9	7.8
BLE0026	383284	6461447	200	150.4	5.44	85.2	81.3
BLE0027	383213	6461374	100	149.9	5.35	82	42.7
BLE0028	383175	6461340	50	150	5.25	81.9	279.2
BLE0029	383154	6461340	25	149.6	5.27	82.4	48.1
BLE0030	383118	6461289	25		5.99	87.8	113.5
BLE0031	383104	6461274	50	149.9	5.25	80.7	14.9
BLE0032	383070	6461240	100	151.7	5.24	81.2	7.5
BLE0033	383000	6461175	200	151.9	5.17	78.2	27.5
BLE0034	381722	6459893	2000	150.4	5.41	85.2	12.8
BLE0035	379606	6457770	5000	152.7	5.54	88.3	8.1

Appendix 5. Previous depictions of the Scanner Pockmark Complex



Figure 53. Figure presented by Hovland and Sommerville (1985) showing the location of gas seepage within the Scanner Pockmark Complex.

Bathymetry based on the data collected in 1983 during the CONOCO site survey (GEOTEAM, 1983). Darker areas indicate areas of exposure of firm clay at seabed. The Scotia Pockmark Complex lies at the northern edge of this map.

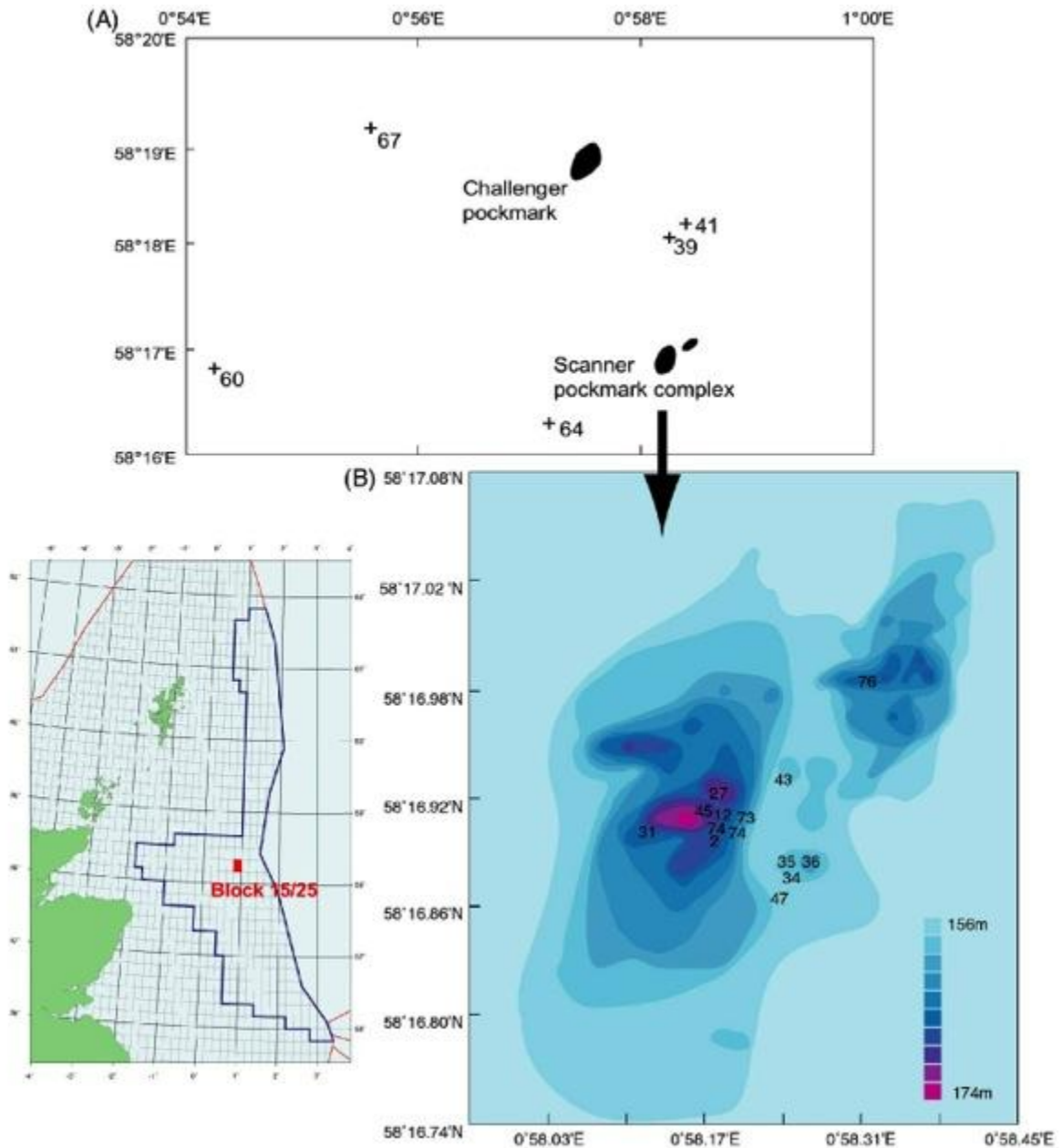


Figure 55. Location of stations samples during RRS Challenger Cruise 70 to the Scanner and Challenger pockmarks in 1990.

Note that the sample station initial digit 7 was omitted for clarity, e.g. 34 is Station 734. Figure extracted from the technical report produced for the Strategic Environmental Assessment – SEA2 by Dando (2001).

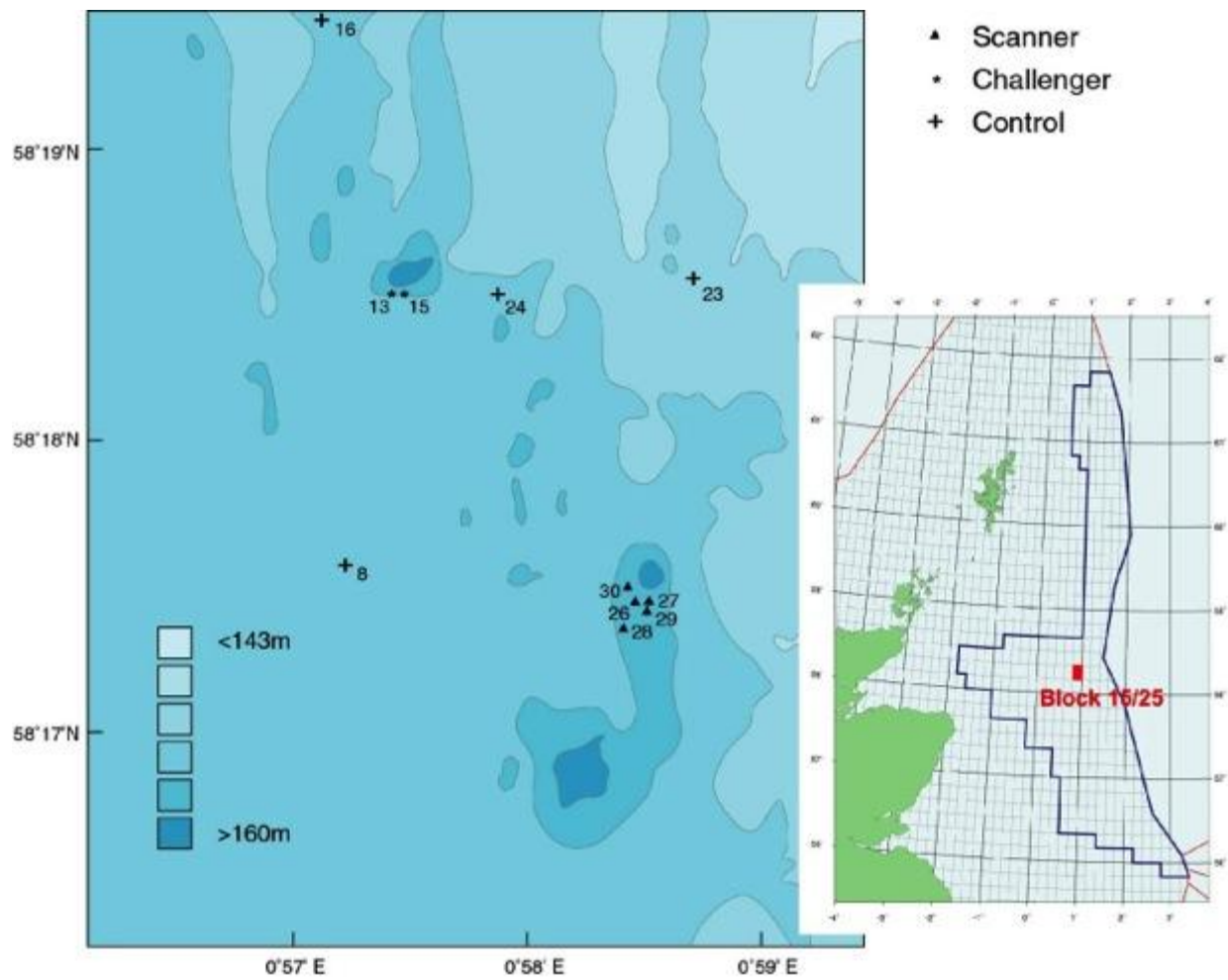


Figure 56. Location of stations sampled during the 1991 RRS Challenger Cruise 82.

Note that in this figure the stations (8)27 to (8)30 sampled located within the Scotia Pockmark Complex are labelled with a triangle, which stands for Scanner Pockmark Complex. Figure extracted from Dando (2001).

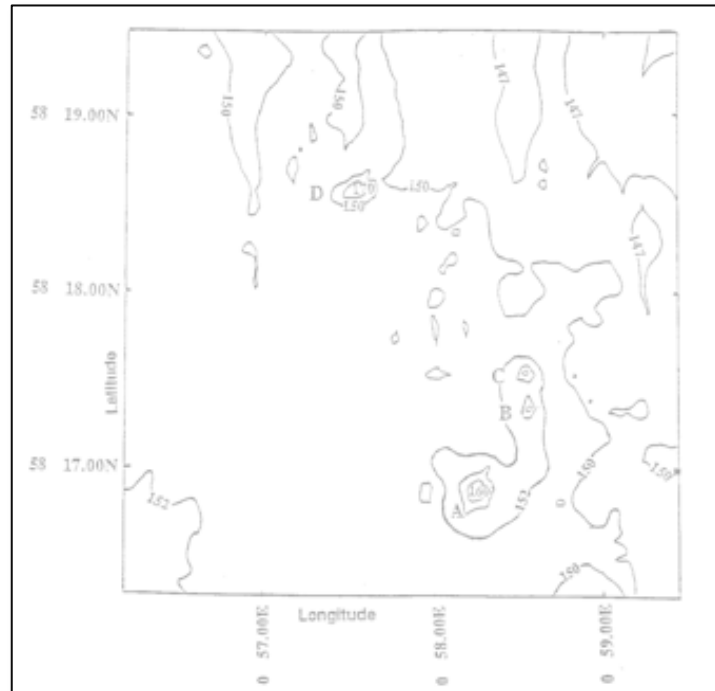


Figure 57. Figure extracted from the 1991 Challenger 82 cruise report (Dando, 1991).

Note that Scotia is recognised to be a pockmark complex comprised of two depressions (B and C), whereas Scanner is still described as a single pockmark (A).

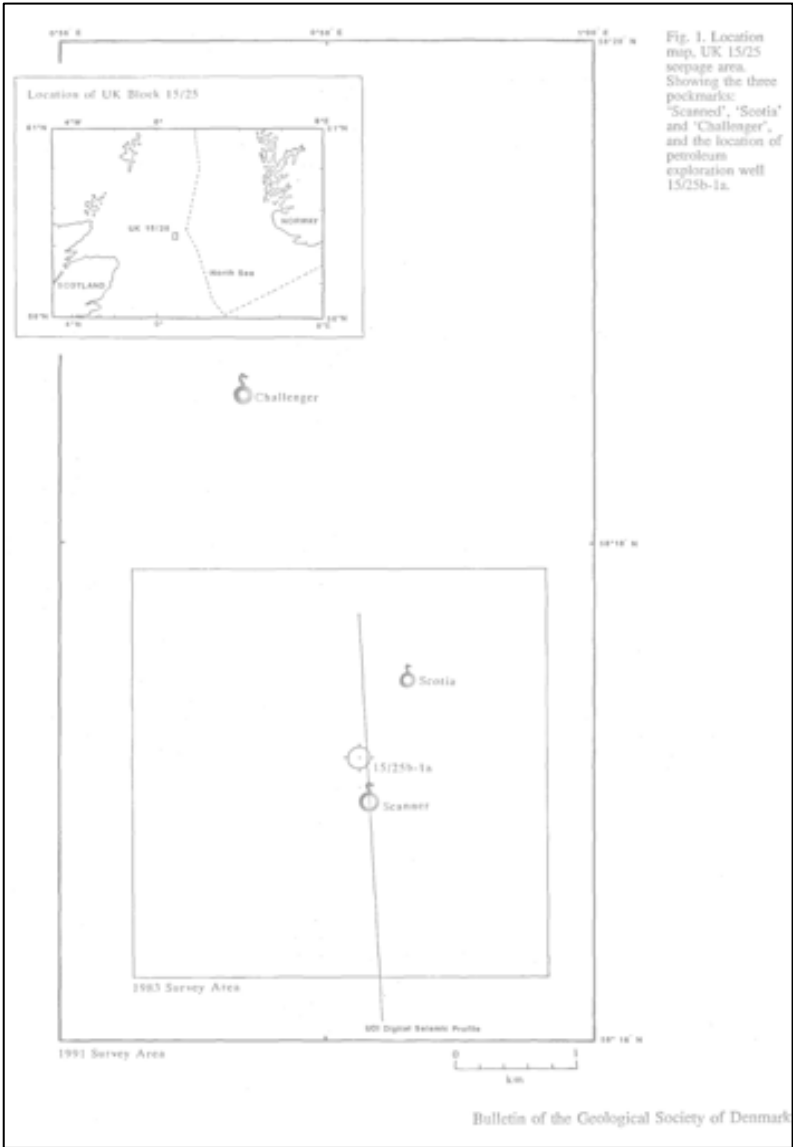


Figure 58. Figure extracted from Judd *et al.* (1994).

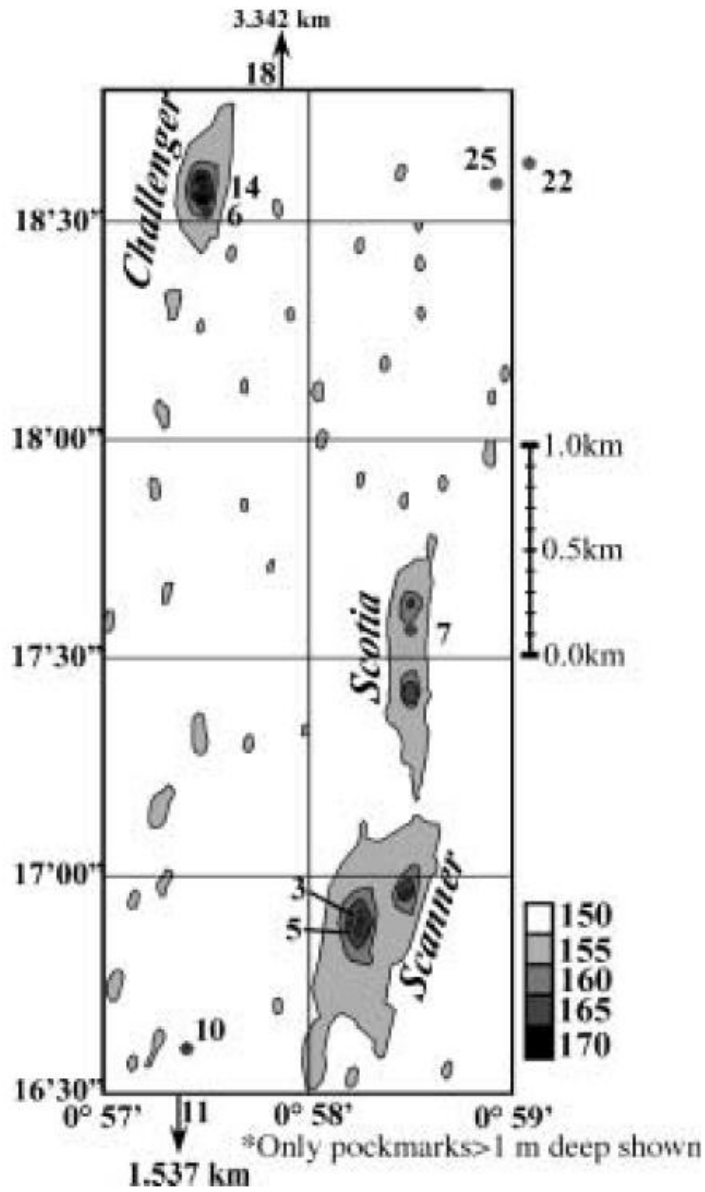


Figure 59. Map showing the pockmarks Challenger, Scotia, and Scanner, compiled from MBES data acquired by the UK government (Department of Trade and Industry) in 2000 as part of the Strategic Environmental Assessment process.

Both Scanner and Scotia are recognised as pockmark complexes rather than comprising one single depression. (Source: Leifer and Judd, 2002).

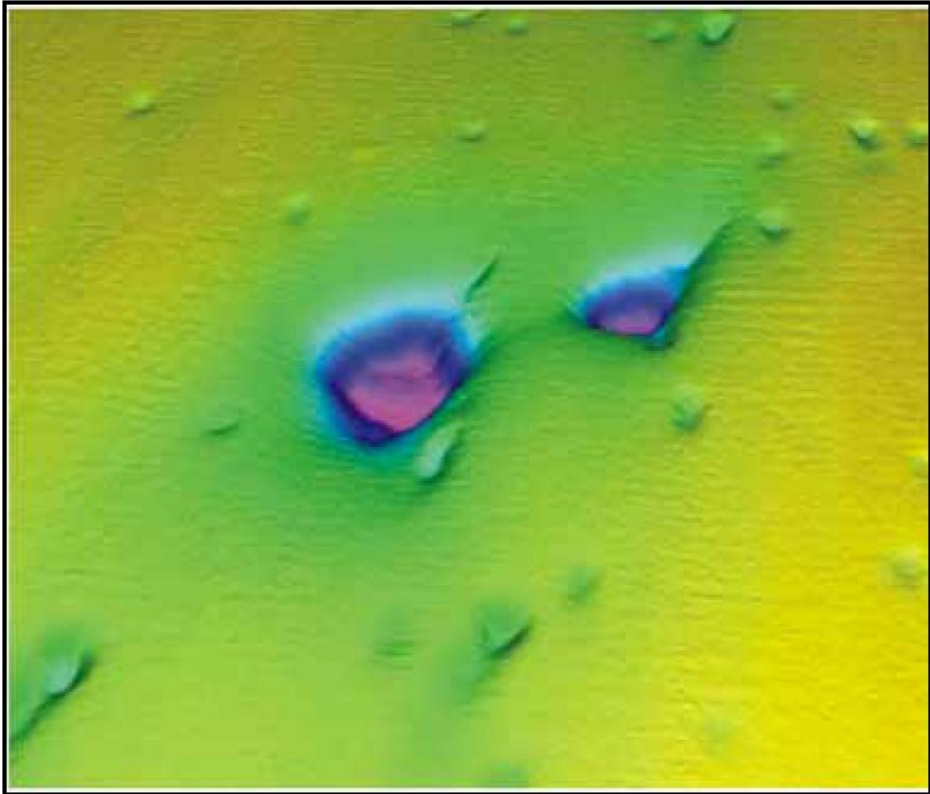


Figure 60. 3D view of the Scanner Pockmark Complex. Figure extracted from Judd (2001).

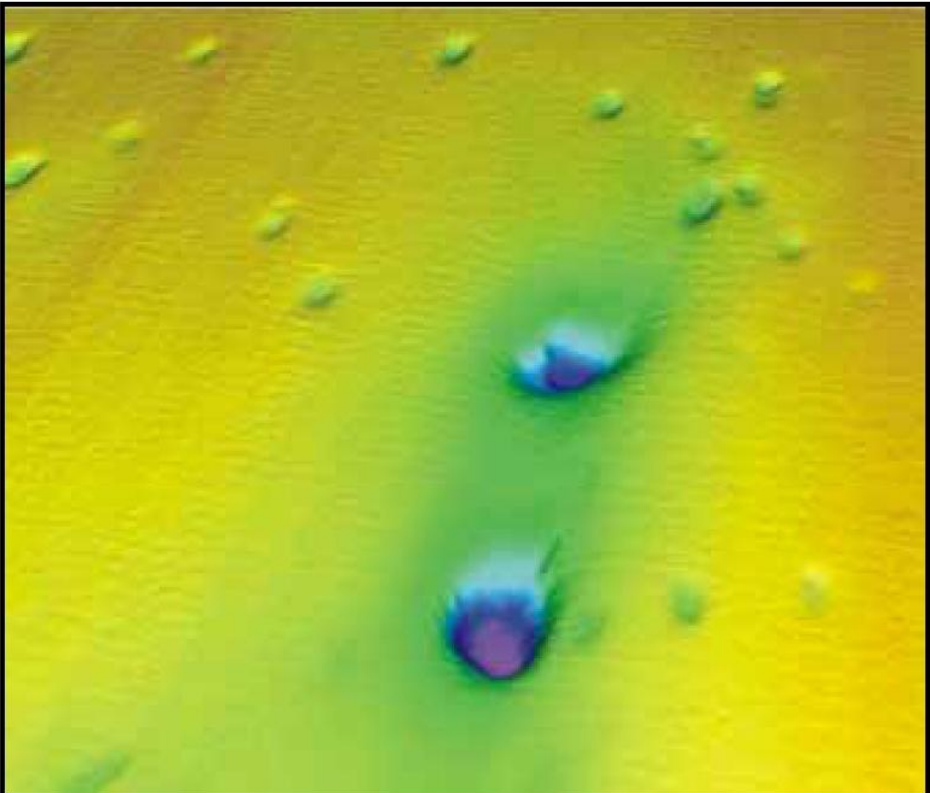


Figure 60. 3D view of the Scotia Pockmark Complex. Figure extracted from Judd (2001).

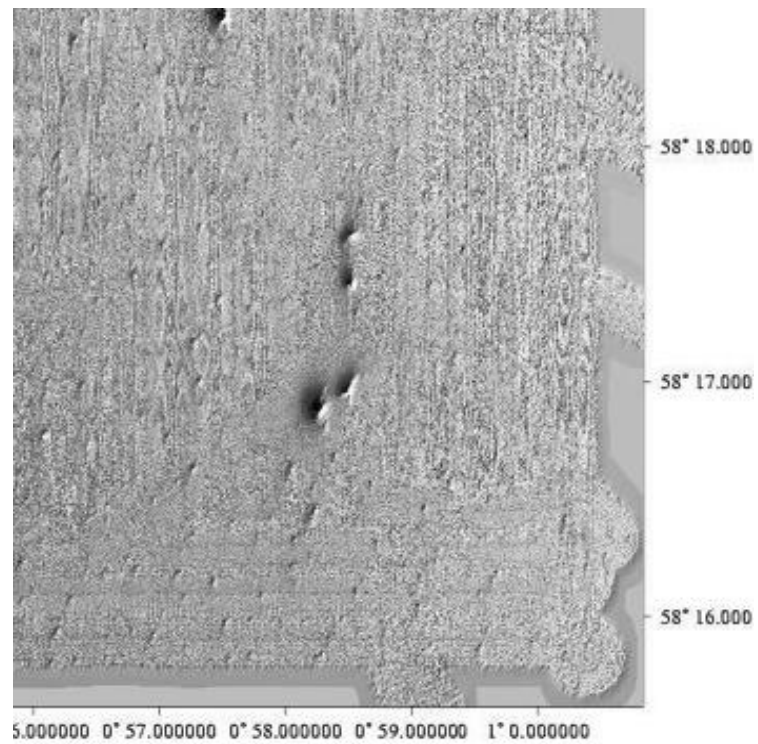


Figure 61. Bathymetric data collected, in 2005, during the IFM-GEOMAR cruise (ALKOR 259), on board of the RV Alkor.

Source : GEOMAR

Appendix 6. Pockmarks Summary

Table 6. Pockmark characteristics inferred from the interpretation of the JNCC multibeam dataset.

<i>ID</i>	<i>Area</i>	<i>Pockmark Depth</i>	<i>Lateral Collapse</i>	<i>High Backscatter</i>	<i>In/Out of SCI</i>
1	1236	0.68	N	-	In
2	1297	0.74	N	-	Out
3	1361	0.82	γ?	-	In
4	1364	0.83	γ?	-	Out
5	1384	0.72	N	-	In
6	1413	0.75	γ?	-	In
7	1453	0.84	N	-	In
8	1529	0.76	N	-	In
9	1552	0.84	N	-	In
10	1577	0.83	γ?	Y	In
11	1597	1.04	N	-	In
12	1603	0.84	N	-	In
13	1639	0.95	N	-	In
14	1711	1.04	N	Y	In
15	1788	0.81	N	Y	Out
16	1821	0.72	N	Y	In
17	1834	1.22	Y	-	In
18	1883	0.84	n	-	In
19	1896	1.12	N	-	In
20	1907	0.93	minor	-	In
21	1916	1.1	n	-	In
22	1920	1.23	N	-	In
23	1931	1.11	N	Y	In
24	1962	1.05	N	-	In
25	2028	0.86	N	-	In
26	2121	0.84	N	-	In
27	2184	1.13	n	-	In
28	2312	1.46	N	Y	In
29	2457	1.35	N	-	In
30	2510	1.11	N	-	In
31	2517	1.25	γ?	Y	In
32	2545	1.91	N	Y	In

Geological investigation of pockmarks in the Scanner Pockmark SCI area

33	2621	1.11	n	-	In
34	2656	1.35	N	Y	In
35	2657	1.39	N	-	In
36	2705	1.08	N	Y	In
37	2777	2.14	N	-	In
38	2888	1.8	N	Y	In
39	3016	1.63	N	-	Out
40	3030	2.44	N	Y	In
41	3057	1.62	n	Y	In
42	3074	1.83	y?	Y	In
43	3112	1.59	N	Y	In
44	3153	1.51	N	Y	In
45	3182	1.85	N	-	In
46	3205	2.26	N	-	In
47	3245	2.11	Y	Y	In
48	3295	1.73	Y	Y	Out
49	3356	1.51	N	-	In
50	3475	1.95	N	Y	In
51	3827	1.13	N	-	In
52	3832	2.15	N	Y	In
53	4652	2.39	N	-	In
54	4709	1.73	N	Y	In
55	4936	3.06	N	Y	In
56	4953	3	N	Y	In
57	5396	1.59	N	-	In
58	5497	1.98	N	-	In
59	6455	2.73	N	Y	In
60	6948	4.32	N	Y	In
61	15716	4.12	Y	Y	Out
62	16617	4.64	N	Y	In
63	25848	6.12	N	Y	In
64	72419	14.63	Y	Y	In
65	76008	12.04	Y	Y	In
66	98049	15.32	Y	Y	In
67	221625	16.67	Y	Y	In

Glossary

Acquisition footprint	Area of the seafloor represented by a single datapoint. This is the area insonified by a single sounding.
Authigenic	Formed <i>in situ</i> ; crystallized in place.
BGS	British Geological Survey
Biogenic gas	Gas generated by microbes, including bacteria and arachaea.
BODC	British Oceanographic Data Centre
DDM	Digital Depth Model
DECC	Department of Energy and Climate Change
Holocene	The geological epoch beginning at the end of the last ice age, spanning the last 10,000 years. Together with the preceding Pleistocene epoch forms the Quaternary period
JNCC	Joint Nature Conservation Committee
MDAC	Methane-Derived Authigenic Carbonate
Pleistocene	The geological epoch from 2.5 million to 10,000 years ago. This period of time was characterized by frequent climatic changes from ice ages to interglacial conditions.
PSA	Particle Size Analysis
Quaternary	Geological period covering the last 2.5 million years comprising the Pleistocene and the Holocene.
ROV	Remotely Operated underwater Vehicle
SCI	Site of Community Importance
SSS	SideScan Sonar
Thermogenic	Term applied to gas derived from thermocatalytic processes at high temperatures and pressures deep below the seabed.
TWT	Two-Way-Time
UKCS	United Kingdom Continental Shelf
WGB	Witch Ground Basin, the topographical depression in the central North Sea reaching more than 150m water depth, 200km north east of Aberdeen.
WGF	Witch Ground Formation, a geological stratigraphic unit based on seismic data; thought to be of Late Glacial to Holocene age.

References

British Geological Survey holds most of the references listed below, and copies may be obtained via the library service subject to copyright legislation (contact libuser@bgs.ac.uk for details). The library catalogue is available at: <http://geolib.bgs.ac.uk>.

- ANDREWS, I.J., LONG, D., RICHARDS, P.C., THOMSON, A.R., BROWN, S., CHESHER, J.A. and MCCORMAC, M., 1990. *United Kingdom offshore regional report: The Geology of the Moray Firth*. London: HMSO for the British Geological Survey. 93pp.
- AUSTEN, M.C., WARWICK, R.M. and RYAN, K.P., 1993. *Astomonema southwardorum* sp. nov., a gutless nematode dominant in a methane seep area in the North Sea. *Journal of the Marine Biological Association of the United Kingdom*, 73, 627-634.
- BERRY, J.A. and WELLS, P.G. 2004. Integrated fate modeling for exposure assessment of produced water on the Sable Island Bank (Scotian Shelf, Canada). *Environmental toxicology and chemistry*. 23, 2483-2493.
- BOETIUS A. 2004. *Cruise report He 208: Methane Seepage in the North Sea*. WP1 Deliverable 1.2.5. MPI-Bremen (Germany), 23 pp.
- BRADSHAW C., VEALE L.O. and BRAND A.R. 2002. The role of scallop-dredge disturbance in long-term changes in Irish Sea benthic communities: a re-analysis of an historical dataset. *Journal of Sea Research*, 47, 161-184.
- BRADWELL, T., STOKER, M., GOLLEDGE, N., WILSON, C., MERRITT, J., LONG, D., EVEREST, J., HESTVIK, O.B., STEVENSON, A., HUBBARD, A., FINLAYSON, A. and MATHERS, H. 2008. The northern sector of the Last British Ice Sheet: maximum extent and demise. *Earth Science Reviews*, 88, 207-226.
- BRITISH GEOLOGICAL SURVEY. 1986. Fladen, Sheet 58° N-00°, Sea Bed Sediments. 1:250000. (Keyworth, Nottingham: British Geological Survey).
- BRITISH GEOLOGICAL SURVEY. 1988. Fladen, Sheet 58° N-00°, Quaternary Geology. 1:250000. (Keyworth, Nottingham: British Geological Survey).
- CEFAS and JNCC, 2013. Braemar CSAC, Scanner CSAC and Turbot Bank SMPA Search Location Survey Report. 132pp.
- CLAYTON, C.J. and DANDO, P.R. 1996. Comparison of seal leakage and surface seepage rates. In: D. Schumacher & M.A. Abrams, eds. - Hydrocarbon Migration and its near-surface expression. American Association of Petroleum Geologists Memoir 66, 169-171.
- DANDO, P. R., 1990. *Survey report: RRS Challenger Cruise 70*, Plymouth Marine Biological Association of the United Kingdom, 19 pp.
- DANDO, P.R., 1991. *Cruise report for RRS "Challenger" Cruise 82*. Plymouth Marine Biological Association of the United Kingdom, 53 pp.
- DANDO, P.R. 2001. A review of pockmarks in the UK part of the North Sea, with particular respect to their biology. *Technical report produced for Strategic Environmental Assessment – SEA2*. UK: Department of Trade and Industry.
- DANDO, P.R. 2010. Biological communities at marine shallow-water vent and seep sites. In: Kiel, S. (Ed.), The vent and seep biota – from microbes to ecosystems. *Topics in Geomicrobiology*, 33, 333-378
- DANDO, P.R., AUSTEN, M.C., BURKE, R.A., KENDALL, M.A., KENNICUTT II, M.C., JUDD, A.G., MOORE, D.C., O'HARA, S.C.M., SCHMALJOHANN, R., and SOUTHWARD, A.J. 1991. Ecology of a North Sea pockmark with an active methane seep. *Marine Ecology Progress Series*, 70, 49-63.
- DECC, 2011. Offshore Oil & Gas Licensing 27 Seaward Round Central North Sea Habitats Regulations Assessment Appropriate Assessment. *Department of Energy and Climate Change, UK*, 26 pp plus appendices. <https://www.gov.uk/government/consultations/27th-seaward-licensing-round>
- DECC, 2013. Offshore Oil & Gas Licensing 27th Seaward Round Central North Sea Blocks 9/27, 15/20f, 15/24a, 15/25c, 16/2c, 16/16. Habitats Regulations Assessment Appropriate Assessment. 34 pp.
- ELKINS, S.R. 1977. *Recent sediments of the Northern North Sea: factors controlling their composition and distribution*. M.Sc thesis, University of Minnesota.
- ENVISION, 2013. PMPA Video Analysis Report: Scanner Pockmark, 2012-1035-Scanner Report for CEFAS. 11pp.
- ERLENKEUSER, H. 1979. Environmental effects on radiocarbon in coastal marine sediments. 453-469 In: Berger, R. and Suess, H.E. (eds) *Radiocarbon Dating*, University of California Press.
- GAFEIRA, J, LONG, D and DIAZ-DOCE, D. 2012. Semi-automated characterisation of seabed pockmarks in the central North Sea. *Near Surface Geophysics*, 10, 303-314.

- GAGE, J.D., ROBERTS, J.M., HARTLEY, J.P. and HUMPHERY, J.D. 2005. Potential impacts of deep-sea trawling on the benthic ecosystem along the northern European continental margin: a review. *In: Barnes, P. W. & Thomas, J. P. Eds. Benthic habitats and the effects of fishing. American Fisheries Society Symposium* 41: 503-517.
- GEOTEAM 1983. Site survey Location 15/25b –A, Conoco Report No. 0664.
- HALL-SPENCER, J., ALLAIN, V. and FOSSÅ, J.H. 2002. Trawling Damage to Northeast Atlantic Ancient Coral Reefs. *Proceedings of the Royal Society Of London, B.* 269, 507-511.
- HEDGES, R.E.M, HOUSLEY, R.A., LAW, I.A., PERRY, C. and HENDY, E. 1988 Radiocarbon dates from the Oxford AMS System, *Archaeometry Datalog* 8, *Archaeometry* 30, 291-305.
- HOLMES, R. 1977. Quaternary deposits of the central North Sea 5. The Quaternary geology of the UK sector of the North Sea between 56° and 58° N. *Report of the Institute of Geological Sciences*, No. 77/14.
- HOLMES, R. and STOKER, S.J.. 2005 Investigation of the origin of shallow gas in outer Moray Firth open blocks 15/20c and 15/25d. British Geological Survey, Report CR/05/030N. 34pp.
- HOVLAND, M. 2012. The geomorphology and nature of seabed seepage processes, *In: Bathymetry and Its Applications*, Blondel, P. (Ed.), InTech, 148 pp. Available from: <http://www.intechopen.com/books/bathymetry-and-its-applications/the-geomorphology-and-nature-of-seabed-seepage-processes>.
- HOVLAND, M. and IRWIN, H. 1989, Hydrocarbon leakage, biodegradation and the occurrence of shallow gas and carbonate cement: Norwegian Petroleum Society Conference on Shallow Gas and Leaky Reservoirs.
- HOVLAND, M, and JUDD, A.G. 1988. *Seabed pockmarks and seepages impact on geology, biology and the marine environment*. Graham & Trotman, London.
- HOVLAND, M. and SOMMERVILLE, J. 1985. Characteristics of Two Natural Gas Seepages in the North Sea. *Marine and Petroleum Geology*, 2, 319-326.
- HOVLAND, M., TALBOT, M.R., QVALE, H., OLAUSSEN, S. and AASBERG, L. 1987. Methane-related carbonate cements in pockmarks of the North Sea. *Journal of Sedimentary Research*, 57, 881 – 892.
- HOVLAND, M., HEGGLAND, R., DE VRIES, M.H. and TJELTA, T.I. 2010. Unit pockmarks and their potential significance for predicting fluid flow. *Marine and Petroleum Geology*, 27, 1190-1199.
- HOVLAND, M., JENSEN, S. and FICHLER, C. 2012. Methane and Minor Oil Macro-Seep Systems — Their Complexity and Environmental Significance. *Marine Geology*, 332–334, 163-173.
- JOHNSON, H., RICHARDS, P.C., LONG, D., AND GRAHAM, C.C, 1993. United Kingdom Offshore Regional Report, The Geology of the Northern North Sea. *British Geological Survey Regional Report*.
- JOHNSON, T.C. and ELKINS, S.R. 1979. Holocene deposits of the northern North Sea: evidence for dynamic control of their mineral and chemical composition. *Geologie en Mijnbouw*, 58, 353-366.
- JONES, R. W., 1993. Preliminary observations on benthonic foraminifera associated with biogenic gas seep in the North Sea, *In: Applied Micropalaeontology* (Editor: Jenkins, D.G.), pp. 69-91. Kluwer Academic Publishers.
- JUDD, A.G. 2001. Pockmarks in the UK Sector of the North Sea, Technical Report TR_002, Technical report produced for Strategic Environmental Assessment - SEA2, DTI.
- JUDD, A.G. and HOVLAND, M. 2007. *Seabed Fluid Flow. Impact of geology, biology and the marine environment*. Cambridge University Press. 475 pp.
- JUDD, A.G., LONG, D. and SANKEY, M. 1994. Pockmark formation and activity, UK block 15/25, North Sea. *Bulletin of the Geological Survey of Denmark*, 41, 34-49.
- KROST, P., BERNHARD, M., WERNER, F. and HUKRIEDE, W. 1990. Otter trawl tracks in Kiel Bay (Western Baltic) mapped by side-scan sonar. *Meeresforsch* 32, 344-353.
- LEIFER, I. and JUDD, A.G. 2002. Oceanic methane layers: the hydrocarbon seep bubble deposition hypothesis. *Terra Nova*, 14, 417–424.
- LEIFER, I. and PATRO, R.K. 2002. The bubble mechanism for methane transport from the shallow sea bed to the surface: A review and sensitivity study. *Continental Shelf Research*, 22, 2409–2428.
- LONG, D. 1991. The identification of features due to former permafrost in the North Sea. *In: Forster, A., Culshaw, M.G., Cripps, J.C., Little, J.A. and Moon, C.F. (eds) Quaternary Engineering Geology*, Geological Society of London, *Engineering Geology Special Publication*, No 7, 369-372.
- LONG, D. 1992. Devensian Late-glacial gas escape in the central North Sea. *Continental Shelf Research*. 12, 1097-1110.
- LONG, D. and MORTON, A.C. 1987. An ash fall within the Loch Lomond Stadial. *Journal of Quaternary Science*, 2, 97-101.
- LONG, D., BENT, A., HARLAND, R., GREGORY, D.M., GRAHAM, D.K. and MORTON, A.C. 1986. Late Quaternary palaeontology, sedimentology and geochemistry of a vibrocore from the Witch Ground Basin, central North Sea. *Marine Geology*, 73, 109-123.

MUSSON, R.M.W. 1996. The seismicity of the British Isles. *Annals of Geophysics*, 39 (3).

PFANNKUCHE, O., 2005. *Cruise Report ALKOR 259: Methane Cycle at Shallow Gaseous Sediments in the Central North Sea*. GEOMAR, Kiel. 42pp.

PFANNKUCHE, O., 2006. *Preliminary Report ALKOR 290: Gas seeps in the central and northern North Sea*, GEOMAR, Kiel. 8pp.

STOKER, M.S. and LONG, D., 1984. A relict ice-scoured erosion surface in the central North Sea. *Marine Geology*, 61, 85-93.

STOKER, M.S., LONG, D. and FYFE, J.A., 1985. *A revised Quaternary stratigraphy for the central North Sea*. British Geological Survey, Report No. 17/2.